Theses and Dissertations 1. Thesis and Dissertation Collection, all items

1993-12

Characterization of tidal currents in Monterey Bay from remote and in-situ measurements

Petruncio, Emil T.

Monterey, California. Naval Postgraduate School

http://hdl.handle.net/10945/44439

NAVAL POSTGRADUATE SCHOOL
Monterey, California

AD-A277 844

DTIC
ELECTE
APR 06 1994
S F D

THESIS

CHARACTERIZATION OF TIDAL CURRENTS
IN MONTEREY BAY
FROM REMOTE AND IN-SITU MEASUREMENTS

by

Emil T. Petruncio

December, 1993

Thesis Advisor:	Leslie K. Rosenfeld
Co-Advisor:	Jeffrey D. Paduan

Approved for public release; distribution is unlimited.

DTIC QUALITY INSPECTED 3

94-10354

9 4 4 5 060

REPORT DOCUMENTATION PAGE	Form Approved OMB No. 0704

1. AGENCY USE ONLY *(Leave blank)*	2. REPORT DATE 1993, December	3. REPORT TYPE AND DATES COVERED Master's Thesis

4. TITLE AND SUBTITLE CHARACTERIZATION OF TIDAL CURRENTS IN MONTEREY BAY FROM REMOTE AND IN-SITU MEASUREMENTS	5. FUNDING NUMBERS
6. AUTHOR(S) Petruncio, Emil T.	

7. PERFORMING ORGANIZATION NAME(S) AND ADDRESS(ES) Naval Postgraduate School Monterey CA 93943-5000	8. PERFORMING ORGANIZATION REPORT NUMBER

9. SPONSORING/MONITORING AGENCY NAME(S) AND ADDRESS(ES)	10. SPONSORING/MONITORING AGENCY REPORT NUMBER

11. SUPPLEMENTARY NOTES The views expressed in this thesis are those of the author and do not reflect the official policy or position of the Department of Defense or the U.S. Government.

12a. DISTRIBUTION/AVAILABILITY STATEMENT Approved for public release; distribution is unlimited.	12b. DISTRIBUTION CODE A

13. ABSTRACT *(maximum 200 words)*

A first order description of tidal heights and currents in Monterey Bay is provided. Analysis of sea level records indicate that a mixed, predominantly semidiurnal tide nearly co-oscillates within the bay. Analysis of month-long moored ADCP records obtained in the winter and summer of 1992 reveals that tidal-band currents account for approximately 50 percent of the total current variance in the upper ocean (20-200 m). A relatively strong (7 cm/s) fortnightly tide (MSf) is present in both seasons. Considerable rotation of the semidiurnal ellipse orientations occurs with depth during both seasons. A month-long record of surface current measurements obtained with CODAR, an HF radar system, during September 1992 reveals that the Monterey Submarine Canyon clearly influences the strength and direction of semidiurnal (M2) tidal currents. Good agreement exists between the strenght and orientation of ADCP- and CODAR-derived tidal ellipses, with the exception of the constituent K1. Large, spatially uniform K1 surface currents (20-30 cm/s) appear to be the result of diurnal sea breeze forcing.

14. SUBJECT TERMS Monterey Bay, Monterey Submarine Canyon, Sea Level, Tides, Currents, CODAR, HF Radar, ADCP, Internal Waves, Remote Sensing, Sea Breeze	15. NUMBER OF PAGES 120
	16. PRICE CODE

17. SECURITY CLASSIFICATION OF REPORT Unclassified	18. SECURITY CLASSIFICATION OF THIS PAGE Unclassified	19. SECURITY CLASSIFICATION OF ABSTRACT Unclassified	20. LIMITATION OF ABSTRACT UL

DTIC QUALITY INSPECTED 3

Characterization of Tidal Currents in Monterey Bay
from Remote and In-Situ Measurements

by

Emil T. Petruncio
Lieutenant , United States Navy
B.S., United States Naval Academy

Submitted in partial fulfillment
of the requirements for the degree of

MASTER OF SCIENCE IN METEOROLOGY AND PHYSICAL OCEANOGRAPHY

from the

NAVAL POSTGRADUATE SCHOOL
December 1993

Author: _____
Emil T. Petruncio

Approved by: _____
Leslie K. Rosenfeld, Thesis Advisor

_____
Jeffrey D. Paduan, Thesis Co-Advisor

_____
Curtis A. Collins, Chairman
Department of Oceanography

ABSTRACT

A first order description of tidal heights and currents in Monterey Bay is provided. Analysis of sea level records indicate that a mixed, predominantly semidiurnal tide nearly co-oscillates within the bay. Analysis of month-long moored ADCP records obtained in the winter and summer of 1992 reveals that tidal-band currents account for approximately 50 percent of the total current variance in the upper ocean (20-200 m). A relatively strong (7 cm/s) fortnightly tide (MSf) is present in both seasons. Considerable rotation of the semidiurnal ellipse orientations occurs with depth during both seasons. A month-long record of surface current measurements obtained with CODAR, an HF radar system, during September 1992 reveals that the Monterey Submarine Canyon clearly influences the strength and direction of semidiurnal (M2) tidal currents. Good agreement exists between the strength and orientation of ADCP- and CODAR-derived tidal ellipses, with the exception of the constituent K1. Large, spatially uniform K1 surface currents (20-30 cm/s) appear to be the result of diurnal sea breeze forcing.

TABLE OF CONTENTS

ACKNOWLEDGEMENTS

Drs. Leslie Rosenfeld and Jeff Paduan were more than co-advisors during this project - they were role models. I owe them my sincere gratitude for providing the guidance which kept me from going adrift during high tide, and the motivation which kept me from running aground during low tide.

I also wish to thank Mr. Michael Cook of the Naval Postgraduate School Oceanography Department for sharing his knowledge of tides and his expertise in computer programming throughout the course of this project. LCDR Rost Parsons, USN also lent valuable assistance in writing a tidal currents error analysis program.

I am especially grateful to my wife Angela, for her steadfast support throughout this endeavor, and for knowing when I needed to work and when I needed to play.

I. INTRODUCTION

The forcing of the global tides by the gravitational attraction of the sun and moon has been studied for centuries, and the physics governing the open ocean equilibrium response to this forcing is reasonably well understood. Over the continental slope and shelf however, the physics becomes more complicated as bathymetric, geometric, and meteorological factors increase in importance. The interaction of the deep ocean tides with the variable topography of the continental margins gives rise to site-specific sea level and current oscillations which can at times be the largest physical signal in the coastal ocean. The sea level response to tidal forcing is generally uniform in amplitude and phase over many kilometers, and thus can be accurately analyzed and predicted given a sea level record of sufficient length. Coastal tidal currents, however, pose a more difficult prediction problem. Due to the sensitivity of current flow to friction, density stratification, and geometry, tidal currents remain coherent in direction and strength over only a few hundred meters in the horizontal, and a few meters in the vertical (Godin, 1991). Thus it is almost universally true that tidal heights are well modelled and predicted, while tidal currents are not.

The focus of this thesis is on a description of the tidal-period signals in Monterey Bay. Specifically, the magnitude

1

and spatial variability of tidal sea level and current fluctuations are examined in an effort to answer the following questions:

1. Is the sea level response to tidal forcing simultaneous and uniform in amplitude across the bay, or do tidal-period sea level fluctuations propagate noticeably within the bay?

2. Do the amplitude and direction of upper ocean tidal currents vary with depth, or do they remain constant?

3. Do the amplitude and direction of surface tidal currents remain constant across the bay, or do they exhibit significant horizontal variability?

Acoustic Doppler Current Profiler (ADCP) measurements obtained from a mooring near the mouth of the Bay are used to investigate the vertical structure of the tidal currents in the upper 200 m of the water column, while tide gauge and HF radar measurements are used to examine the horizontal variability of the tide within the bay. The proximity of the moored ADCP to the "footprints" of two Coastal Ocean Dynamics Applications Radar (CODAR) antennae provides a unique opportunity to study the tidal currents with both in-situ and remote sensors. The measurement locations, including the two tide gauges, the offshore mooring, and the CODAR observation bins are presented in Figure 1.
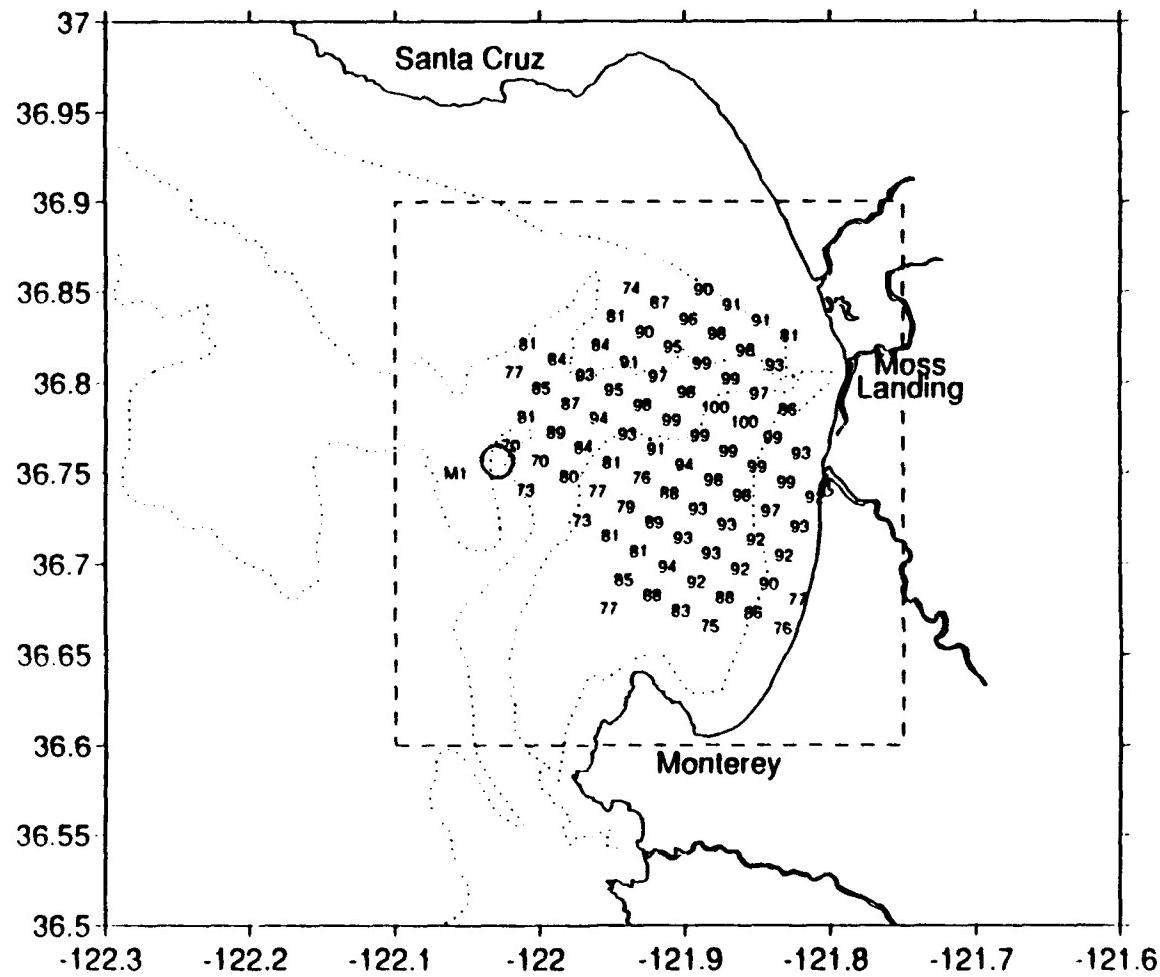
Figure 1. Locations of Tidal Height and Current Measurements. Tide gauges were located in Santa Cruz and Monterey. Numbers represent the percent coverage of measurements obtained at each CODAR gridpoint. The circle labeled "M1" indicates the watch circle of the moored ADCP. The inner box is the area depicted in subsequent figures throughout this text.

The extreme changes in bathymetry within Monterey Bay and the rich field observations available make this an especially interesting location to study tidal-period motions. Previous studies suggest that while oceanic currents are dominant at the mouth of the Bay, tidal currents play a significant role in the circulation of the inner Bay (Stoddard, 1971 and Shea and Broenkow, 1982). The Monterey Submarine Canyon, one of the deepest in the world, is a source of persistent baroclinic tidal energy. Broenkow and Smethie (1978) observed large internal waves with semidiurnal periods near the head of the canyon, and strong near-bottom semidiurnal currents have been observed at several locations along the canyon axis (Shepard et al., 1979). Preliminary investigations of the ADCP data used for this study indicate that even at the mouth of the Bay tidal period currents account for a significant portion of the total current variance.

Knowledge of coastal tidal circulation is of great benefit to physical and chemical oceanographers, as well as to marine biologists. Fine-scale resolution of tidal flow is essential to accurately model nutrient and pollution transport along the coast. Within Monterey Bay, improved current modeling will benefit efforts to protect the ecological and aesthetic resources of this newly designated National Marine Sanctuary.

The military applications of tidal analysis, prediction, and modeling are also numerous. Sea level and current fluctuations due to tides affect navigation, amphibious

4

landings, minefield planning, mine hunting operations, search-and-rescue operations, and oil spill clean-up. Fronts generated by tidal mixing may have an impact on acoustic forecasting. There are many scenarios in which careful study of the tides can contribute to the success of military operations in the littoral zone.

The results of the present study are presented in the following order: Background on tidal theory and previous studies of Pacific coast and Monterey Bay tides is presented in Chapter II. Sources of data and methods of analyses used in this study are discussed in Chapter III. Observations of tidal heights and currents are presented in Chapter IV, and an analysis of the dynamics involved in the observed semidiurnal, diurnal, and long period tides is presented in Chapter V.

II. BACKGROUND

A. TIDAL THEORY

The periodic changes in gravitational pull exerted between the earth, moon, and sun due to their complex, yet quantitatively predictable orbits, and the periodic global variations in the strength of these forces due to the spin of the earth on its axis, result in numerous tidal components or "constituents". The dominant constituents have periods close to 24 and 12 hours (the "diurnal" and "semidiurnal" constituents), however there are hundreds of lesser constituents, with periods ranging from several hours to thousands of years. The equilibrium theory of tides, which assumes that the earth is covered with water of uniform depth and density and that the ocean surface responds instantaneously to the gravitational pull of the moon and sun, is a simplification of the actual ocean response but is useful in calculating the relative importance of the various constituents. A partial list of the nearly 400 constituents, with their relative magnitude as predicted by equilibrium theory, is presented in Table 1. Pierre Laplace's dynamic theory of tides, which accounts for factors such as the depth of the ocean, the irregular boundaries of the ocean basins, friction, and the Coriolis effect, describes tides as shallow-

water waves that respond to periodic astronomical forcing. These waves have the same frequencies as the forcing constituents, but are not necessarily in phase with the astronomical forcing.

TABLE 1 PRINCIPAL HARMONIC COMPONENTS			
Name of constituent	Symbol	Period in solar hours	Coefficient ratio M_2 :100
Semidiurnal components			
Principal lunar	M_2	12.42	100.0
Principal solar	S_2	12.00	46.6
Larger lunar elliptic	N_2	12.66	19.2
Luni-solar semidiurnal	K_2	11.97	12.7
variational	μ_2	12.87	3.1
Diurnal components			
Luni-solar diurnal	K_1	23.93	58.4
Princ. lunar diurnal	O_1	25.82	41.5
Princ. solar diurnal	P_1	24.07	19.4
Larger lunar elliptic	Q_1	26.87	7.9
Smaller lunar elliptic	M_1	23.10	3.3
Long-period components			
Lunar fortnightly	Mf	327.86	17.2
Luni-solar fortnightly	MSf	354.37	0.9
Lunar monthly	Mm	661.30	9.1
Solar semiannual	Ssa	2191.43	8.0

(After Werner, 1992 and Schureman, 1988)

7

B. HARMONIC ANALYSIS

One of the immediate tasks in tidal analysis is to determine the amplitudes and phases of the various constituents. In the case of sea level, the harmonic representation of these constituents is:

$$A(t) = A_o + \sum_{i=1}^{N} A_i \cos(\sigma_i t - \phi_i) \qquad (1)$$

where A(t) is the total sea level, A_o is the mean sea level, A_i is the amplitude of the *i*th constituent, σ_i is the frequency, and ϕ_i is the phase lag (or epoch). The phase lag, which is expressed in angular measure, may be expressed more fully as $\phi_i = G_i - V_i$, where V_i is the phase of the Equilibrium tide of the *i*th constituent at the start of the record (relative to the Greenwich Meridian), and G_i is the angle by which the *i*th constituent in the observed tide lags the corresponding Equilibrium tide response. By convention, G is expressed relative to Greenwich Mean Time (GMT), and is referred to as the "Greenwich Phase". Although Greenwich Phases may be expressed relative to the local time zone, they would require subsequent conversion to GMT if comparison with phases obtained in other time zones was desired (for the construction of co-tidal charts, etc...). In this study, the

8

Greenwich phases of the various constituents are expressed relative to GMT.

Currents are represented in a similar fashion, the main difference being that two components of flow (usually the u-component, positive in the eastward direction, and v-component, positive northward) are analyzed. The harmonic decomposition produces amplitude and phase information for each component of flow which is used to reconstruct u and v as a function of time for that particular constituent. The harmonic representation of currents is as follows:

$$U(t) = u_o(t) + \sum_{i=1}^{N} u_i \cos(\sigma_i t - \phi_i) + i[v_o(t) + \sum_{i=1}^{N} v_i \cos(\sigma_i t - \theta_i)] \quad (2)$$

The first two terms on the right side of the equation are the mean and periodic parts of the east-west component of flow, and the final two terms are the mean and periodic parts of the north-south component. Setting $A_1 = u_i \cos\phi_i$, $B_1 = u_i \sin\phi_i$, $A_2 = v_i \cos\theta_i$, and $B_2 = v_i \sin\theta_i$, then dropping the constituent numbering suffix i and setting

$$a^+ = [(\frac{A_1 + B_2}{2})^2 + (\frac{A_2 - B_1}{2})^2]^{1/2}, \qquad a^- = [(\frac{A_1 - B_2}{2})^2 + (\frac{A_2 + B_1}{2})^2]^{1/2},$$

$$\varepsilon^+ = \arctan(\frac{A_2 - B_1}{A_1 + B_2}), \qquad \text{and} \qquad \varepsilon^- = \arctan(\frac{A_2 + B_1}{A_1 - B_2}),$$

9

and applying some algebra (Godin, 1972), the tidal currents contribution for any constituent is then seen to be

$$U(t) = U^+(t) + U^-(t) = a^+ \exp i(\varepsilon^+ + \sigma t) + a^- \exp i(\varepsilon^- - \sigma t) \qquad (3)$$

$$= \exp\left[i\left(\frac{\varepsilon^+ + \varepsilon^-}{2}\right)\right]\left[(U_{maj})\cos\left(\left(\frac{\varepsilon^+ - \varepsilon^-}{2}\right) + \sigma t\right) + i(U_{min})\sin\left(\left(\frac{\varepsilon^+ - \varepsilon^-}{2}\right) + \sigma t\right)\right]$$

$$(4)$$

Equation (3) reveals that this contribution consists of two vectors, $U^+(t)$ and $U^-(t)$, each rotating at the angular speed of σ cycles per hour. The former vector has length a^+, rotates counterclockwise, and is at ε^+ radians counterclockwise from the positive X (east/west) axis at time $t=0$; while the latter has length a^-, rotates clockwise, and is at ε^- radians counterclockwise from the positive X axis at $t=0$. The net rotational effect is that the composite vector U(t) moves counterclockwise if $a^+ > a^-$, clockwise if $a^+ < a^-$, and linearly if $a^+ = a^-$. Equation (4) shows that over a time period of $1/\sigma$ hours, the path of the composite vector traces out an ellipse (or a line segment, if moving linearly) whose respective semimajor (U_{maj}) and semiminor axis (U_{min}) lengths are $a^+ + a^-$ and $a^+ - a^-$, and whose angle of inclination (in the counterclockwise direction) from the positive X axis is $(\varepsilon^+ + \varepsilon^-)/2$ radians. A depiction of these tidal ellipse parameters is presented in Figure 2.
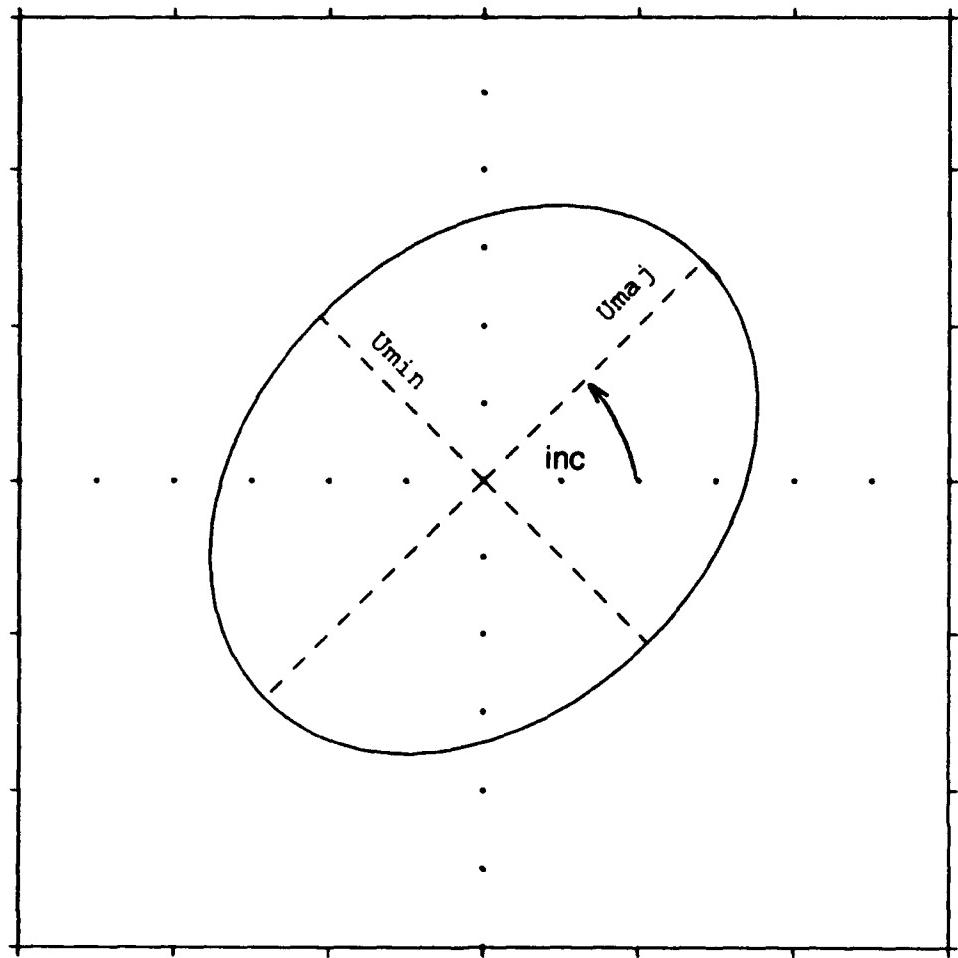
**Figure 2.** Tidal Ellipse with an Inclination of 45°.

All tidal current ellipses exhibit 180° ambiguity with
respect to the angle of inclination, since this angle
indicates the offset from due east for one or the other end of
the semimajor axis. The actual position of the tidal current
vector for a given moment in time will point in the same
direction regardless of which end of the semimajor axis is

chosen as the reference, but the angles describing the inclination of the ellipse and phase of the current vector change by 180°, depending on which end is chosen. This ambiguity should be borne in mind when comparing the phase angles of various tidal current constituents.

If the amplitude and phase lag of every constituent at a particular location could be determined, then one could calculate the time history and future of the tide at that location for all time (or at least until the orbits of the earth, moon, and other celestial bodies undergo significant changes). While the amplitudes and phases of the various gravitationally forced tidal constituents are constant over time, the determination of their values is not a trivial matter. Short time series may prevent the resolution of important constituents which are narrowly separated in frequency. Meteorological factors, such as seasonal changes in the direction of prevailing winds and diurnal changes due to land/sea breeze cycling cause periodic sea level and current oscillations with tidal-band frequencies. The tides themselves contribute to non-gravitational forcing of tidal-band currents through internal wave generation and nonlinear interaction among stronger constituents.

In general, the tides can be described reasonably well by determining the amplitudes and phases of just a few of the major constituents. The strongest semidiurnal constituent is the principal lunar, or M2 tide, which is a result of the

combined effect of the moon's orbit around the earth and the earth's spin about its axis. Other significant semidiurnal constituents are the S2 (principal solar), N2 (larger lunar elliptic), and K2 (luni-solar). The largest diurnal constituent is the luni-solar diurnal, or K1 tide, which arises from interactions of orbital motions with periods of a lunar and a solar day with those of a tropical month (Werner, 1992). Other important diurnal constituents are the O1 (principal lunar diurnal) and P1 (principal solar diurnal).

One common classification of tides at a given locality is the ratio of the sum of the amplitudes of the major diurnal constituents, K1 and O1, to the sum of the amplitudes of the major semidiurnal constituents, M2 and S2. This ratio, called the form number, is expressed mathematically as: $F = (K_1 + O_1)/(M_2 + S_2)$. The form number is larger for locations which have a large diurnal inequality, and is maximum where there is only one high water a day. Traditional classification of tides according to their form number is (Pugh, 1987 and Werner, 1992):

1. F=0 to 0.25, semidiurnal: two highs and two lows daily of approximately equal height.

2. F=0.25 to 1.50, mixed, mainly semidiurnal: two highs and two lows daily but unequal in time and height.

3. F=1.50 to 3.00 mixed, mainly diurnal: two highs and two lows daily but strongly unequal in time and height.

4. F=3.00 to infinity, diurnal: one daily high water, almost no semidiurnal signature.

The form number provides a rough comparison of the diurnal and semidiurnal sea level response, however this description may not be useful to describe the tide regime in very shallow seas and estuaries, where shallow water distortions cause significant sea level changes with shorter periods in addition to the normal diurnal and semidiurnal fluctuations.

C. PACIFIC COAST TIDES

Numerous global numerical solutions of Laplace's tidal equations indicate that the tides along the west coast of North America are of the mixed, mainly semidiurnal type. According to Defant (1961), the form number in San Francisco is equal to 0.90. Most global models depict an amphidrome of the M2 tide located in the northeast Pacific, with the phase propagating northward along the west coast of North America. Models of tidal elevation amplitude and current flow off the California coast have been in existence since at least 1970. Munk, Snodgrass, and Wimbush (1970) modeled the tidal responses along the California coast as the sum of Kelvin, Poincare, and forced waves over a step-shelf topography. Their models accounted for many of the characteristics of the observed sea level changes and current fields off southern California, including the northward progression of tidal heights and alongshore orientation of currents. A model to

predict the amplitude and phase of barotropic tidal currents at any offshore location using only data from an alongshore array of coastal sea level stations was developed and tested by Battisti and Clarke (1982). Both the Munk, Snodgrass, and Wimbush (MSW) model and the Battisti and Clark (BC) model were compared to extensive observations of tidal currents made off of northern California during the Coastal Ocean Dynamics Experiment (CODE).

1. Tides Seaward of the Continental Shelf

Noble et al. (1987), conducting a study of currents seaward of the continental shelf during CODE, found significant energy peaks in the semidiurnal band and smaller peaks in the diurnal band. They found that tidal current energy was most significant over the basin and middle slope, where it contributed 40-60% of the variance in the alongslope current field and 10-45% of the cross-shelf field. Over the upper slope, tidal current amplitudes were comparable to those over the middle slope and basin, but subtidal currents were at maximum strength and dominated the current variance. Their study confirmed that M2 was the dominant constituent, containing 50-75% of tidal current variance. The barotropic M2 currents were found to rotate counterclockwise at most sites, and were approximately in phase vertically over the upper slope and basin. Over the upper and middle slope, barotropic M2 current ellipses were generally oriented

15

alongslope, while over the basin no obvious direction of orientation was found. S2 currents were approximately half the strength of M2, and rotated counter-clockwise only over the upper slope. While barotropic currents accounted for over 50% of the M2 current signal over the upper slope and basin, baroclinic currents strongly dominated the M2 currents over the middle slope. According to Noble et al., "...the large variations of the estimated amplitude and phase of the M2 current for successive 75-day blocks of record indicate that the internal tides over the middle slope and basin can have a stable phase over several months."

The diurnal currents fell into two basic categories. Those over the basin (category one) were depth independent, aligned alongslope, and rotated counterclockwise. The diurnal currents over the middle and upper slope (category two) rotated clockwise, were oriented cross slope, and exhibited vertical and horizontal phase shifts.

Noble et al. found that a barotropic Kelvin wave propagating poleward along the coast would exhibit many of the characteristics of the M2 currents and the category one diurnal currents. In particular, Kelvin waves have counterclockwise-rotating velocity ellipses that are depth independent and aligned with the large-scale topography of the continental margin. The category two diurnal currents, those found over the middle and upper slope, were best modeled by continental shelf waves (CSW). Although they both propagate

16

with the coast to the right, diurnal CSWs and Kelvin waves have quite different spatial structures. CSWs have clockwise rotating ellipses which may be oriented either with or against the local topography. Because of its shorter decay scale the CSW is seen only over the shelf and slope. The CSW also features much slower propagation speed and a much smaller sea level deflection. Noble et al. found the BC model to be ineffective in predicting the observed diurnal currents, probably because the CSW signature at the coastal sea level stations is masked by the much stronger Kelvin wave deflection. They found the BC model to work much better with the M2 currents, since they are primarily a Kelvin wave feature. In particular, the BC model correctly predicted counterclockwise rotating M2 ellipses oriented along slope, with semimajor axis amplitudes of 3 to 4 cm/s and semiminor axes of 0.2 to 0.4 cm/s.

2. Tides over the Continental Shelf

Rosenfeld and Beardsley (1987), studying barotropic semidiurnal currents over the northern California shelf during CODE, found these currents to be aligned primarily in the alongshore direction and counterclockwise in their direction of rotation. Although they observed little variation among the currents in the cross-shelf direction, they found significant alongshore variability which was not well predicted by the MSW model. In an effort to account for the

alongshore variations (current ellipse major axes were observed to vary from 1 to 6 cm/s over distances less than 100 km), Rosenfeld and Beardsley devised a model with topographic effects roughly similar to the California coast (sinusoidal bumps with an alongshore scale much smaller than the barotropic Rossby radius of deformation, and an onshore-offshore scale much smaller than the alongshore scale). The results of a perturbation analysis conducted with this model suggest that the alongshore speed changes are driven by the onshore and offshore boundary conditions (classic Kelvin wave behavior offshore, which matches Noble's observations, and no normal flow onshore); the tidal flow must speed up as it passes through constrictions, which were represented in the model by bumps in the coastline.

Fernandez (1993), using a single phased-array HF radar system located about 15 miles south of Monterey Bay at Granite Canyon, measured surface tidal currents in the alongshore direction during a two month period in the summer of 1990. Focusing on a 7.5 km-square area located over a narrow portion of the shelf, Fernandez found the strongest constituents to be M2 (5.4 cm/s), S2 (2.9 cm/s), and K1 (2.8 cm/s). The radar-derived M2 current strength was in agreement with M2 currents measured 100 miles further south along the coast and reported by MSW (1970).

The discussion up to this point has focused mainly on the increased energy of the barotropic tides as they encounter

18

the shallower waters along the continental margins. Internal waves can also contribute significantly to tidal period current velocities over the shelf. Wunsch (1975) showed that energy associated with internal waves approaching sloping topography will be focused toward the shallowest region. Internal waves with frequencies greater than a certain critical frequency will be refracted upslope. This critical frequency (ω_c) is expressed as:

$$\omega_c = [\frac{f^2 + a^2N^2}{a^2 + 1}]^{\frac{1}{2}} \qquad (5)$$

where f is the inertial frequency, a is the bottom slope, and N is the buoyancy frequency. Internal waves with frequencies less than the critical frequency will be reflected in the downslope direction. At the critical frequency, generation of internal waves is particularly intense and the predicted velocity along the bottom is large (Hotchkiss and Wunsch, 1982). Lab experiments conducted by Wunsch (1975) demonstrated that at high frequencies, $\omega \geq \omega_c$, intensification occurs at the apex (the intersection of the bottom and the sea surface), causing the internal waves to break "catastrophically." These breakdowns of the internal waves resembled bores in some cases and breaking waves in others.

Equation (5) can alternately be used to solve for the critical slope necessary for generation of an internal tide

19

with a specified frequency. According to Baines (1973), the internal tide generating process is generally strongest at or near the shelf break, where the generating force is largest. Baines states that on the shelf (depth $\leq$ 100 m), baroclinic tidal energy is frequently observed to be concentrated in the lowest vertical mode. It should be noted that regardless of the slope of the topography, only those internal waves with periods less than the inertial period will propagate freely, while those with longer periods will remain trapped at their point of generation.

Rosenfeld (1990) revisited the CODE shelf data to examine the baroclinic energy in the semidiurnal tidal currents. There were several occasions over the 8-month period during which the semidiurnal tidal energy increased well above the background level. In one case the semidiurnal tidal currents were as high as 30 cm/s. Focusing on these events, which coincided with relaxations in the upwelling regime, Rosenfeld showed that the kinetic energy of the semidiurnal tidal band increased due to increased stratification (and thus, increased internal wave activity). Upon examining the horizontal current and temperature fluctuations in the semidiurnal band, she found them to be consistent with a first baroclinic mode internal wave with a horizontal wavelength of 20-30 km. The topography of the slope in the vicinity of the current meters from which the data was drawn suggests that the internal waves observed over

the shelf were probably generated near the shelf break, which follows Baines' theory. The slope goes from super-critical (too steep for semidiurnal internal tide generation) to subcritical in the vicinity of the shelf break, about 20 km offshore. At the semidiurnal frequency, the topography of the entire shelf in the CODE region remains subcritical, which is favorable for propagation of semidiurnal internal tides generated at the shelf break.

3. Tides in Monterey Bay

a. Tidal Heights

Tidal sea level fluctuations in the Bay have been studied at least since 1963, when the National Ocean Service (NOS) installed a tide gauge at Monterey. NOS operated a tide gauge at Moss Landing during 1976-1977 in conjunction with the California Marine Boundary Program (Schomaker, 1983). Currently tide gauges are maintained at Santa Cruz and Monterey. The NOS Tide Tables 1992 predict the Monterey tidal heights to lag those in Santa Cruz by six minutes. Lazanoff (1971) and Schomaker (1983) used two-dimensional, implicit finite difference schemes to model the barotropic tides within the bay. While they were generally successful in modeling tidal heights (model heights were within 4 cm of the predicted heights), they failed to accurately model observed currents in either pattern or speed. Lazanoff's model currents were an order of magnitude too large, and Schomaker's were too weak.

Both Lazanoff and Schomaker forced their models with sea levels which were constant in phase across the mouth of the bay. Schomaker attempted to incorporate the six minute lag between Monterey and Santa Cruz (predicted by NOS) within her model, but this increased the errors in modeled sea level and did not improve the modeled currents. The lack of success in modeling Monterey Bay tidal currents with barotropic models was attributed to the possible influence of baroclinic energy on the tidal currents (Schomaker, 1983).

b. Tidal Currents

Although there are few published reports specifically addressing the tidal currents in Monterey Bay, there have been several short term observations of tidal band phenomena in the bay. Observations of near-surface tidal currents in Monterey Bay can be traced back to McKay (1970). Using a geomagnetic electrokinetograph (GEK), McKay observed downcanyon surface flow during rising tide and upcanyon surface flow during falling tide. Currents as high as 50 cm/s were observed near the canyon head. Stoddard (1971) used 38 parachute drogues to study currents in the Bay over a 4-month period. The depth of the chutes was approximately 8 m. Tracking the drogues with a radar located at NPS, Stoddard was able to observe currents over the southern portion of the Bay. The drogue tracks indicate that near the mouth of the Bay, oceanic currents dominate the flow, while inside the Bay tidal

currents are important. Nearly all of the drogues launched over the middle and southern edges of the canyon moved in clockwise spirals, reaching maximum speeds of 25 cm/s. Analysis of several of the circular drogue tracks indicate a semidiurnal period. Koehler (1990) analyzed ship-mounted Acoustic Doppler Current Profiler (ADCP) measurements and hydrographic data obtained near the mouth of the Bay during a May 1988 NPS student cruise. Correlations between current flow and surface tidal heights were weak, however one series of ADCP measurements indicated upcanyon flow at 20 cm/s during the ebb tide and downcanyon flow at 18 cm/s during flood. Koehler noted internal waves near the mouth of the Bay with amplitudes of 30 m, with the highest levels of baroclinic energy occurring near the shelf break. Heard (1992) made ship-mounted ADCP current measurements between 10 and 30 m along a 3.6 km transect which crossed the canyon near the 40 m depth contour. His measurements revealed oscillatory currents of semidiurnal period with speeds of 6-18 cm/s between 10 and 30 m, oriented in a northeast-southwest fashion.

Neal (1992) found that HF radar measurements might be useful for studying tidal surface currents in Monterey Bay. He used data obtained with the same sensors used in this study: a moored, downward-looking ADCP located near the mouth of the bay, and two Coastal Ocean Dynamics Applications Radar (CODAR) systems located on the shores of the Bay at Moss

Landing (near the center of the bay) and Pacific Grove (at the southern end of the bay). Comparisons of the radar-derived surface currents with wind data and ADCP current data revealed good correlations for events with periods longer than one week. Neal found good agreement between the CODAR and ADCP-derived currents during an oceanic (non-wind driven) event with a period of about two weeks, which is suggestive of (among other possibilities) a fortnightly tidal current. For events with periods less than one week, the radar-derived currents were not coherent with either the winds or the ADCP measurements except at tidal periods. The radar measurements were coherent with the winds at diurnal periods and with the ADCP measurements at both diurnal and semidiurnal periods.

Several observations of near-bottom currents in Monterey Canyon were conducted by Naval Postgraduate School (NPS) students between 1965-1975. These studies revealed strong semidiurnal currents in the along-axis direction near the head of the canyon, at depths ranging from 91 to 485m. Several of these studies (Gatje and Pizinger (1965), Njus (1968), and Caster (1969)) correlated downcanyon flow with the surface flood tide and upcanyon flow with the ebb tide. Dooley (1968) observed sudden bursts of cold, upcanyon flow near the canyon head, followed by warmer downcanyon flow. The dominant period of these flows was 12 hours, but he did not correlate these flows with the surface sea level. Hollister (1975) found that currents at 30 m above bottom were

semidiurnal and oriented in the along axis direction, while currents at 60 m above bottom flowed across the canyon and exhibited a weak semidiurnal signal. Shepard et al. (1979) conducted research on currents in numerous canyons, including Monterey Canyon. They made observations along the canyon axis at 1061 m and 1445 m near the mouth of Monterey Bay, and compared them to the shallower measurements made by NPS. Shepard et al. concluded that internal waves were generated within the canyon and were propagating upcanyon between stations at shallower depths but downcanyon at greater depths. They found that correlations between flow in the canyon and tidal sea level at Monterey were much stronger at the shallower stations near the canyon head than they were at the deep stations near the mouth of the bay.

Broenkow and Smethie (1978), studying vertical temperature distributions obtained during a 24 hour period on 7-8 August 1971, observed large internal tides at two stations near the head of Monterey Canyon. In water depths of 130 m and 250 m, they observed internal tidal oscillations with amplitudes of 80 m and 120 m, respectively. The oscillations were roughly semidiurnal in period and approximately 180° (7 hours) out of phase with the predicted tidal heights for the same time period. Additionally, Broenkow and Smethie observed cool patches of water located near the head of the canyon during both upwelling and non-upwelling wind conditions, and a tendency for the center of the Bay to be cooler than the

north or south ends. Based on their observations of the large internal tides, and assuming a covarying tide within the bay, Broenkow and Smethie suggested "tidal pumping" of water up and down the canyon as a mechanism to account for the cool patches.

Shea and Broenkow (1982) pursued the idea of tidal pumping in the bay, using a conceptual model of volume convergence (on the falling internal tide) and divergence (on the rising internal tide) to explain nutrient enrichment observed on the shelf along the flanks of the canyon. The currents associated with the cross-shelf transport of a large volume (560×10^6 m^3) of cold, high density water that originated in the canyon were calculated to be on the order of 9 cm/s, between 10 and 40 m in depth (Shea and Broenkow (1982)). Observations of isopycnal spacing by Heard (1992) suggested a smaller volume (63×10^6 m^3) and associated current speeds of 4 cm/s between 10 and 30m.

III. DATA AND METHODS

A. SEA LEVEL MEASUREMENTS

Hourly sea level measurements recorded at Monterey and Santa Cruz between 1 January - 31 December 1992 were provided by NOS, which is part of the National Oceanic and Atmospheric Administration (NOAA). The sea level data for this time period was free of gaps and coincided with the current measurements. During the time period of this study, both the Monterey and Santa Cruz tide gauges were of the stilling well type. The stilling well is basically a stand pipe which houses a float, the level of which represents sea level. Water enters the stilling well through a small orifice at the bottom, which is usually located approximately 2 m below Mean Lower Low Water (MLLW) (Lentz, 1993). The orifice serves to damp out higher frequency oscillations. The float is attached through a system of gears and a counterweight to an automatic recorder. The level of the float is sampled every 6 minutes and automatically recorded by the punching of a binary code on a paper tape.

Possible sources of error in tide gauge measurements include currents in the vicinity of the stilling well (strong currents will cause a lower sea level in the well due to the Bernoulli effect), wave induced errors, marine fouling, and

27

density changes due to river discharge or the advection of cooler or warmer waters in the vicinity of the well. According to Shih and Baer (1991), these effects can introduce errors on the order of several centimeters. Lentz reports the rms errors associated with a stilling well tide gauge measurement to be on the order of 1.5 cm or less.

The 366-day sea level records were subjected to harmonic analysis in order to extract the tidal signals. The harmonic analysis was conducted using a least squares tidal heights analysis computer program developed by Dr. Michael Foreman of the Institute of Ocean Sciences, Patricia Bay, Sidney, British Columbia (Foreman, 1984). The program, based on the least squares method described by Godin (1972), is in common use throughout Canada and has several desirable features. Among them are the permission of gaps within the data record and compensation for smoothing effects due to prefiltering of the data. A standard list of 69 constituents is used for the analysis, with 77 additional shallow water constituents available for inclusion. The program output lists the amplitudes and Greenwich Phases of each resolved constituent, as well as a time series of hourly tidal height values (in the same units and covering the same time period as the input) based on the analysis results.

As a check on the program performance, the results of the Monterey and Santa Cruz analyses were compared to least squares analyses conducted by NOS for the same locations and

28

time periods. Since the NOS program uses fewer constituents, the constituent list in the Foreman program was reduced to match the NOS list for this comparison. The analyses were nearly identical, with phase differences of 0.5° or less and height differences of 0.9 cm or less for the major diurnal and semidiurnal constituents. Differences were slightly greater when the full package of 69 constituents was used with the Foreman program.

B. CURRENT MEASUREMENTS

1. Time Periods of Current Studies

Currents in the upper 200 m of the ocean were investigated using moored ADCP data obtained during the periods 17 January - 19 February and 1 September - 4 October 1992. These times were chosen for two reasons: The current records for these two periods were nearly gap-free, and the periods represent different synoptic flow regimes and density stratification conditions. A detailed discussion of the Central California marine climate is presented in detail in Chapter IV; at this point it will suffice to say that the density of the upper ocean is expected to be uniform in the winter due to strong wind mixing and stratified in the late summer. The seasonal variations in upper ocean mixing can be demonstrated in a general sense by comparing vertical temperature profiles. Temperature profiles obtained within a

few kilometers of the ADCP during two cruises of the R/V Point Lobos are presented below in Figure 3.
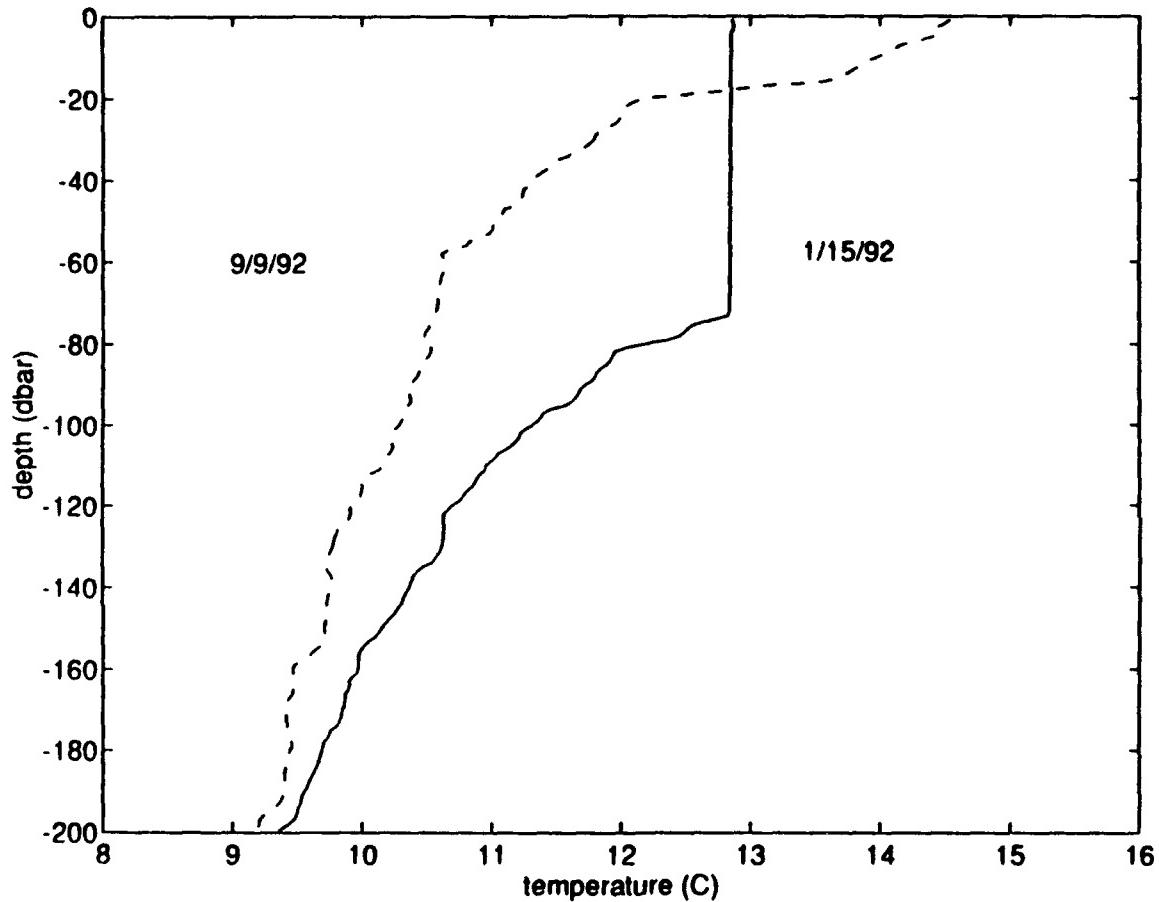

Figure 3. Temperature Profiles Obtained at 36° 46.7′ N, 122° 01.0′ W. On 15 January 1992, a mixed layer extends down to approximately 75 m. On 9 September 1992, the water column appears continuously stratified.

Surface currents (those in the upper meter of the bay) were investigated with remotely-sensed HF radar measurements

obtained during September 1-30 1992. During this time period, the radar systems operated continuously, making current measurements every two hours. This time period coincides with the second set of ADCP measurements. The various sensors and the time periods of measurement used in this study are summarized below.

TABLE 2   INSTRUMENTS AND TIME PERIODS USED IN THIS STUDY

Instrument	Duration of Measurements (1992)
Tide Gauges	1 January - 31 December
Moored ADCP	17 January - 19 February, 1 September - 4 October
HF Radar	1 - 30 September

2. ADCP Data

The Monterey Bay Aquarium Research Institute (MBARI) operates a mooring to obtain weather and oceanic data near the mouth of Monterey Bay, at 36° 44.9′ N, 122° 02.3′ W. The water depth at the mooring location is approximately 1200 m (see Figure 1). The downward-looking ADCP used in this study is one of the instruments mounted on the mooring. The ADCP

31

measures current by transmitting short acoustic pulses into a column of water along lines of position defined by four directional transducers, and then determining the Doppler shift present in the sound backscattered from plankton and other small-scale inhomogeneities in the water. The Doppler shift is proportional to the relative velocity between the scatterers and the transducer. By assuming that the scatterers are drifting with the current, the velocity indicated by the measured doppler shift is then seen to represent the current velocity in the water column. By knowing the precise geometry of the transducer beams, three orthogonal current velocity components for each "depth bin" are computed by combining the measurements from any three of the four beams. The MBARI ADCP is programmed to separate the current measurements into 8 m depth bins. The transducer heads are located at a depth of approximately 1.27 m, and a blanking interval of 4 m below the transducer heads was selected. As a result of this configuration, the first depth bin measures currents between 5 and 13 m, but measurements made within this bin are highly contaminated by reflections from surface waves and turbulence. The second depth bin is therefore the first reliable depth bin. Due to decreased accuracy in the lower bins, the deepest bin used in this study was bin 25, which measures currents centered at a depth of 201 m. The ADCP sampled every 15 minutes, 110 pings per sample, with one second between pings.

Sources of error in ADCP measurements are random "ping-to-ping" errors, ADCP bias errors, and relative motion introduced by the movement of the ADCP through the water. In the case of the MBARI mooring, movement of the ADCP occurs as the mooring buoy travels within its watch circle. The random ADCP errors, which are a function of operating frequency, depth bin size, and the number of pings per ensemble, are calculated to be between 0.5-1.0 cm/s for the MBARI ADCP.

ADCP bias, according to *Principals of Operation: A Practical Primer* (RD Instruments, 1989), depends on a variety of factors including temperature, mean current speed, beam geometry, etc... and is typically on the order of 0.5-1.0 cm/s. Both the ADCP bias and the random errors are an order of magnitude smaller than the measured currents and are thus considered negligible.

The effects of buoy drift on the current measurements were less obvious. The buoy, which is moored in 1200 m of water over the canyon axis, is subject to the combined action of the winds and currents. Analysis of Global Positioning System (GPS) position data obtained from a single channel Magellan GPS unit on the buoy indicated movement within a watch circle approximately 1.8 km in diameter (see Figure 1). In order to estimate the errors in the tidal currents analyses due to relative motion imparted by buoy drift, the time series of GPS latitude and longitude readings were used to compute the approximate velocity of the buoy through the water. A

despiking routine was used to remove buoy velocities calculated from obvious position errors, and then buoy velocities corresponding to each ADCP current measurement were obtained by linear interpolation. The errors associated with this periodic buoy motion are discussed in Chapter IV.

The 15 minute ADCP data was smoothed by the successive application of three moving-average filters, and then subsampled to obtain hourly current readings. The pre-filtering, which follows Godin (1972) and Foreman (1984), eliminates short period fluctuations that are of no relevance to tidal analysis. Hourly subsampling was required in order to meet the standard format requirements of the least squares program. The hourly u and v current data were then screened for 3-beam "percent good" values of less than 75%. Current readings which fell into this category were flagged and replaced with gaps. (Using this criteria, only one data gap occurred in the September-October time series, and there were none in the January-February time series). The hourly u and v values for each depth bin were then subjected to least squares harmonic analysis, using Foreman's tidal currents analysis program. Since the record lengths (804 hours) were too short to resolve P1 and K2, these relatively important constituents were inferred from their amplitude and phase relationships to K1 and S2, as observed in the tidal heights analyses. This is an acceptable method of inferring tidal current constituents, as long as the measurements are not made

34

in the vicinity of an amphidrome (Godin, 1972). Compensation for the false amplitudes introduced by pre-filtering are accomplished within the analysis program, based on the filter length definitions included in the input files. The program output includes the ellipse semi-major and semi-minor axis lengths, the ellipse inclination, and the Greenwich Phases for each resolved constituent. A synthesized time series of tidal current u and v components, based on the analysis results, is also included in the program output.

A depth-averaged analysis of the data was performed in order to minimize the effects of any wind contamination that might be present in the upper depth bins. The depth-averaged analyses were accomplished by averaging the hourly current readings for bins 2-25 and then running the least squares analysis on the averaged data. It should be noted that a depth-averaged tidal analysis will not necessarily yield the barotropic tidal currents. If a true integral of the entire water column were performed, baroclinic effects would be removed, but a true depth integral is impossible to accomplish. Additionally, the presence of friction also introduces vertical shear.

3. HF Radar data

HF radar measures currents in the upper one meter of the ocean by resonant backscatter of radar signals from surface gravity waves (Crombie, 1955; Barrick et al., 1977).

The dominant returning signals are reflected (Bragg-scattered) from ocean waves moving directly toward or away from the radar. The wavelength of the ocean waves which cause a resonant reflection of the radar signal is one-half the radar wavelength. Spectral analysis of the returning signal reveals two dominant peaks in the frequency spectrum surrounded by a continuum of smaller peaks. The frequencies of the dominant peaks are at the Doppler shift associated with the phase velocities of the ocean waves responsible for the resonant Bragg scattering, divided by their wavelength. The current measurement is based not on the actual Doppler shift associated with the phase velocity of the wave, but on small deviations from this expected Doppler shift. Slight changes from the expected Doppler shift are attributed to surface currents advecting the ocean wave field (Crombie, 1972; for a review see Fernandez, 1993).

During this study, NOAA operated two HF radar sites on the shores of Monterey Bay, one near the center of the Bay at Moss Landing, and one at the southern end of the Bay at Pacific Grove. These instruments were of the Coastal Ocean Dynamics Applications Radar (CODAR) design (Barrick et al., 1986). These particular instruments provide useful coverage to approximately 22 km offshore (Neal, 1992). The average depth observed, based on the radar operating wavelength, is 0.5 m. Horizontal range resolution is 2 km; each CODAR gridpoint represents the center of a 2 km by 2 km box. CODAR

36

measurements are recorded every two hours, and each measurement is the result of 26 minutes of radar transmissions. Both CODAR sites independently gather radial current vectors, and a central site then uses both sets of radial current vectors to resolve the total current vectors. The CODAR system software computes the surface current velocity uncertainties at all gridpoints. If velocity uncertainty is greater than 10 cm/s at a gridpoint, the data for the point is discarded. Barrick et al. list the average surface current velocity uncertainties as ± 2-3 cm/s rms errors and the bearing uncertainties as $\pm 2.5°$ rms.

Since total current vectors cannot be resolved along the line which runs directly between the two CODAR sites (the "baseline"), the CODAR system software artifically determines the onshore current velocity along the baseline by interpolation of velocities further offshore. Inshore of the baseline, the software reduces the onshore current velocities from their artificial value at the baseline to zero at the coastline. For this reason, CODAR-derived current measurements along and inshore of the baseline should be interpreted with caution. The baseline is marked by a dashed line on all CODAR plots used in this report.

Time series of two-hourly CODAR-derived surface currents obtained during September 1992 were subjected to least squares harmonic analysis using the Foreman tidal currents analysis program. Analyses were only performed on

37

data from gridpoints which reported acceptable current measurements (based on the 10 cm/s uncertainty criteria) at least 70% of the time. As in the case of the ADCP data, the P1 and K2 constituents were inferred from K1 and S2, using amplitude and phase relationships derived from the tidal heights analyses.

4. Precautions

CODAR and ADCP current measurements are conducted at different depths, and on different temporal and spatial scales. CODAR measures currents within the top meter of the ocean, covers 4 km^2 bins, and averages over 26-minute period transmissions made every two hours. The second depth bin of the MBARI ADCP (the shallowest reliable depth bin) measures currents between 13 and 21 m below the surface, and its ensembles are averaged over 110 seconds every 15 minutes. Additionally, the mooring to which the ADCP is fixed was observed to move within a watch circle of nearly two km in diameter. Due to the different dynamics and noise sources which affect the currents measured by each system, the measurements should not be expected to match precisely. In a comparison of measurements obtained with these same two systems in March through May 1992, Neal (1992) did find good agreement for low frequency currents with periods greater than 10 days and for fluctuations in the diurnal and semidiurnal tidal bands.

IV. OBSERVATIONS

A. TIDAL HEIGHTS

The amplitudes and phases of the dominant diurnal and semidiurnal constituents, based on analysis of the year-long records of tide gauge measurements, are listed on the following page in Table 3. The amplitudes are also depicted in a bar graph in Figure 4. In general, the results for Monterey and Santa Cruz are very similar. Both locations are characterized by a mixed, predominantly semidiurnal tide. The form numbers for Monterey and Santa Cruz are 0.955 and 0.948, respectively. M2 is seen to be the dominant constituent in the bay, followed by K1, O1, and S2. N2 and P1 are seen to be practically equal in both locations, and are followed in strength by Q1 and K2. The remaining constituents analyzed had amplitudes less than that of K2.

In addition to the tide gauge errors discussed in Chapter III, sea level fluctuations associated with periodic atmospheric pressure changes, wind forcing, and unresolved tidal constituents will contribute to errors in the tidal analysis. The errors associated with the analyzed amplitude and phases for the major constituents were determined by calculating the variance in residual sea level within the

TABLE 3 DOMINANT TIDAL CONSTITUENTS IN TIDAL HEIGHTS

	Monterey		Santa Cruz	
	Amplitude (cm)	Greenwich Phase (deg)	Amplitude (cm)	Greenwich Phase (deg)
M2	49.1 ± .1	182.0 ± .3	49.6 ± .4	178.2 ± .4
K1	36.5 ± .1	219.6 ± .2	36.3 ± .2	219.0 ± .2
O1	22.8 ± .1	203.0 ± .2	22.9 ± .2	202.5 ± .4
S2	13.0 ± .1	180.7 ± .5	12.8 ± .4	177.1 ±1.7
N2	11.2 ± .1	155.9 ± .6	10.9 ± .4	150.3 ±2.0
P1	11.4 ± .1	216.1 ± .5	10.7 ± .1	215.2 ± .9
Q1	4.1 ± .1	195.6 ± 1.4	4.1 ± .2	194.0 ±2.3
K2	3.7 ± .1	171.8 ± 1.8	3.6 ± .4	165.4 ±6.1
MM	2.1 ± .6	255.3 ± 16.6	2.2 ± .5	267.0±13.1
MSf	0.4 ± .6	333.0 ± 84.2	0.6 ± .5	34.5 ±48.1

constituent frequency bands (semidiurnal, diurnal, fortnightly, etc...), and then computing the propagation of this uncertainty in the subsequent amplitude and phase calculations. This method follows Filloux and Snyder (1979). Equations used to calculate the standard deviations of amplitude and phase may be found in Appendix A.
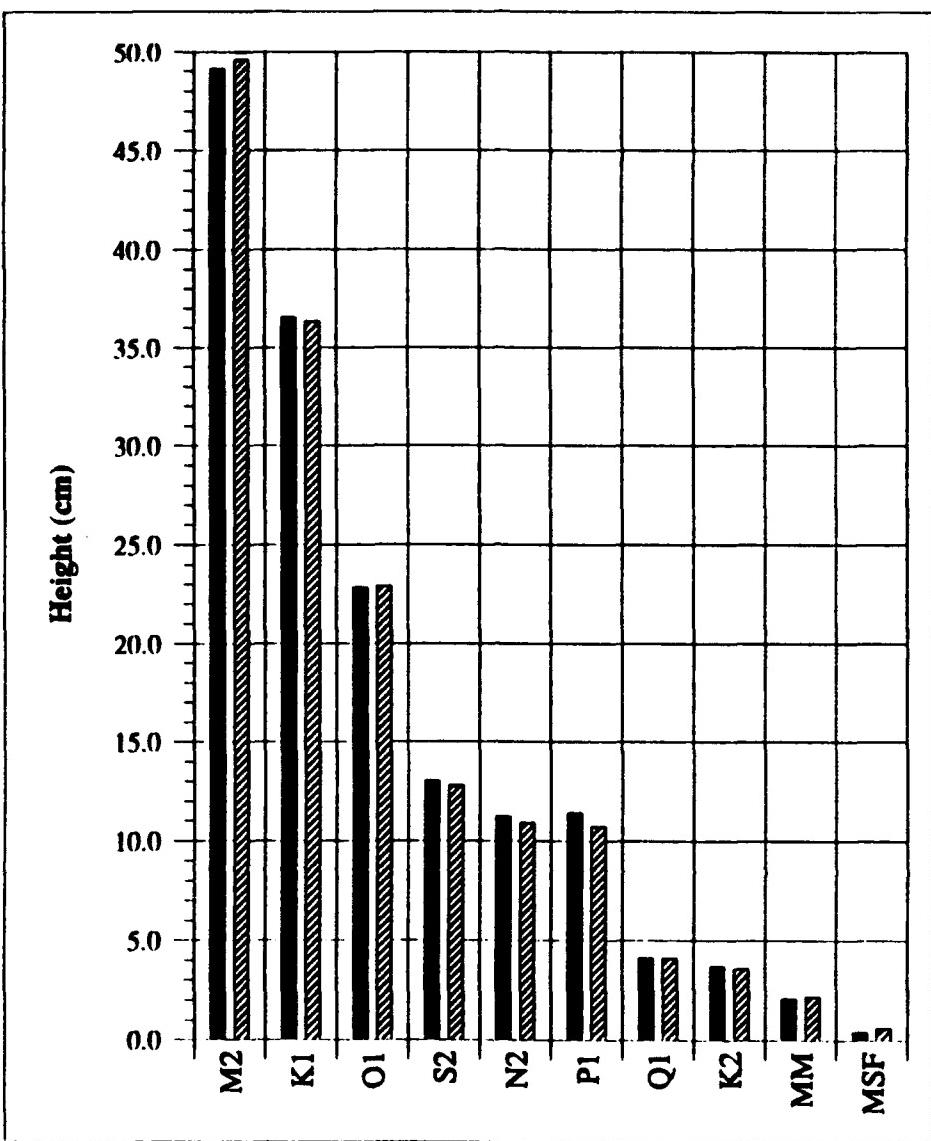
Monterey **Santa Cruz**

Figure 4. Major Tidal Constituent Amplitudes Analyzed in Monterey and Santa Cruz Sea Level Records. The Lunar Monthly (MM) and Luni-solar Fortnightly (MSf) constituents are listed for the purpose of comparison with the current strengths depicted in Figure 10.

The calculated amplitude and phase errors are small, as expected for a year-long time series. Errors tend to be slightly larger in Santa Cruz than in Monterey. Calculated

errors for this study were under 0.5 cm for the dominant constituents.

Werner (1992) discusses tidal propagation in embayments. In bays with widths much greater than the barotropic Rossby radius (W >> a, a=c/f), the tides propagate along the shores of the bay in Kelvin wave fashion, rotating counterclockwise about a nodal point in the center of the bay. The width of Monterey Bay, as measured between Monterey and Santa Cruz, is approximately 46 km, and the barotropic Rossby radius within the Bay is approximately 250 km. Thus, little if any horizontal propagation of the tides is expected within the Bay. The phases listed in Table 3 suggest that the semidiurnal tides occur slightly later in Monterey than in Santa Cruz. The phase differences between Monterey and Santa Cruz can be converted from angular measure to time using the following formula:

$$\Delta G(time) = \frac{\Delta G(^\circ)}{360} \times \frac{1}{\sigma}$$

where σ is the frequency of the constituent. Using the standard deviations of the analyzed phases to put upper and lower bounds on the phase differences, the tidal heights analyses suggest an M2 phase lag between Monterey and Santa Cruz of 7-9 minutes. This delay suggests propagation of the M2 wave between Santa Cruz and Monterey at velocities ranging from 84 to 114 m/s southward. This result is contrary to the

42

northward propagation of the M2 wave along the west coast of North America, however it is in close agreement with the 6 minute lag between Monterey and Santa Cruz predicted by NOS. Significant southward phase speeds can also be calculated for S2 (66-274 m/s) and N2 (44-121 m/s). The phase differences between the other major constituents are not significant when compared to their error estimates. A comparison of M2 phases at Monterey and Moss Landing, based on data listed by Schomaker (1983) also suggested a southward phase speed, with the M2 sea level response occurring 4.35 minutes later in Monterey than in Moss Landing.

B. TIDAL CURRENTS

1. Seasonal Mean Currents

In order to gain perspective on the tidal current observations, a short discussion on the seasonal mean currents in the vicinity of the Bay follows. The classic description of the marine climate off the California coast can be traced back to Skogsberg (1936) and Bolin and Abbot (1963). Upwelling normally occurs along the central California coast during the spring and early summer months, the offshore California Current waters enter the coastal region from September through November, and the California Undercurrent shoals or surfaces from November through February. During the upwelling season, near-surface water offshore of Monterey Bay flows southward due both to local equatorward wind stress and

the influence of the California Current (Hickey, 1979). The core of the California Current, marked by a salinity minimum, is located 100 to 200 km offshore (Chelton, 1984). The average speed of the California Current is generally less than 25 cm/s, however instantaneous flow may reach peaks of 50-70 cm/s (Huyer et al., 1991). Within 150 km of the California coast, there is a fall-winter reversal of the surface flow referred to as the California Countercurrent (Simpson et al., 1986), which has also been referred to as the Davidson Current. This poleward flow may actually be a surface manifestation of the California Undercurrent. The California Undercurrent flows poleward throughout the year and shows considerable variability in strength and depth (Hickey, 1979 and Lynn and Simpson, 1987). Using hydrographic data obtained between 12 and 42 km offshore near Point Sur, California, Tisch et al. (1992) computed maximum California Undercurrent velocities in excess of 35 cm/s, at depths of 70 to 190 m. Strub et al. (1987) used moored current meter data obtained between Monterey and the Gulf of the Farallones to the north to study the seasonal mean currents in the upper ocean. They found the low-passed upper ocean currents to be weak, with alongshore velocities of 10 to 20 cm/s in either direction throughout the year.

There are few direct long-term current measurements in Monterey Bay. Using natural tracers such as nitrates and ammonia, Broenkow and Smethie (1978) inferred northward flow

through the bay, even during the upwelling season, however Breaker and Broenkow (1989) noted cases of southward advection of cold water across the mouth of the Bay. In a study of AVHRR and CTD data obtained during the spring and summer of 1989, Rosenfeld et al. (1993) found the upwelling season in Monterey Bay to be characterized by two basic states. During periods of upwelling favorable winds, cool water from an upwelling center north of Monterey near Pt Ano Nuevo was advected southward into the Bay. When upwelling favorable winds weakened or reversed, rapid onshore advection of warm, fresher oceanic waters was found to occur to a depth of at least 200 m.

The ADCP data obtained for this study showed very weak mean currents at the mouth of the Bay. The depth- averaged currents between 17 and 201 m were weakly northward during both periods: 1.8 cm/s between 17 January-19 February and 2.2 cm/s between 1 September-4 October 1992. These mean current values may be misleading however. As Godin (1991) points out, the mean flow may not be significant if the low frequency tidal currents are significantly stronger than the mean. In other words, if the semimajor axis of one or more low frequency constituents is greater than the mean flow, then the average value cannot be viewed as stationary. In both sets of depth-averaged ADCP tidal current analyses, low frequency currents of 3 to 5 cm/s were analyzed. Low frequency tidal currents are discussed further in Section 4 of this chapter.

The CODAR-derived mean surface currents indicate weak cyclonic flow within the Bay, with mean current speeds near the mouth of the Bay on the order of 10 cm/s and weaker mean flow near the canyon head at 1-2 cm/s.

2. Spectral distributions

Tidal currents accounted for a significant portion of the total current variance in the upper ocean. Spectral densities and variance preserving spectra of the depth-averaged (17-201 m) u and v current components are presented in Figures 5 and 6. Peaks in the diurnal and semidiurnal bands are readily apparent in the u component spectra. The v component exhibits a semidiurnal signal which is much stronger than the diurnal.

Graphs comparing tidal period current variance to the total current variance are presented in Figures 7 and 8. Tidal period current variance was obtained by calculating the variance of the time series synthesized by the Foreman tidal analysis program. Since the synthesized time series are based on the results of the least squares harmonic analyses, and these analyses may be contaminated by periodic meteorological forcing, the "tidal period" current variances may contain non-tidal energy.

Tidal period current variance as a percentage of total current variance is presented in Figure 9. In general, tidal period oscillations accounted for 30 to 60 percent of the
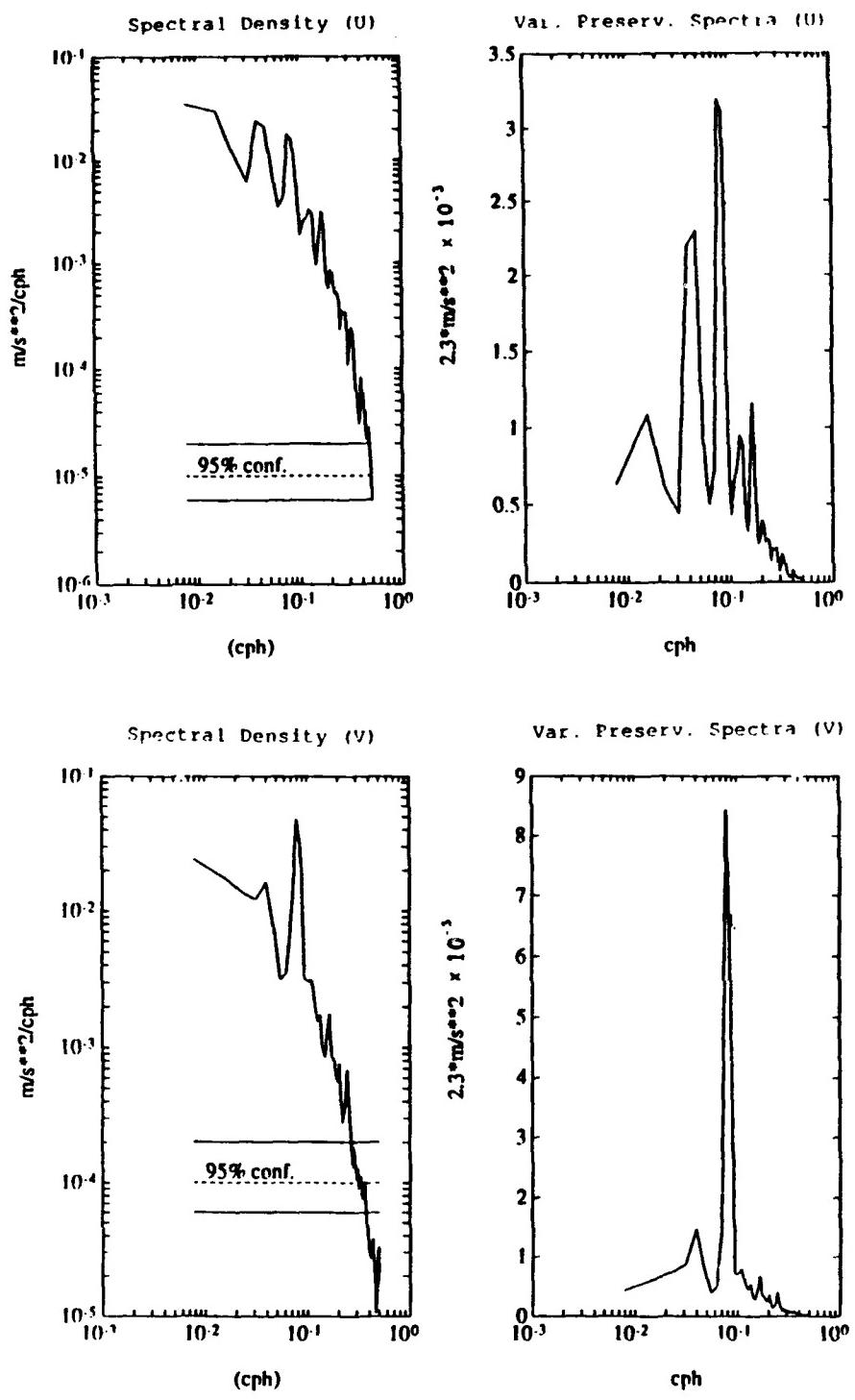
Figure 5. Spectral Density and Variance Preserving Spectra for the U Component (Top) and V Component (Bottom) of Depth-Averaged ADCP Current Measurements Obtained 1/17-2/19/92.

47

Spectral Density (U)

Var. Preserv. Spectra (U)

Spectral Density (V)

Var. Preserv. Spectra (V)
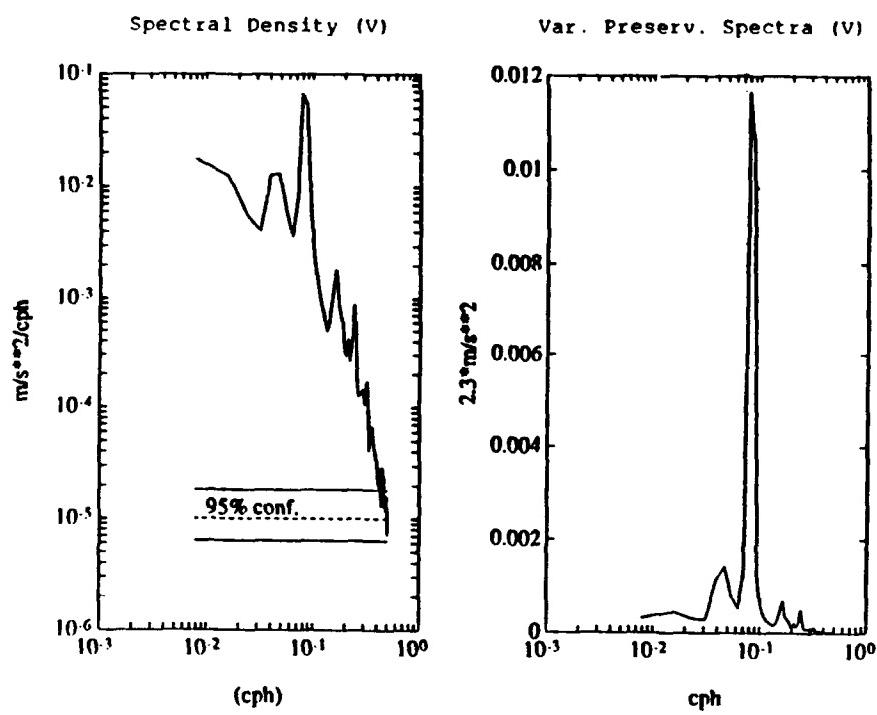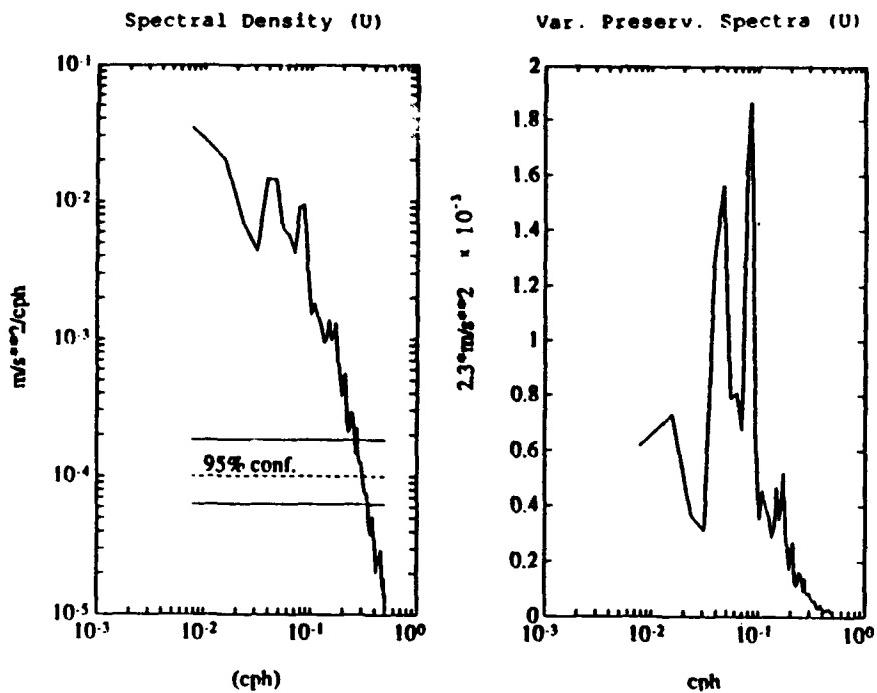
Figure 6. Spectral Density and Variance Preserving Spectra for the U Component (Top) and V Component (Bottom) of Depth-Averaged ADCP Current Measurements Obtained 9/1-10/4/92.

48
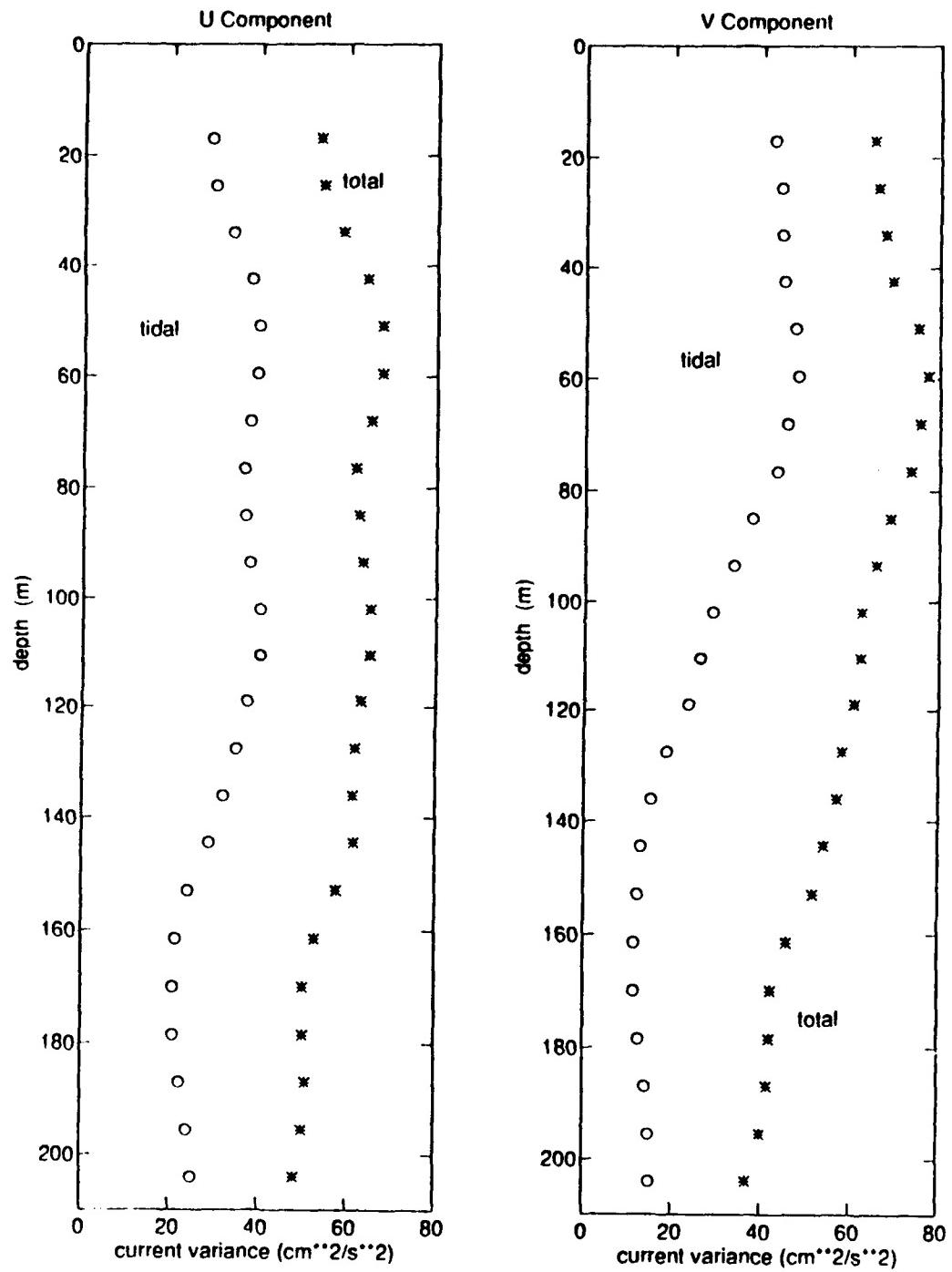
Figure 7. Tidal Current Variance Compared to Total Current Variance During 1/17-2/19/92.
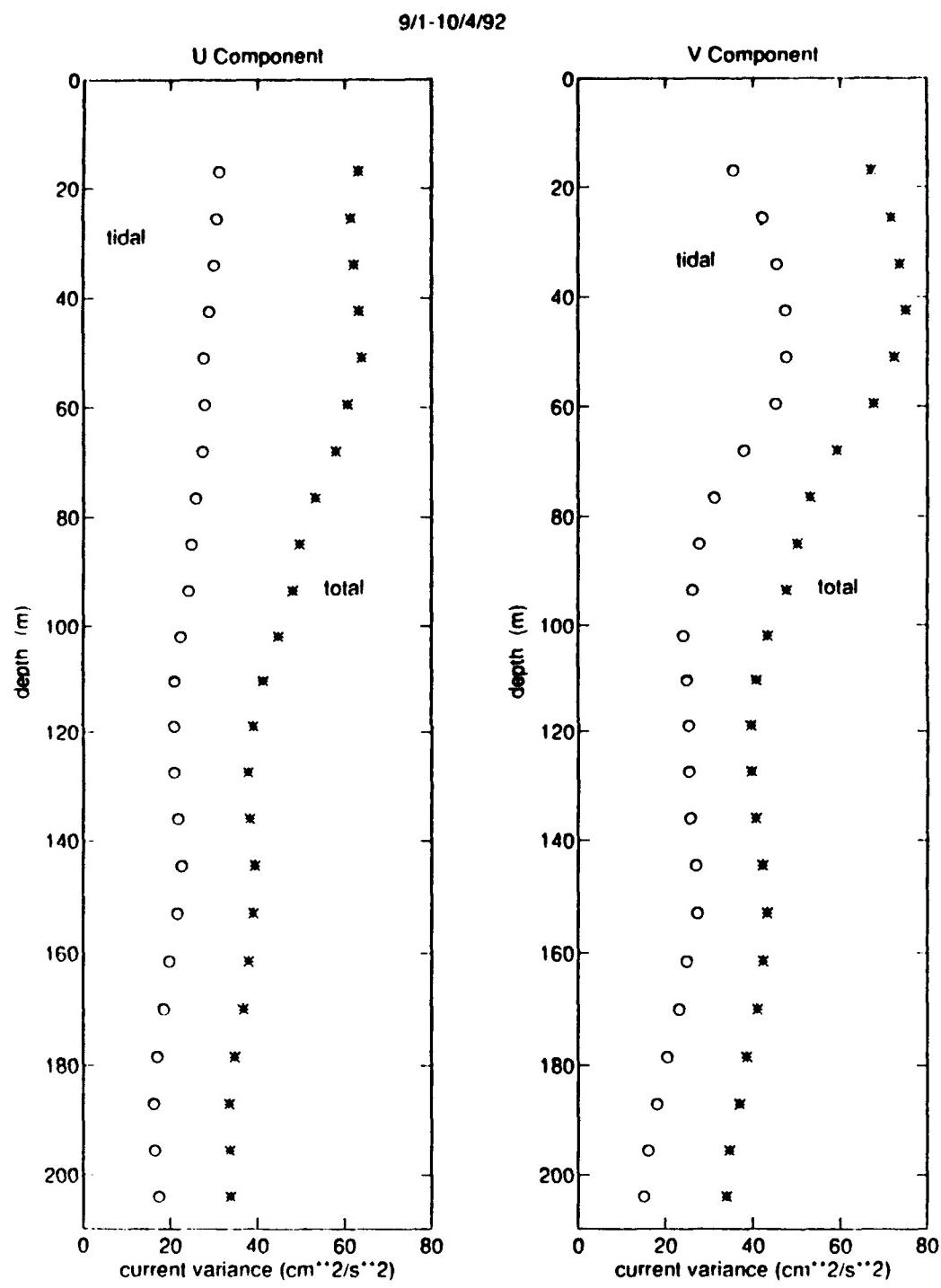
Figure 8. Tidal Current Variance Compared to Total Current Variance during 9/1-10/4/92.

50
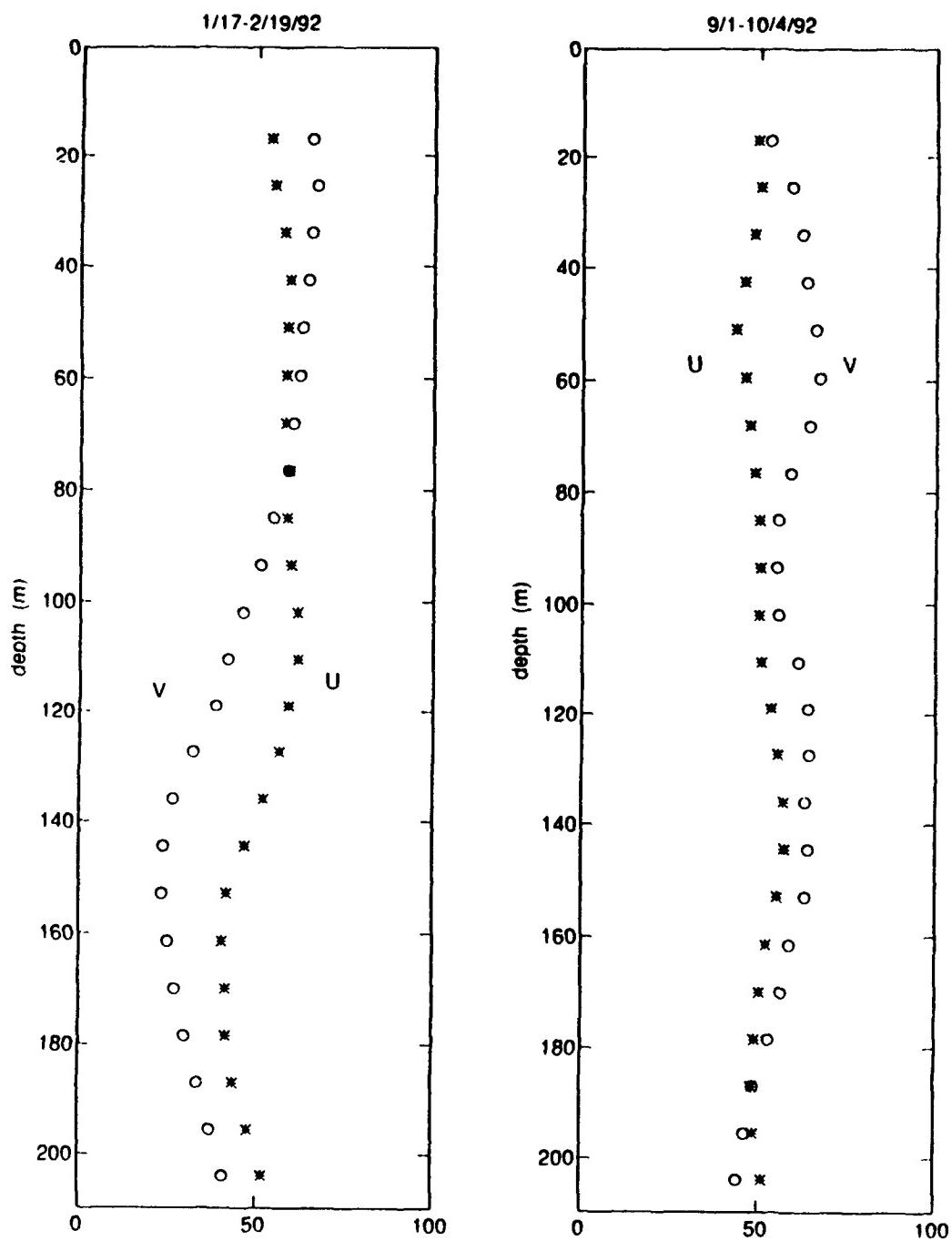
Figure 9. Tidal Current Variance as a Percentage of Total Current Variance.

total current variance. Although power spectra and variances were not calculated for the CODAR time series (due to a strong sea-breeze contribution in the diurnal band), the percentage of total current variance accounted for by tidal currents is expected to increase shoreward due to baroclinic energy which increases towards the head of the canyon.

3. Error Estimates

The error estimates associated with the ADCP-derived tidal currents were calculated using the same theory applied in the calculation of the tidal height errors. The power spectra of the residual currents were analyzed for the variance within the low frequency, diurnal, and semidiurnal frequency bands, and the propagation of this uncertainty in the tidal ellipses was calculated. Error calculation for currents is somewhat more involved than it is for tidal heights, since errors must be computed for the lengths of the ellipse axes, the angle of inclination, and the phase of the constituent. Equations for current ellipse error calculations may be found in Appendix B.

An attempt was made to determine the errors due to the relative motion introduced by the drift of the MBARI mooring buoy within its watch circle. Ideally, this motion could be subtracted from the measured current velocity in order to obtain more accurate current velocities. This correction was difficult to make accurately, however, since the Global

Positioning System (GPS) position data was transmitted from the buoy every 20-30 minutes, while current measurements were recorded every 15 minutes. Additionally, significant gaps of 17 and 25 hours occurred in the GPS data between 17 January and 19 February 1992. Due to the uncertainties involved in matching interpolated buoy velocities with the ADCP measured current velocities, corrections for buoy drift were attempted only with the depth-averaged currents. The calculated "buoy drift" errors are discussed in the next section.

4. Depth-Averaged Tidal Currents

The amplitudes of the semi-major axes of the major tidal current constituents analyzed in the depth-averaged ADCP measurements are presented in Figure 10. Tables 4(a) and 4(b) present the depth-averaged ellipse parameters and their standard deviations for the dominant tidal period currents, and Table 5 presents semi-major axis lengths before and after subtracting the relative motion introduced by the buoy drift.

The depth-averaged ellipse plots are presented in Figures 11 through 13. The phase of each constituent ellipse is plotted with respect to the time of local high tide for that constituent. This was accomplished by determining the phase difference between the Greenwich Phase of the constituent in the tidal heights analyses (an average of the phases at Monterey and Santa Cruz was computed for each constituent) and the Greenwich Phase of the constituent in the

tidal current analyses. The resulting phase difference of *N* degrees is indicated on the plots by a line extending from the center of the ellipse, at an angle *N* degrees from the semi-major axis (in the direction opposite that of the ellipse rotation, for a positive phase lag).

A comparison of Figures 4 and 10 makes it readily apparent that the relative strengths of the tidal period currents differ significantly from those of the tidal constituents in the sea level response. At first glance, one sees a strong contribution from the low frequency tidal current constituents (MM, the lunar monthly constituent, and MSf, the luni-solar fortnightly) that is completely absent in the tidal heights. Stronger currents in general were present during the second record (1 September - 4 October 1992) indicating the presence of non-stationary tidal-period currents. Proportionately stronger contributions from S2 and N2 as compared to O1 in both records, indicate the presence of internal waves of semidiurnal period.

As can be seen in Figures 11 through 13, the relative motion due to buoy drift had a moderate effect on the size, orientation, and phase of the diurnal and semidiurnal tidal ellipses, and a very minor effect on the low frequency tidal ellipses. Table 5 shows that the buoy motion drift had the greatest proportionate effect on the strength of the S2 component in the first record (1/17-2/19) and the K1 component in both records. Additionally, when buoy motion is accounted

54

for, the depth-averaged K1 current is stronger than M2 in both seasons, suggesting that sea-breeze forcing has a considerable affect on the diurnal band currents in both winter and summer.

## Major Tidal Constituents–Depth-Averaged Current
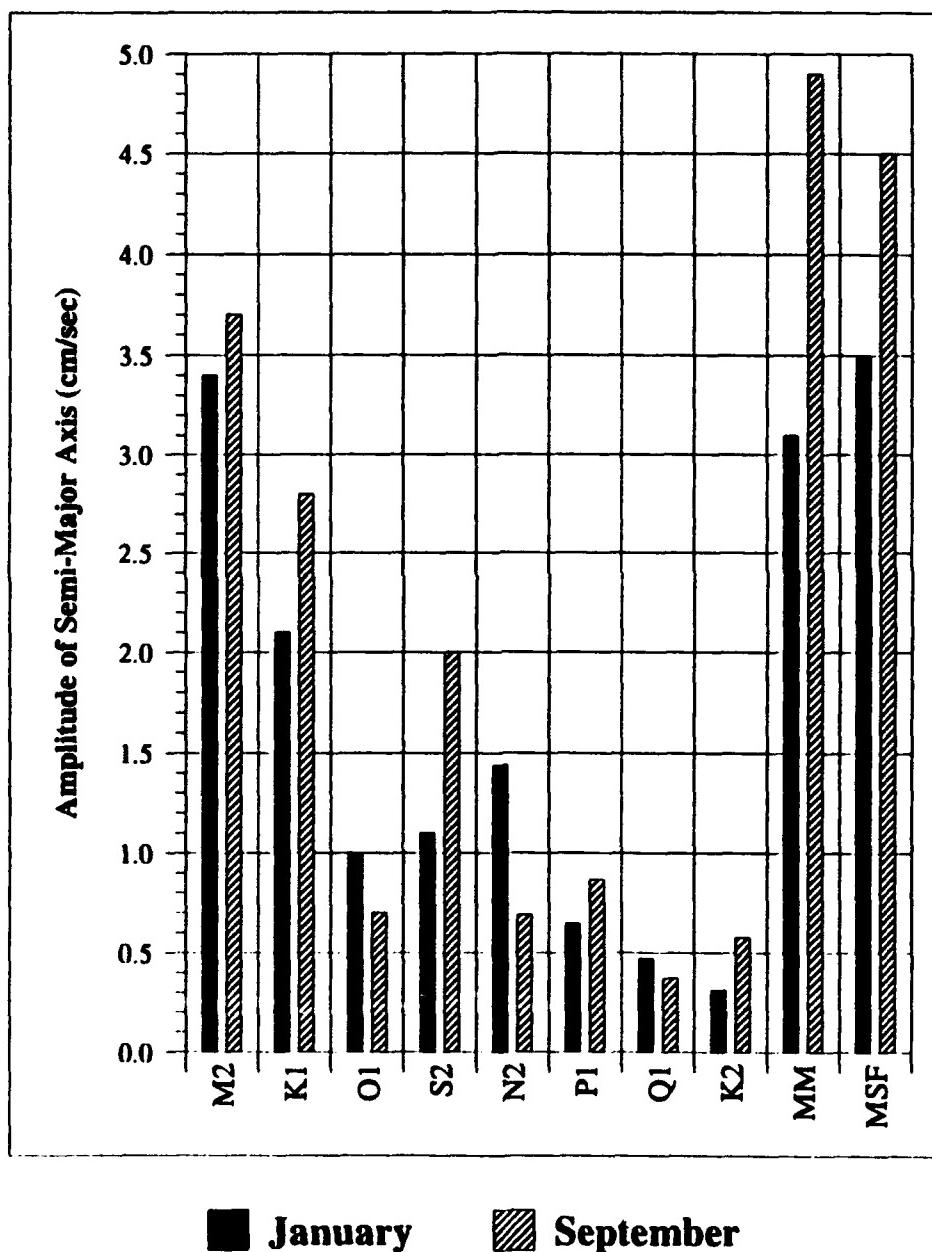
Figure 10. Major Tidal Constituents Analyzed in the Depth-Averaged (17-200 m) ADCP Current Measurements.

TABLE 4(A)   DEPTH-AVERAGED TIDAL ELLIPSE PARAMETERS
1/17-2/19/92

	Semi-major Axis (cm/s)	Semi-minor Axis (cm/s)	Greenwich Phase (deg)	Inclination (deg CCW from east)
MM	3.1 ± 0.8	0.2 ± 0.8	196 ±15	137 ±15
MSf	3.5 ± 0.9	0.3 ± 0.8	186 ±14	140 ±13
O1	1.0 ± 0.1	0.4 ± 0.2	189 ± 6	97 ±12
K1	2.1 ± 0.2	-0.3 ± 0.1	161 ± 4	35 ±11
M2	3.4 ± 0.1	-0.6 ± 0.1	278 ± 1	65 ± 1
S2	1.1 ± 0.1	0.4 ± 0.1	7 ± 4	152 ± 3

Note: Ellipse rotation is CW for negative semi-minor axis values, CCW for positive semi-minor axis values.

TABLE 4(B)   DEPTH-AVERAGED TIDAL ELLIPSE PARAMETERS
9/1-10/4/92

	Semi-major Axis (cm/s)	Semi-minor Axis (cm/s)	Greenwich Phase (deg)	Inclination (deg CCW from east)
MM	4.9 ± 0.7	0.3 ± 0.5	289 ± 8	143 ± 6
MSf	4.5 ± 0.7	0.6 ± 0.5	31 ± 9	143 ± 7
O1	0.7 ± 0.4	0.4 ± 0.3	162 ±52	36 ±44
K1	2.8 ± 0.4	-1.2 ± 0.3	207 ±10	141 ± 9
M2	3.7 ± 0.1	-0.4 ± 0.4	330 ± 1	92 ± 6
S2	2.0 ± 0.1	-0.5 ± 0.3	355 ± 5	102 ±11
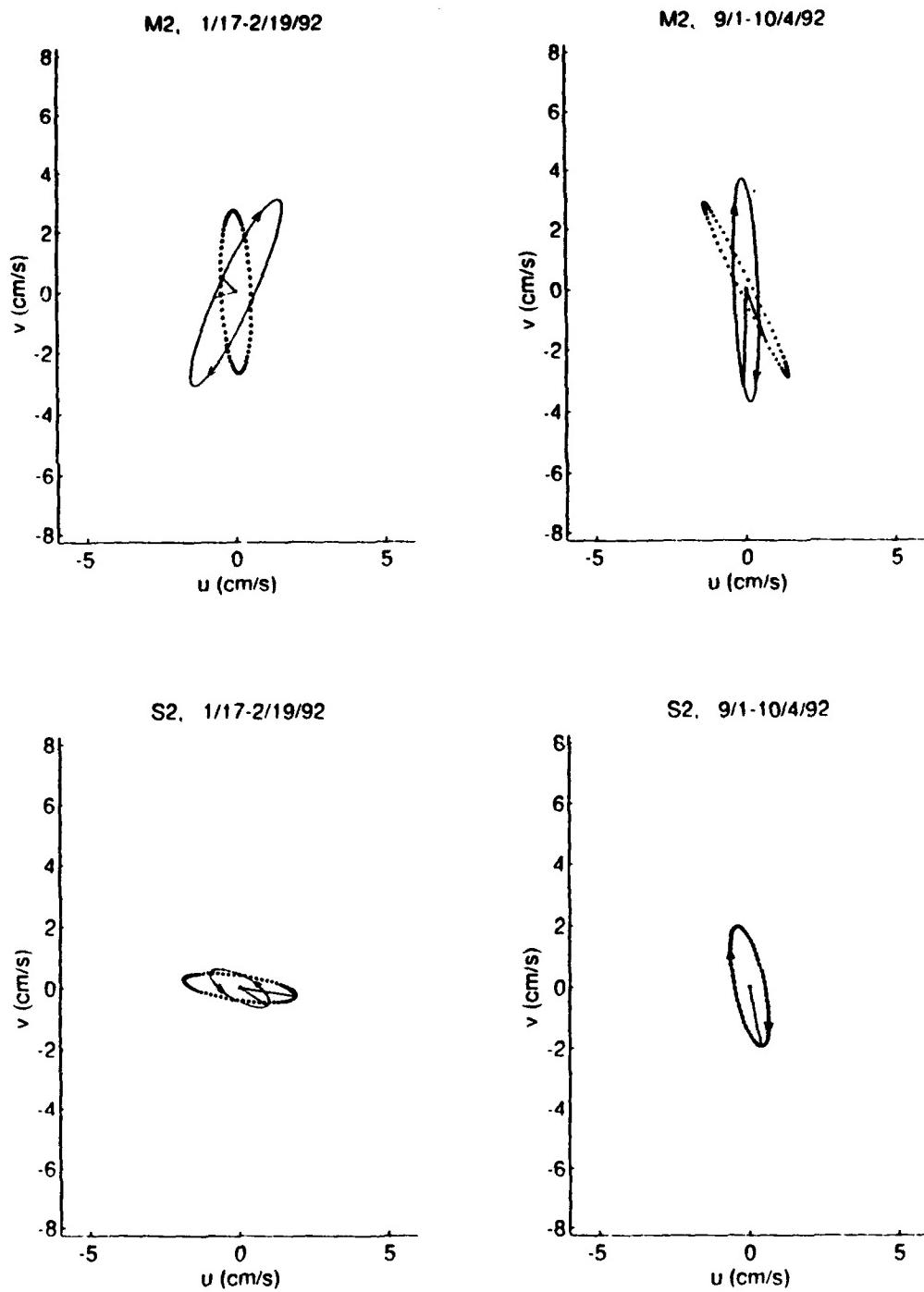
Figure 11. Depth-Averaged Semidiurnal Tidal Ellipses. Ellipses which have been corrected for mooring buoy drift are plotted with dots.
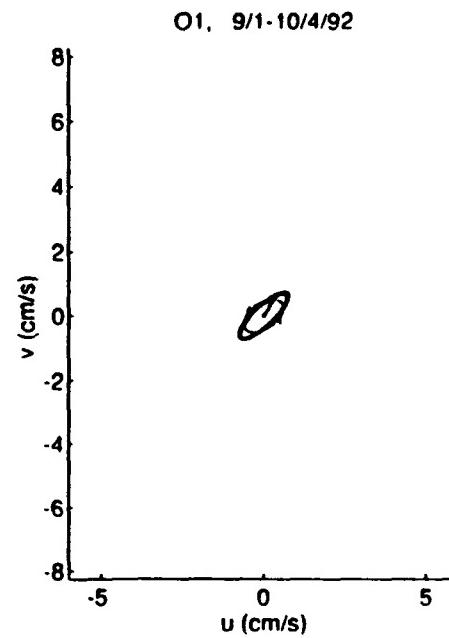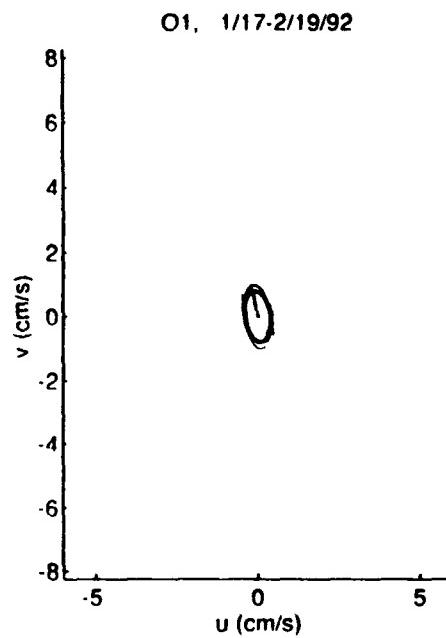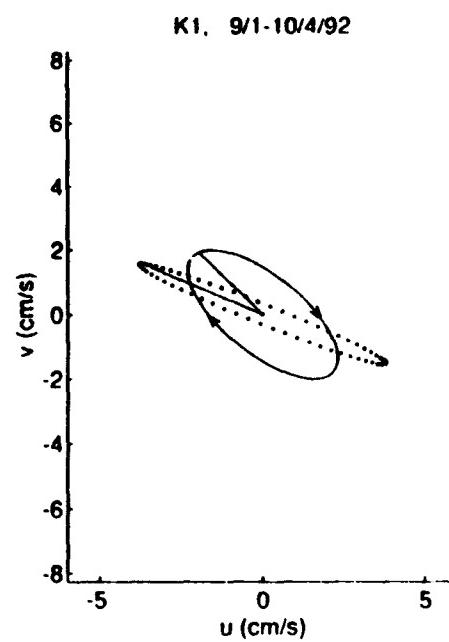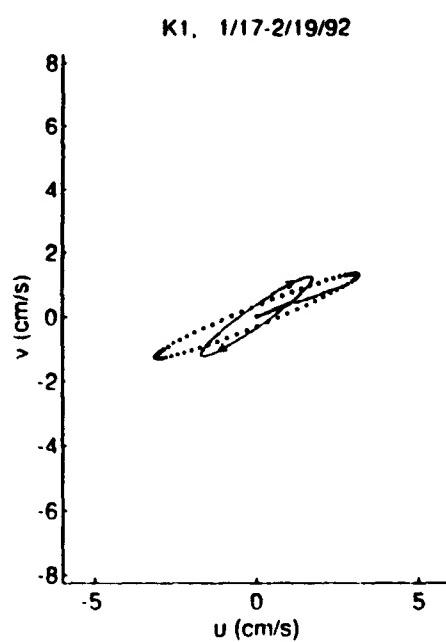
Figure 12. Depth-Average Diurnal Tidal Ellipses. Ellipses which have been corrected for mooring buoy drift are plotted with dots.
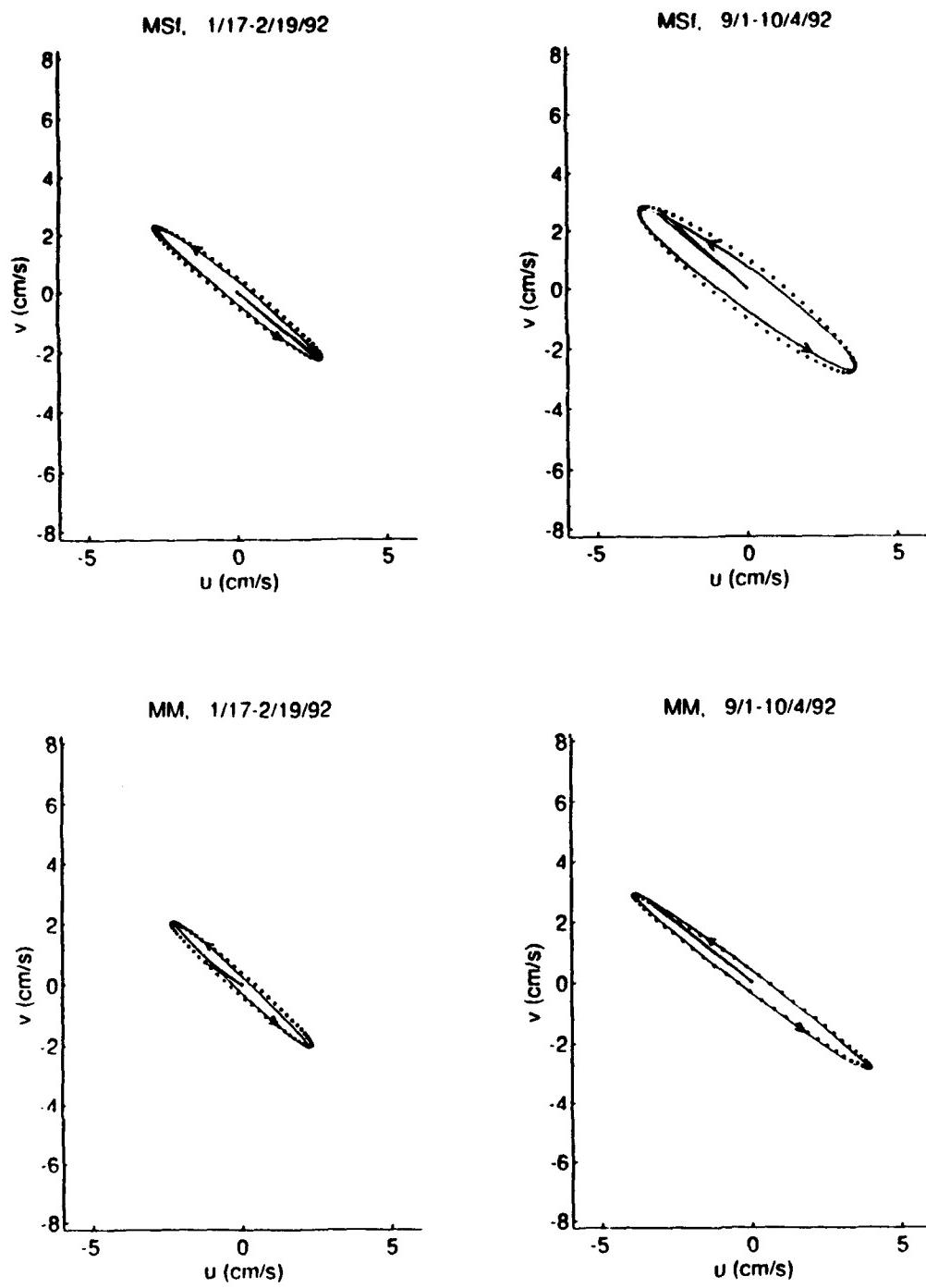
Figure 13. Depth-averaged Low Frequency Tidal Ellipses. Ellipses which have been corrected for mooring buoy drift have been plotted with dots.

TABLE 5. COMPARISON OF DEPTH-AVERAGED TIDAL CURRENT SEMI-MAJOR AXIS LENGTHS (CM/S) WITH AND WITHOUT ADJUSTMENTS FOR MOORING BUOY DRIFT

		W/O ADJ	WITH ADJ	% CHANGE
M2	1/17-2/19	3.4	2.8	18% ↓
	9/1-10/4	3.7	3.2	14% ↓
S2	1/17-2/19	1.1	1.9	73% ↑
	9/1-10/4	2.0	2.3	15% ↑
K1	1/17-2/19	2.1	3.4	62% ↑
	9/1-10/4	2.8	4.1	46% ↑
O1	1/17-2/19	1.0	0.8	20% ↓
	9/1-10/4	0.7	1.0	43% ↑
MSf	1/17-2/19	3.5	3.6	3% ↑
	9/1-10/4	4.5	4.5	0
MM	1/17-2/19	3.1	3.1	0
	9/1-10/4	4.9	4.9	0

Errors in the compensation for buoy motion may be present due to the interpolation of buoy speeds to match the hourly current data, and due to the large gaps in GPS position reports during the first time period (17 January - 19 February). For this reason. buoy motion is neglected in all subsequent depictions of ADCP-derived tidal current ellipses.

With or without corrections for buoy motion, the MM and MSf currents are seen to be at least as strong as M2 and K1 and much stronger than S2 and O1. In both the winter and summer records, the low frequency tidal ellipses are oriented in the northwest-southeast direction and rotate counterclockwise. Potential causes of these strong low frequency signals are discussed in Chapter V (Analysis).

5. Vertical Structure

Plots of the M2, K1, MSf and MM current ellipses analyzed at each ADCP depth bin in the upper 200 m of the ocean (bins 2 to 25) are presented in Figures 14-17. All constituents exhibit considerable variation in the strength, inclination, and direction of rotation with depth.

In general, the M2 currents (Figure 14) rotate clockwise during both periods. In the first record (1/17-2/19), the M2 ellipses are uniform in amplitude and orientation between the top bin (17 m) and bin 10 (81 m). Below bin 10 the orientation of the ellipses turns counterclockwise with depth. Additionally, below bin 10 the

strength of the ellipses decreases to a minimum at bin 19 (153 m) and then begins to increase with depth. The direction of M2 current flow is in opposite directions above and below the minimum. In the second record (9/1-10/4/92) the orientation of the M2 ellipses again turns counterclockwise with depth, however this turning begins at the shallowest bins and continues uniformly with depth. The direction of current flow also changes with depth, however the strength of the ellipses remains generally constant with depth.

A comparison of the M2 ellipses depicted in Figure 14 and the temperature profiles depicted in Figure 2 suggests a relationship between the orientation of the ellipses and stratification. In the winter record, the depth at which the M2 ellipses begin to veer counterclockwise corresponds to the approximate depth of the mixed layer. In the summer record, during which a relatively shallow mixed layer is expected, the M2 ellipses veer counterclockwise at all depths. This relationship is discussed further in Chapter IV.

The K1 ellipses rotate clockwise at most depths, with the exception of the top four bins (the upper 40 m) during the winter record. The orientation of the K1 ellipses and the direction of current flow is generally uniform with depth. Subsurface maxima of the K1 currents occur in both records. The strongest K1 currents occur at bins 7 and 8 (57-65 m) in the first record and at bin 3 (25 m) in the second record.
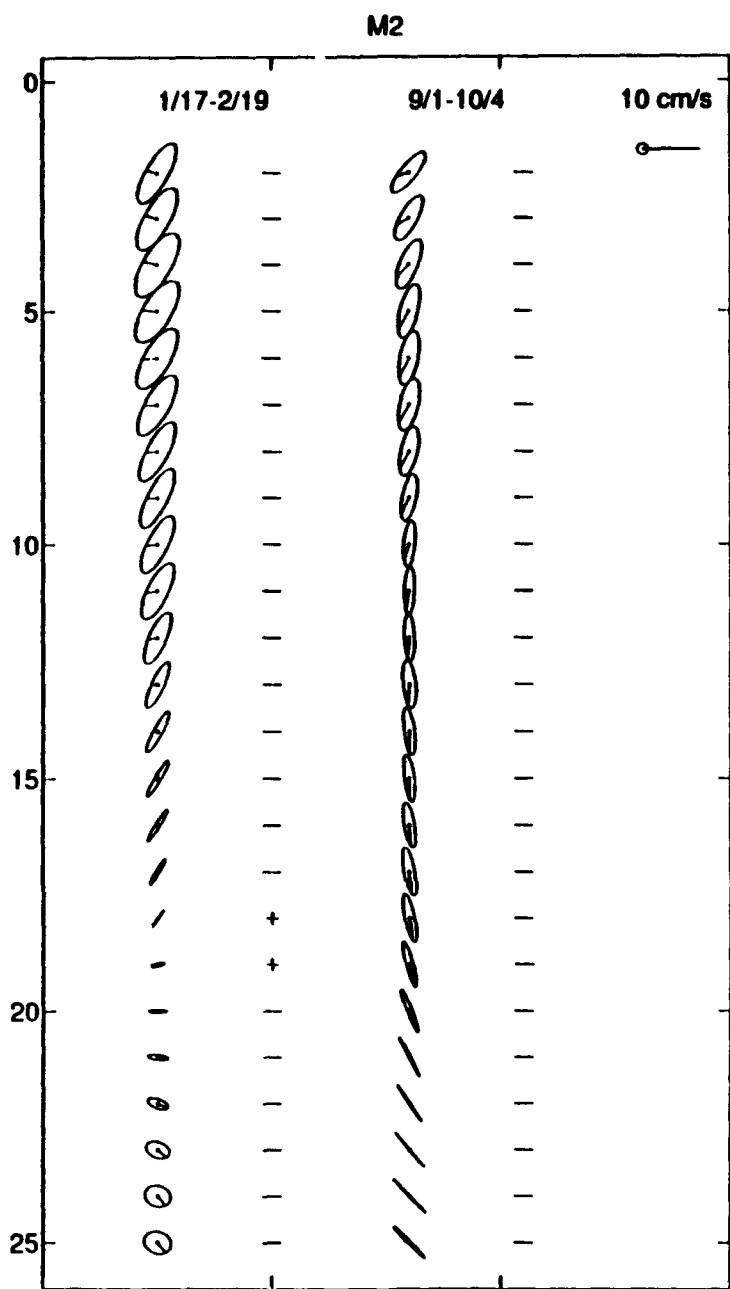
Figure 14. ADCP-Derived M2 Tidal Ellipses. Phases indicate the direction of current flow at the time of high M2 tide. Direction of current vector rotation is indicated with a "-" for clockwise rotation and a "+" for counterclockwise rotation. Ellipses are depicted every 8 m between 17-201 m. The vertical axis is labelled with the ADCP bin numbers.
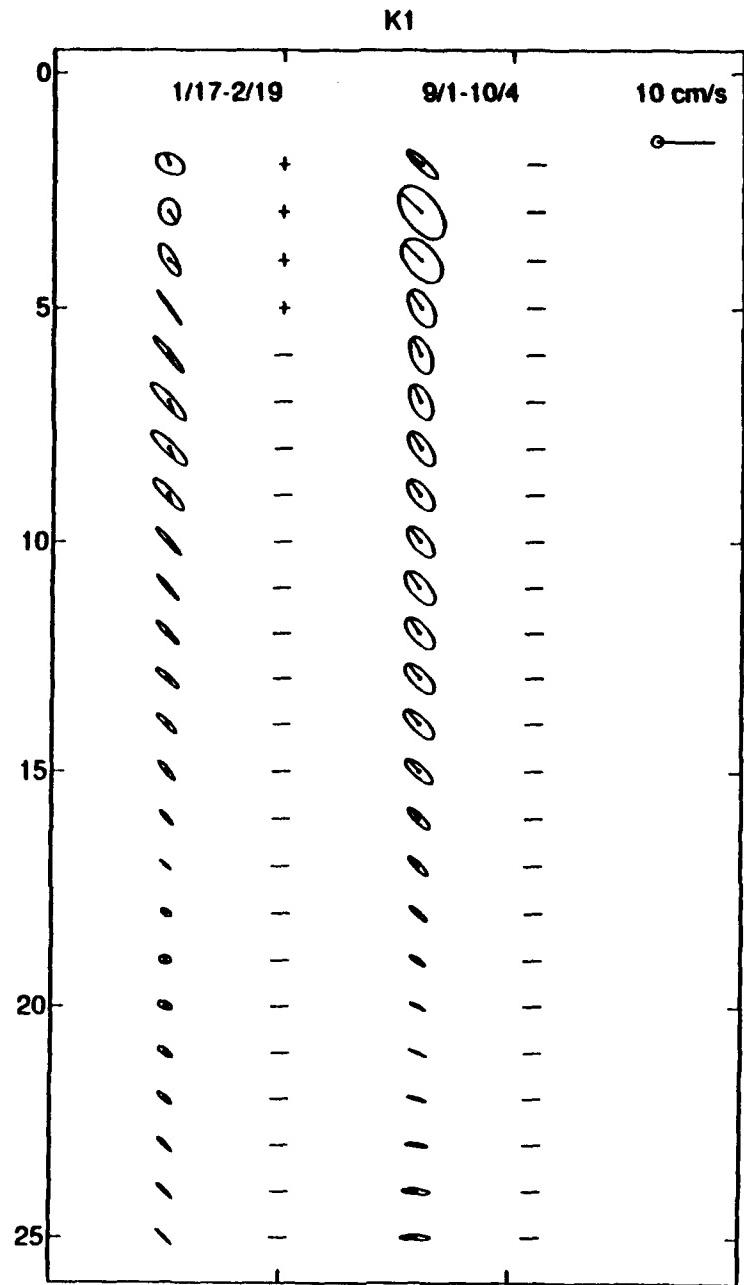
Figure 15. ADCP-Derived K1 Tidal Ellipses. Phases indicate the direction of current flow at the time of high K1 tide. Direction of current vector rotation is indicated by a "-" for clockwise rotation and a "+" for counterclockwise rotation. Ellipses are depicted every 8 m between 17-201 m. The vertical axis is labelled with the ADCP bin numbers.
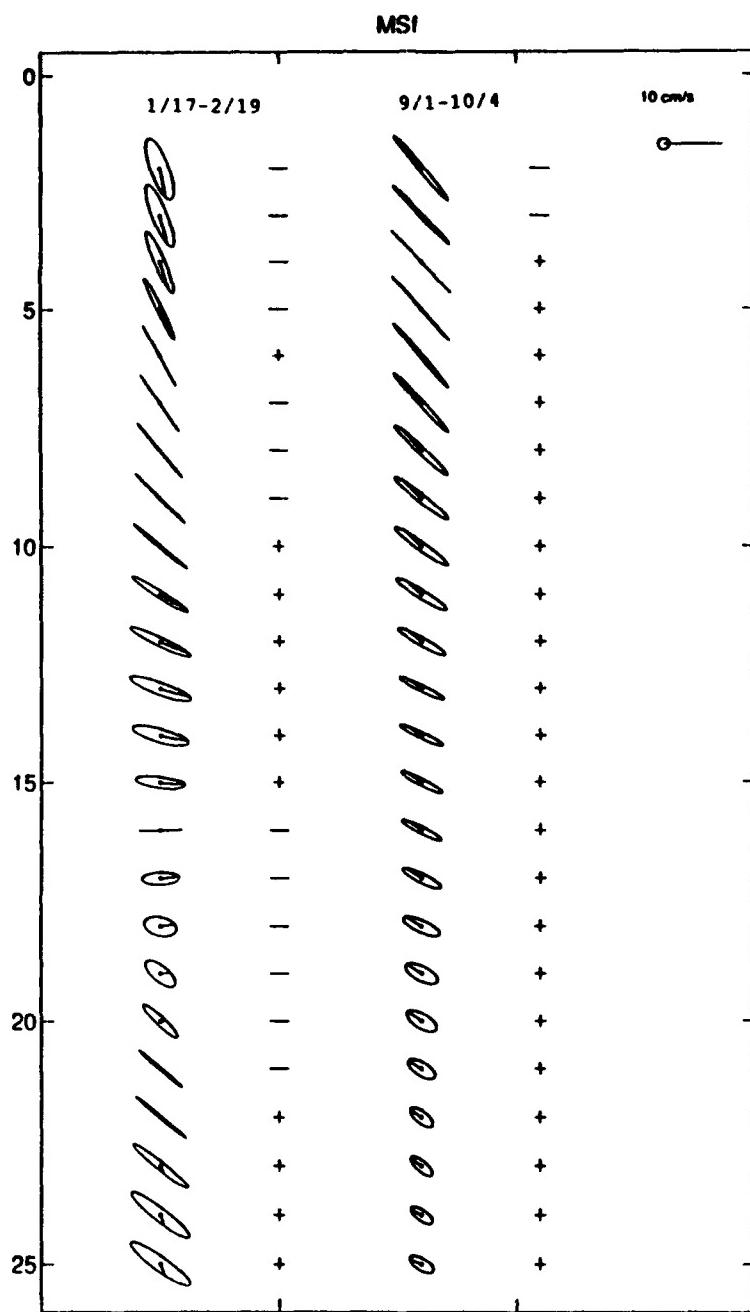
Figure 16. ADCP-Derived MSf Tidal Ellipses. Phases indicate the direction of current flow at high MSf tide. Direction of current vector rotation is indicated by a "-" for clockwise rotation and a "+" for counterclockwise rotation. Ellipses are depicted every 8 m between 17-201 m. The vertical axis is labelled with the ADCP bin numbers.
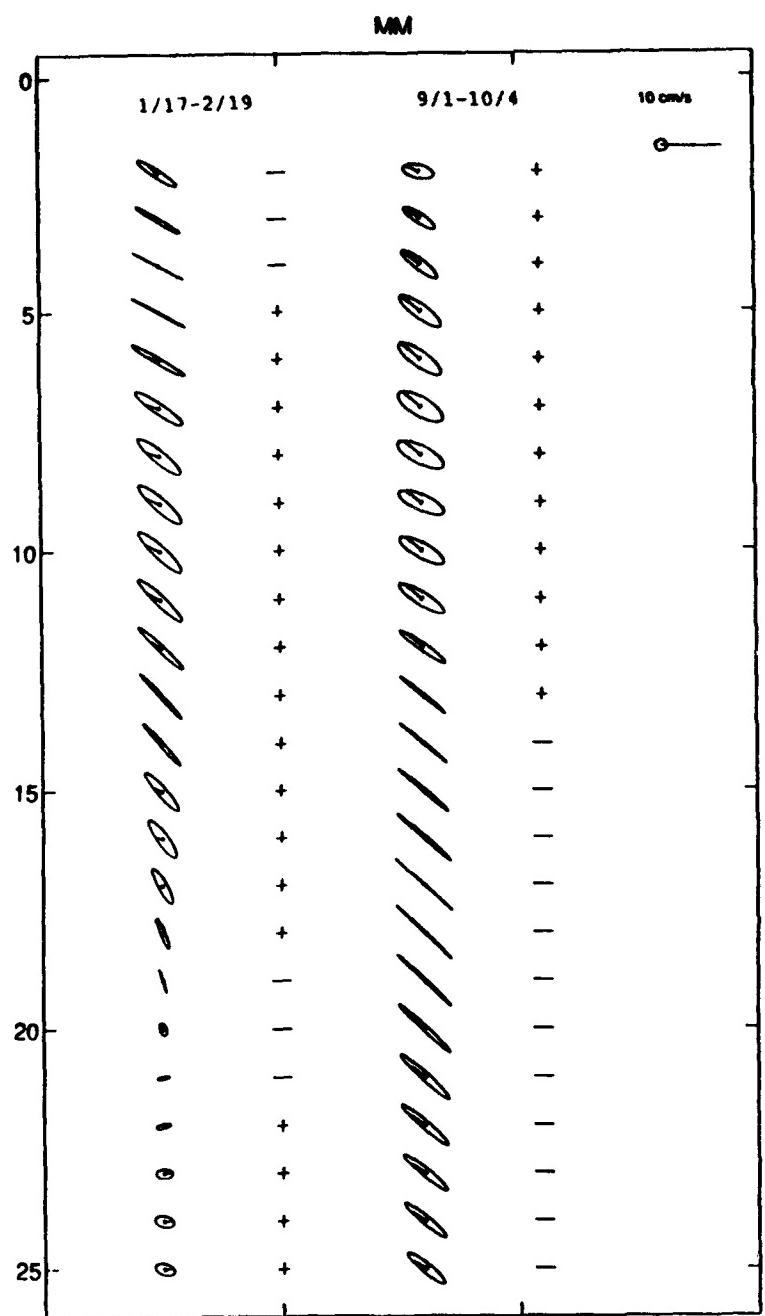
Figure 17. ADCP-Derived MM Tidal Ellipses. Phases indicate the direction of current flow at high MM tide. Direction of rotation is indicated by a "-" for clockwise rotation and a "+" for counterclockwise rotation. Ellipses are depicted every 8 m between 17-201 m. The vertical axis is labelled with the ADCP bin numbers.

The vertical structure of the low frequency currents is complex in the first record and somewhat more uniform in the second. The orientation of the fortnightly (MSf) tidal current ellipses turns both counterclockwise and clockwise with depth in the first record but is generally uniform in the second record. The rotation direction of the MSf current vectors also varies considerably in the first record, but is generally clockwise in the second record.

The orientation of the monthly (MM) tidal current ellipses is generally uniform with depth, with the exception of clockwise turning between 100-200 m in the first record. The rotation of the MM current vectors varies with depth in both records.

6. Horizontal Variation

Plots of the CODAR-derived tidal current ellipses and the corresponding ellipses derived from the shallowest reliable ADCP depth bin (17 m) are presented in Figures 18-20 for the M2, K1 and MSf constituents. These were the strongest constituents in the analysis (the CODAR record length was not long enough to resolve the monthly constituent). The ADCP-derived ellipse on each plot is labelled with the mooring buoy name, "M1". The CODAR "baseline" is indicated with a dashed line on each plot. Differences between the CODAR and ADCP-derived ellipses should be expected due to the different depths at which the measurements were made (0.5 m vs. 17 m)

and the different time periods over which the measurements are averaged (26 minutes vs 110 seconds). As in the vertical ellipse plots, the phase of each constituent ellipse is plotted with respect to the time of high tide for that constituent.

The M2 ellipse plot (Figure 18) reveals the considerable influence of bathymetry on the alignment of the M2 currents. On the shelf (depth < 200 m), the ellipses are generally aligned with bathymetry, while over the canyon, the ellipses are oriented in the along-axis direction near the shallower end and in the cross axis direction over the deeper end. Considerable amplification of the ellipses is evident on the flanks of the canyon and in the vicinity of the canyon head. A comparison of the ADCP-derived ellipse with the CODAR-derived ellipses located nearest the M1 mooring indicates good agreement in terms of ellipse amplitude and the phase lag with respect to M2 tidal heights. The differences in orientation suggest turning of the ellipse axes with depth, which would be expected based on the vertical plot of the ADCP-derived ellipses (see Figure 14).

The CODAR-derived K1 ellipses (Figure 19) are much stronger than expected (the lengths of the semi-major axes are on the order of 30 cm/s) and are oriented very uniformly in the northwest-southeast direction. Note the reduced scale used to plot the K1 ellipses. The CODAR-derived K1 ellipses

are an order of magnitude larger than those derived from the ADCP measurements.

Unlike the M2 currents, the fortnightly (MSf) tidal currents (Figure 20) are strongest over the deeper end of the canyon and weaker near the canyon head. Good agreement exists between the ADCP-derived MSf ellipse and the CODAR-derived ellipses.

The direction of current vector rotation within each ellipse is represented in Figures 21-23. The rotation of the currents follows an interesting pattern in the case of the M2 and MSf ellipses. Figure 21 shows the rotation of the M2 currents to be generally clockwise on the southern end of the Bay and counterclockwise on the northern side of the canyon. This pattern of rotation was the same in the case of the S2 ellipses (not depicted). Nearly all of the K1 currents rotate clockwise (Figure 22), however the MSf currents (Figure 23) rotate in the same manner as the M2 and S2 currents.

The relation of M2 current flow to M2 sea level changes was further investigated by plotting the current vectors which corresponded to high M2 tide, ebb tide (high tide + 1/4 cycle), low tide, and flood tide (high tide + 3/4 cycle). These plots are presented in Figures 24-27. On each plot, the current vector representing M2 current flow measured at ADCP bin 2 (17 m) is labelled "M1". In general, the M2 tidal currents flow towards the southwest when M2 sea level is at high tide (Figure 24). Flow is in the cross-canyon

69

direction at the head of the canyon, and weak convergence occurs over the deep end of the canyon. As the M2 tide falls, the M2 currents clearly converge at the canyon head (Figure 25). The currents over the shallower end of the canyon flow in the up-canyon direction, while the currents on the flanks of the canyon flow inward toward the canyon head. At low M2 tide (Figure 26), semidiurnal flow is generally towards the northeast, opposite the direction of flow during high tide. Flow is in the cross-canyon direction at the canyon head, and weak divergence occurs over the deep end of the canyon. As the M2 sea level begins to rise again (Figure 27), the M2 currents diverge from the canyon head. Flow over the shallow end of the canyon is in the down-canyon direction, and the currents on the flanks of the canyon flow outward away from the canyon head.
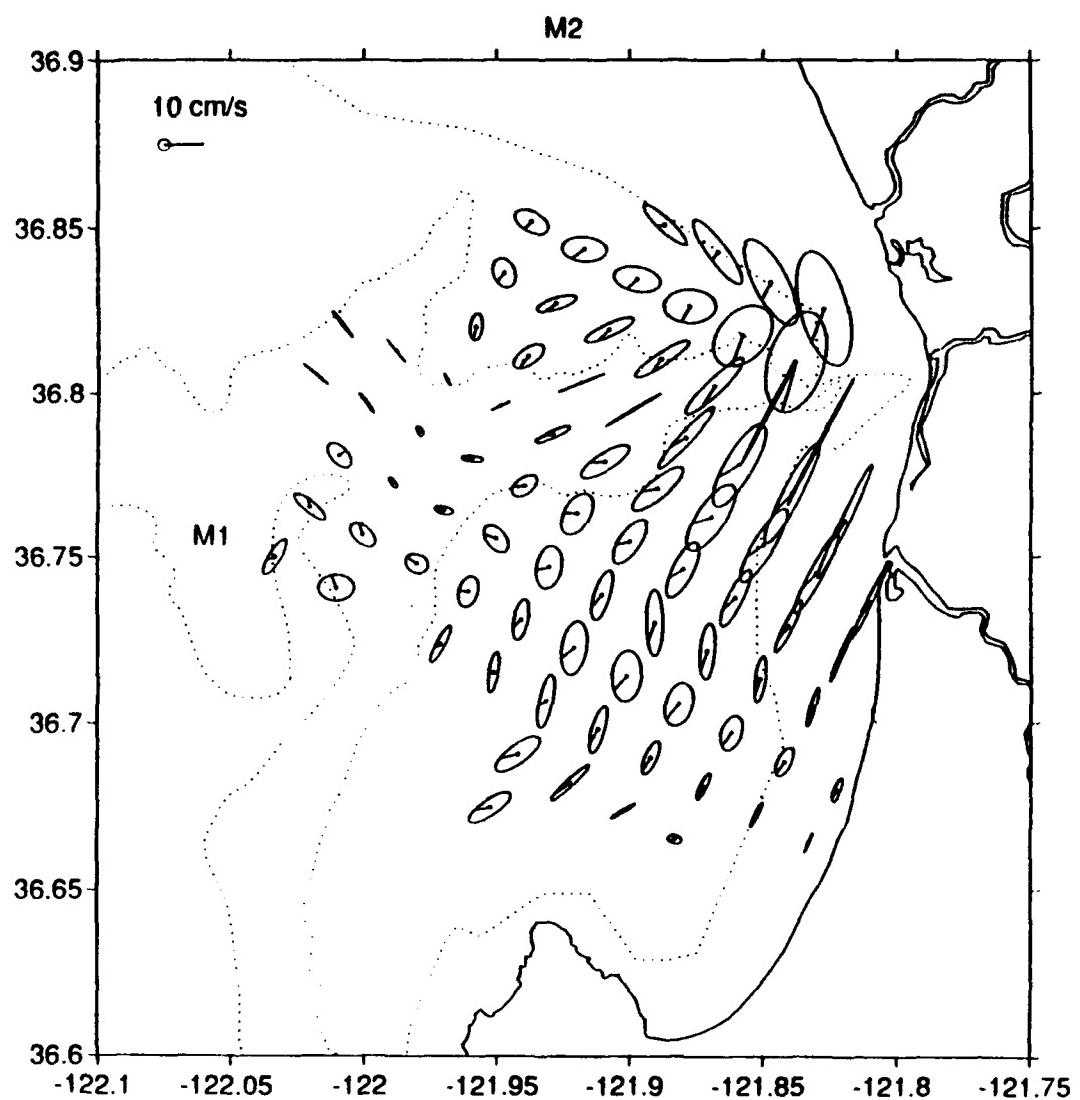
Figure 18. M2 Surface Current Ellipses. The ellipse derived from ADCP bin 2 (17 m) is labelled "M1". The 50 m, 200 m, and 1000 m bathymetry contours are depicted.
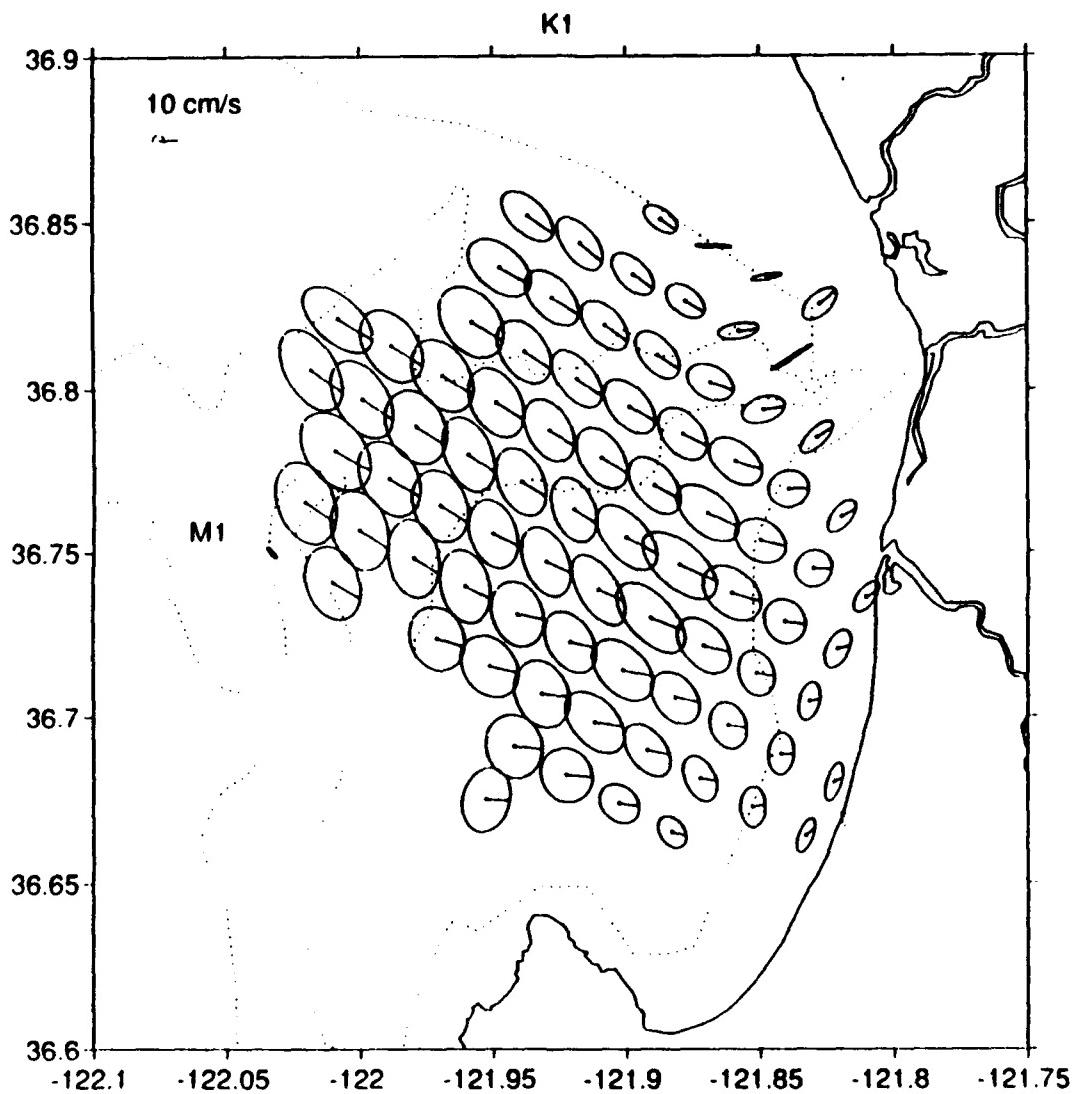
Figure 19. K1 Surface Current Ellipses. The ellipse derived from ADCP bin 2 (17 m) is labelled "M1". The 50 m, 200 m, and 1000 m bathymetry contours are depicted.
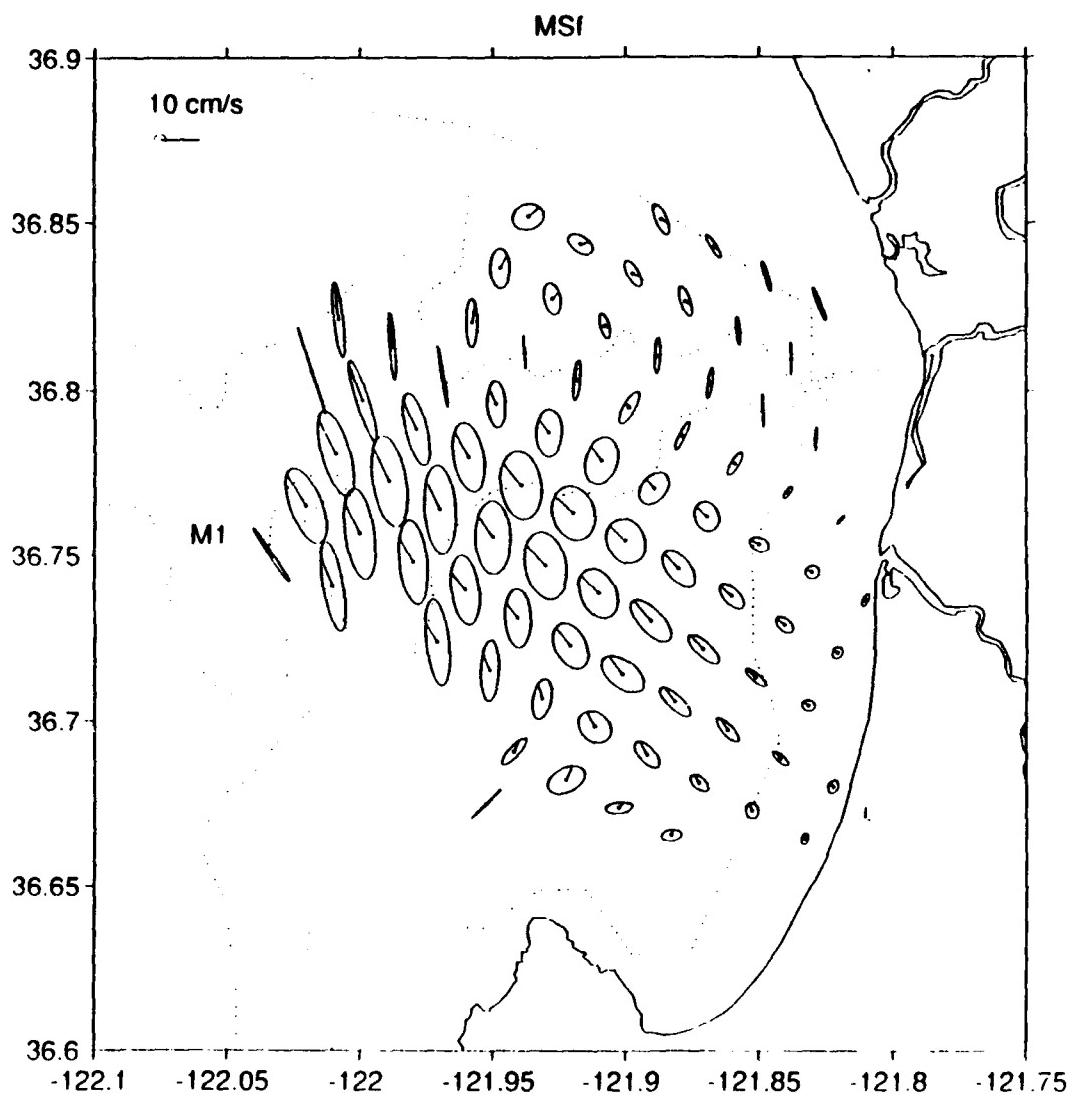
Figure 20. MSf Surface Current Ellipses. The ellipse derived from ADCP bin 2 (17 m) is labelled "M1". The 50 m, 200 m, and 1000 m bathymetry contours are depicted.

73
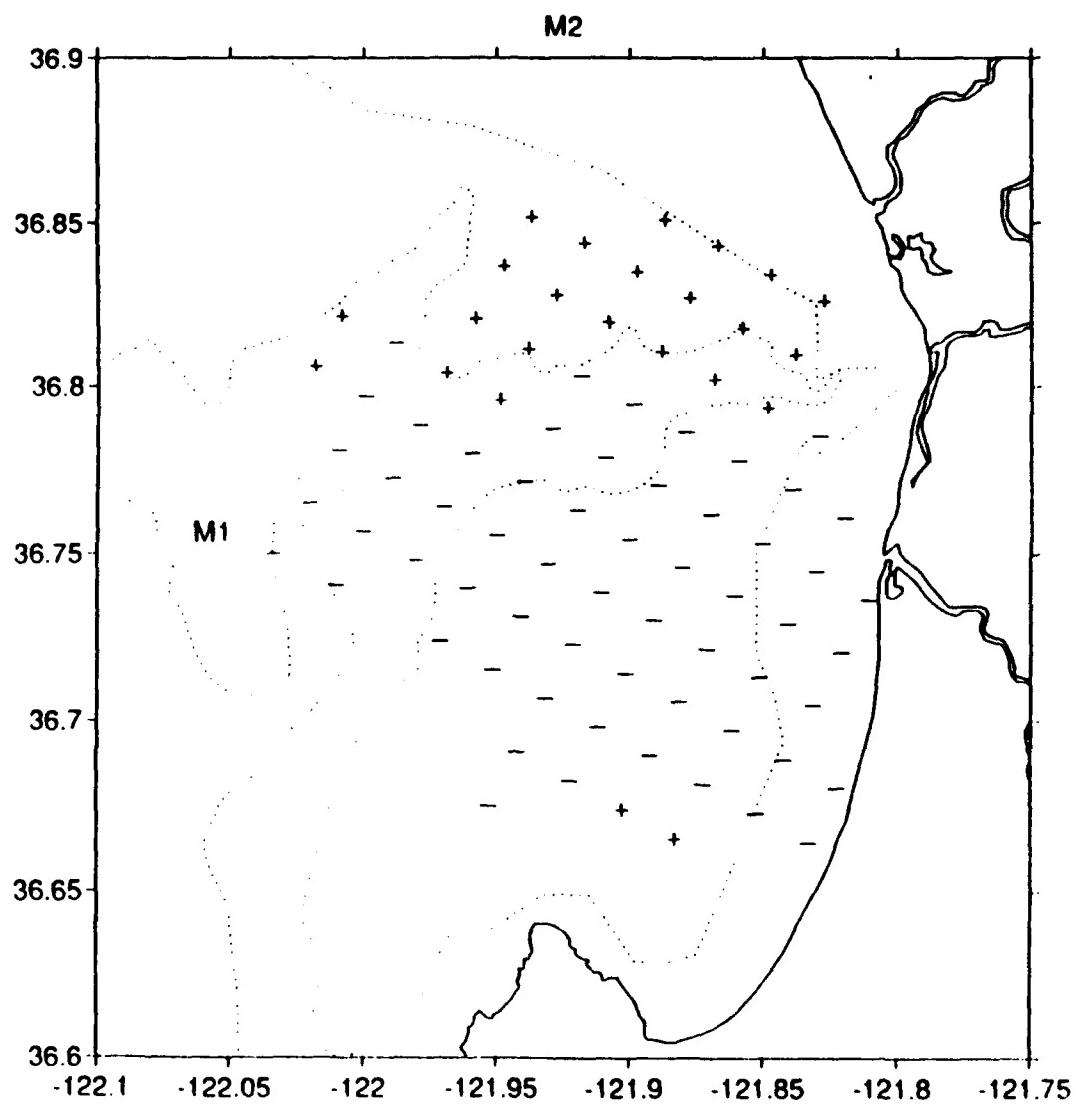
Figure 21. Direction of M2 Current Rotation (- = Clockwise, + = Counterclockwise).
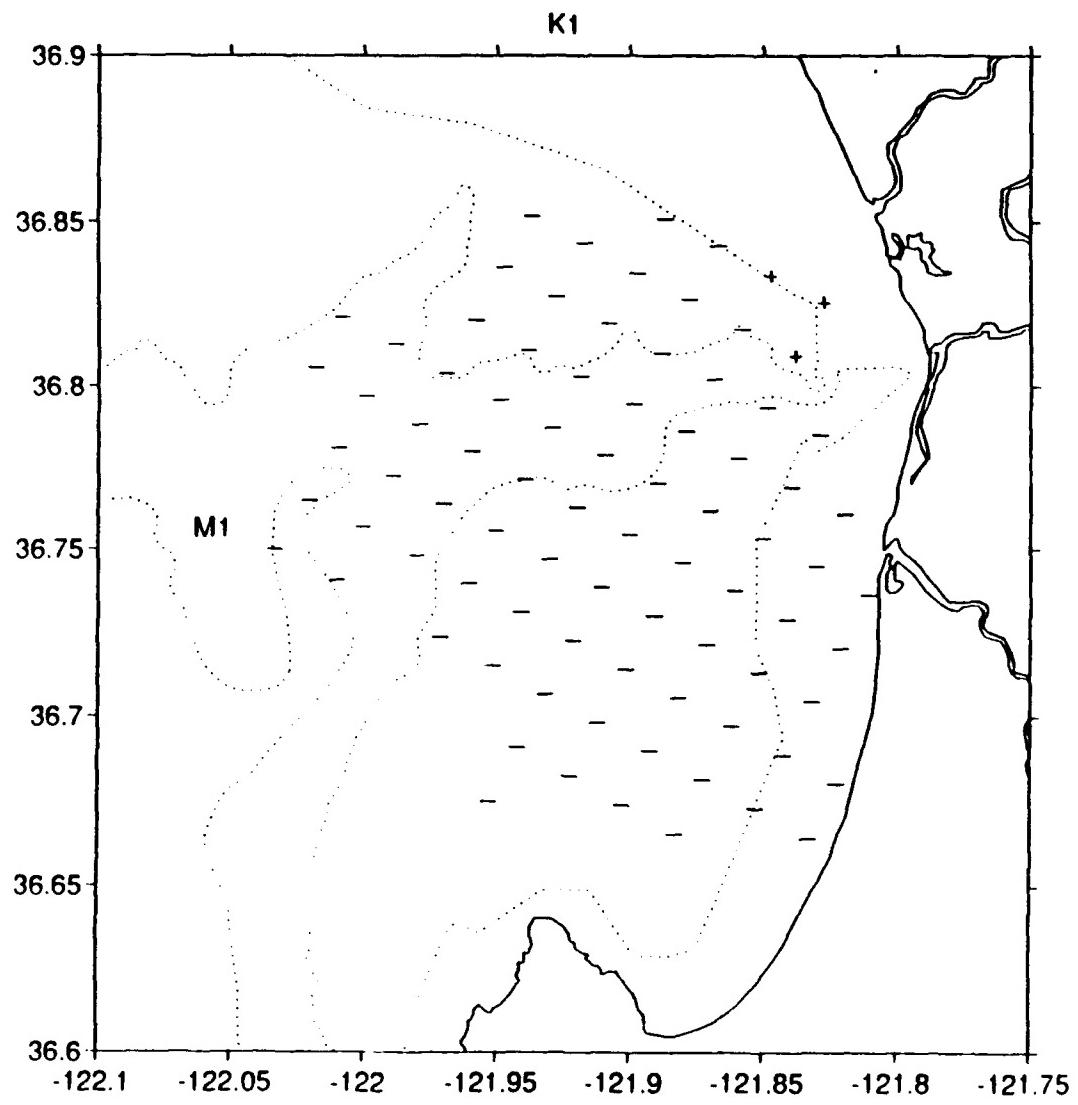
Figure 22. Direction of K1 Current Rotation (- = Clockwise, + = Counterclockwise).
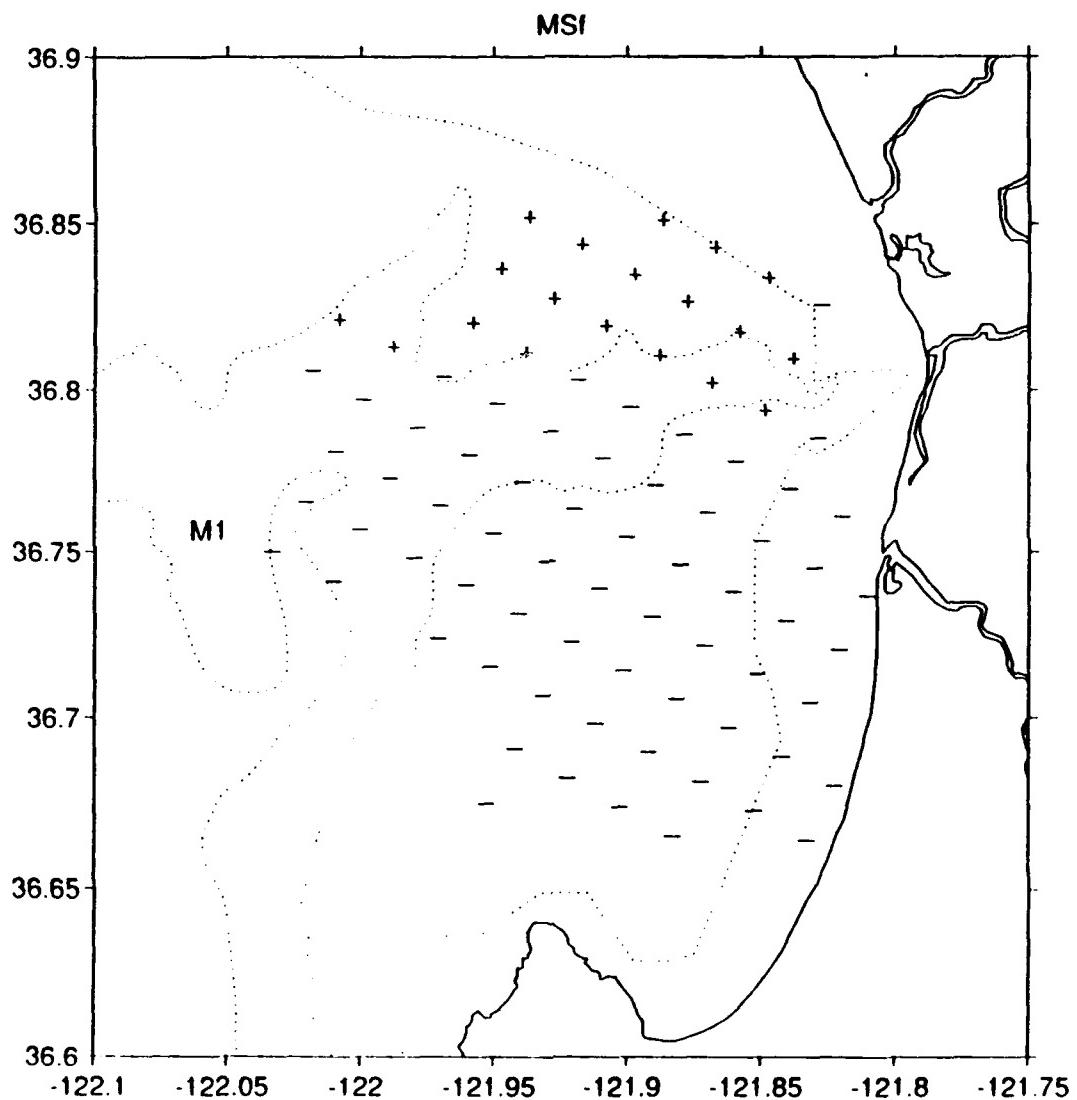
Figure 23. Direction of MSf Current Rotation (- = Clockwise + = Counterclockwise). Note the similarity with the rotation pattern of the M2 currents.
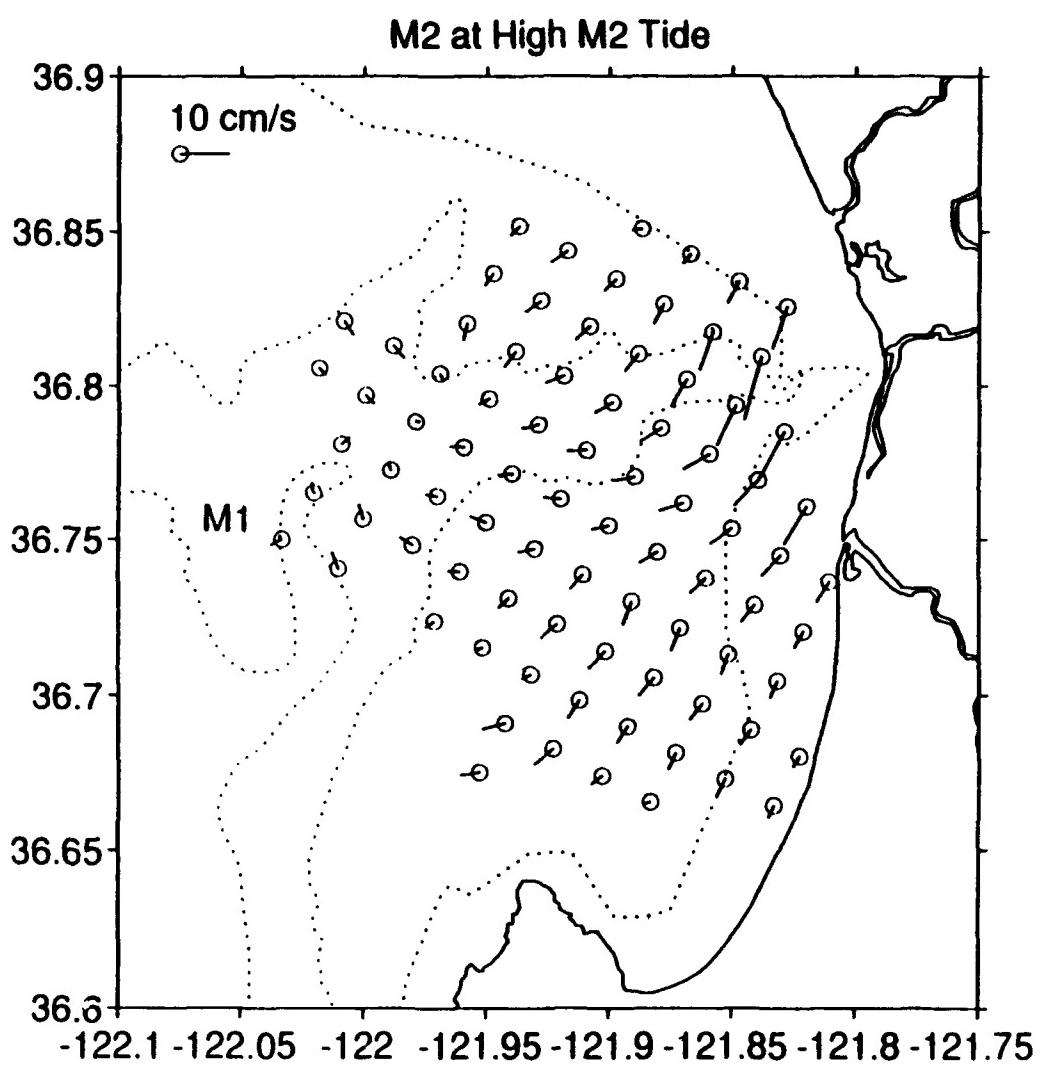
Figure 24. M2 Surface Current Flow During High M2 Surface Tide.
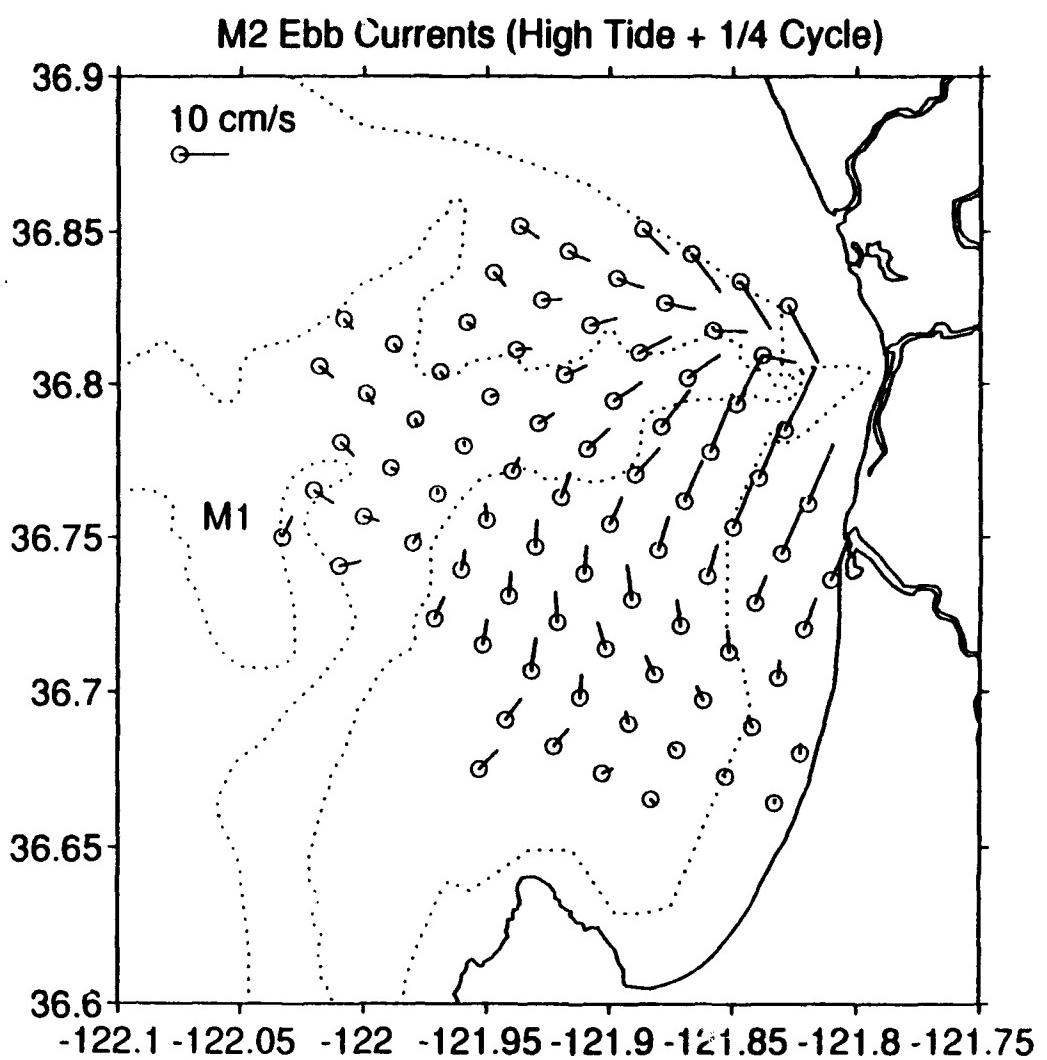
Figure 25. M2 Surface Current Flow During Falling M2 Surface Tide (Ebb Tide).
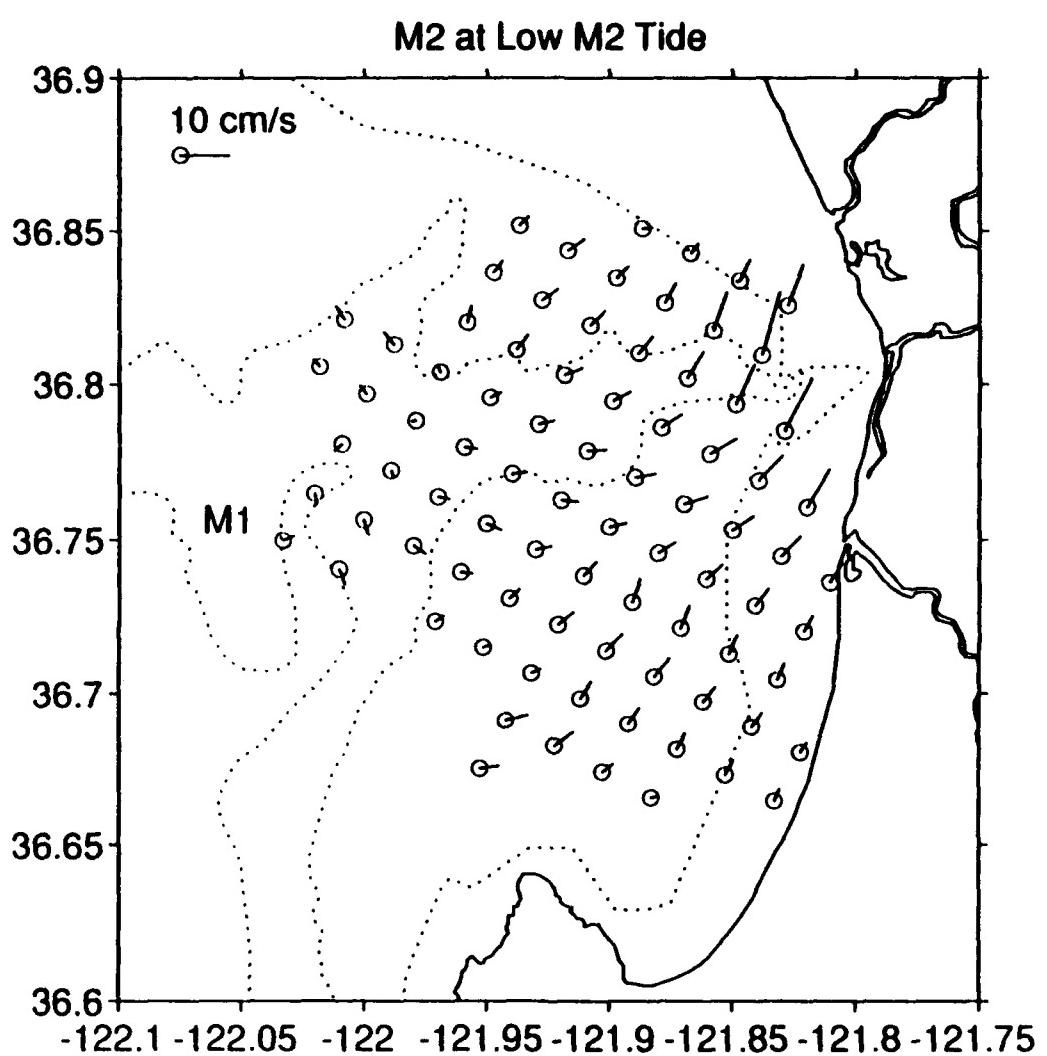
Figure 26. M2 Surface Current Flow During Low M2 Surface Tide.
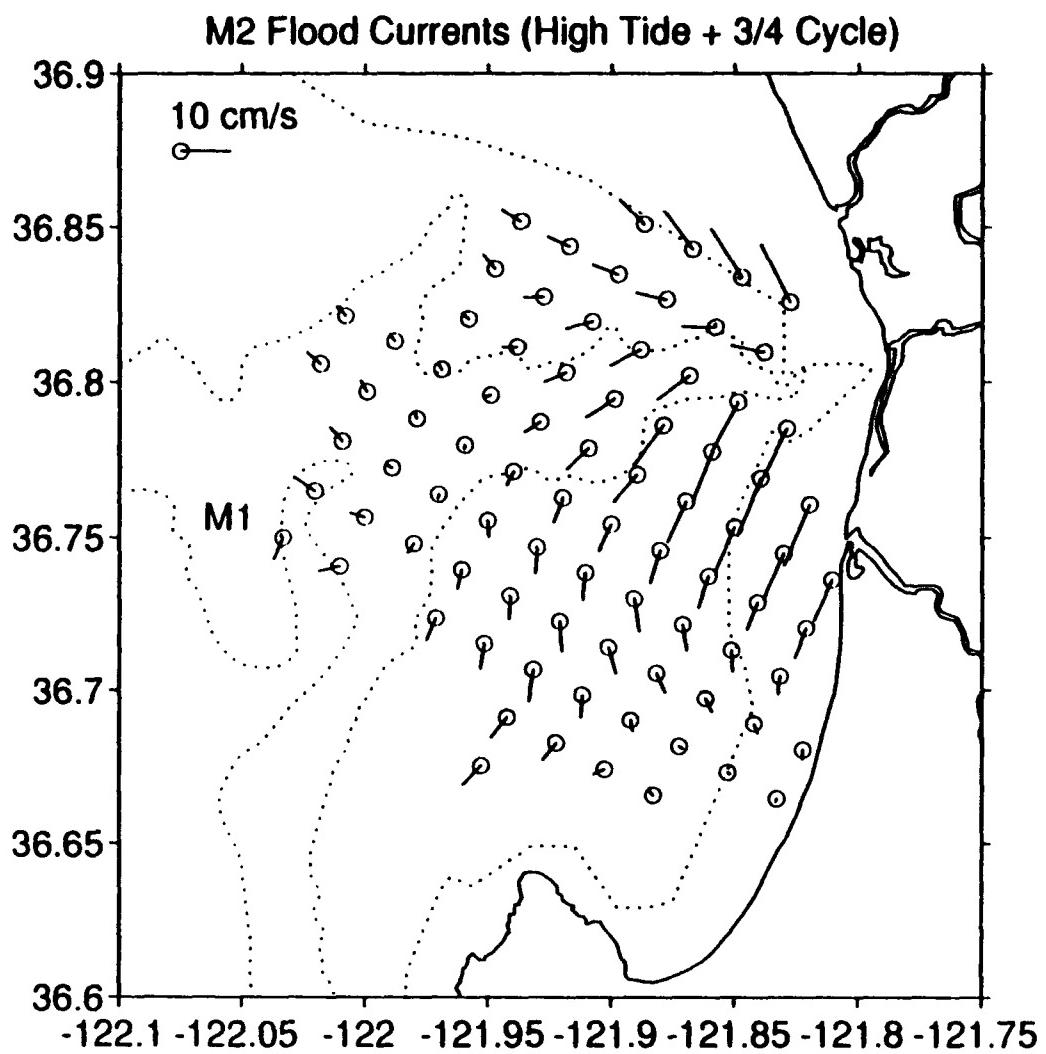
Figure 27. M2 Surface Current Flow During Rising M2 Surface Tide (Flood Tide).

V. ANALYSIS

A. SEMIDIURNAL TIDES

1. Tidal Heights Vs. Tidal Currents

The surface tides in Monterey Bay are dominated by the M2 constituent. Tidal currents also have a strong M2 constituent but have a complex relationship with the semidiurnal sea level changes due to the presence of internal waves and extreme changes in bathymetry within the bay.

As discussed in Chapter II, the barotropic M2 currents would be expected to rotate in the counterclockwise direction under the influence of a poleward propagating Kelvin wave. The vertical profiles of the M2 ellipses at the mouth of the Bay and most of the M2 ellipses analyzed in the surface currents however, indicate clockwise rotation. As discussed in Gill (1982), the direction of current vector rotation associated with an internal wave is clockwise. If clockwise rotation of the M2 ellipses over the axis of the canyon is due to the influence of internal waves of semidiurnal period propagating up the canyon axis, the currents should rotate clockwise in space as one moves seaward, i.e., in the direction *opposite* the direction of propagation. This behavior is evident in the M2 currents over the canyon axis, being more obvious at high and low M2 tide than at flood and

ebb (Figures 24 and 26). Additional evidence for internal waves exists in the vertical structure of the M2 currents (Figure 14). The direction of current flow reverses with depth, and in the first record (1/17-2/19/92) a node is apparent between the flow reversals, which would be expected of a baroclinic mode.

Although the currents over the canyon axis appear to be related to internal waves propagating up the slope, the opposing rotation of the M2 ellipses on the north and south flanks of the canyon (counterclockwise and clockwise, respectively) is more indicative of bathymetric steering of flow into and out of the canyon. This phenomena is further discussed in the next section.

2. Horizontal Variations

According to Shea and Broenkow (1982), at high internal tide large internal waves push cold, high density water up out of the canyon and onto the shelves flanking the canyon head. As the internal wave falls, some of this high density water is left behind, and warmer, less dense water flows down the canyon to take its place (Figure 28). The M2 currents analyzed in this study clearly show convergence toward and divergence away from the canyon head during falling and rising M2 sea levels, respectively. The flow of the surface M2 currents in the vicinity of the canyon head seems
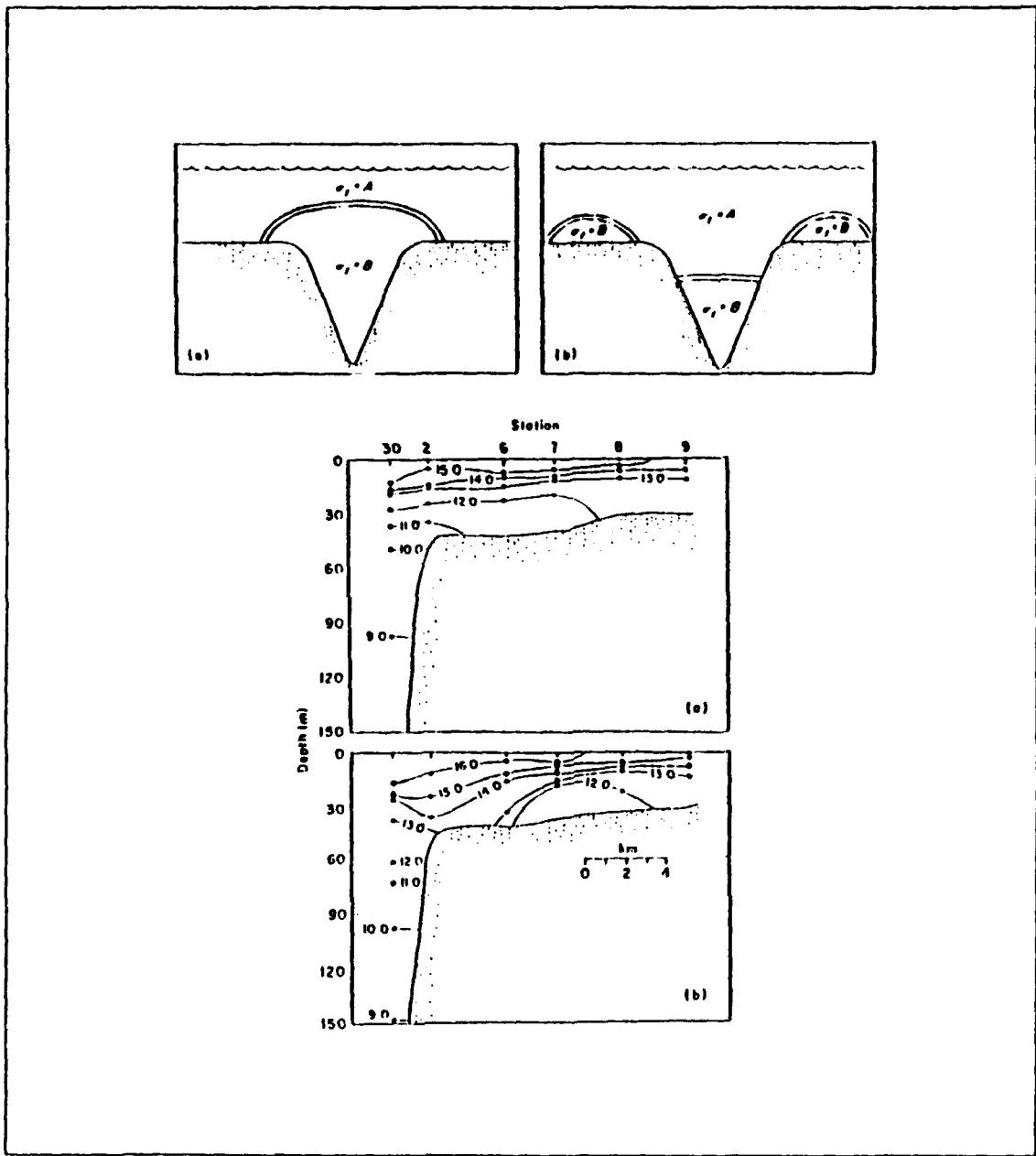
Figure 28. Conceptual Model of "Tidal Pumping" of Higher Density Water from Monterey Canyon to the Shelf by Internal Wave Action. The top figures depict the lifting of high density water out of the canyon during high internal tide (a), and the deposition of some of this water onto the shelves flanking the canyon during low internal tide (b). The bottom figures indicate actual water temperatures during high (a) and low (b) internal tide. (Source: Shea and Broenkow, 1982).

to be in agreement with the "tidal pumping" theory of Shea and Broenkow, if it is assumed that the surface and internal tides are nearly in phase. Heard (1992) analyzed 26 hours of CTD and ADCP measurements obtained near the canyon head, and concluded that the maximum displacement of the semidiurnal internal tide at the canyon head occurred 2.3 hours later than the maximum M2 surface tide at Monterey. It should be noted that the internal tide is not necessarily "phase-locked" with the surface tide, and that variations in the phase lag between the internal and surface tides can be expected when comparing short term observations recorded at different time periods.

The phase differences between the CODAR-derived M2 tidal ellipses and the M2 surface tide indicate that the mid-bay M2 surface currents lag the M2 sea level response by 4 hours (116°). This phase lag results in upcanyon surface flow during falling tide and downcanyon flow during rising tide, which is contrary to the expected direction of "ebb" and "flood" currents. The behavior of the mid-bay surface currents is consistent with a first mode internal wave of semidiurnal period propagating upslope, if the wavelength of the internal wave is approximately 30 km (twice the distance between the head of the canyon and the mouth of the bay) and the displacment of the isopycnals near the head of the canyon is approximately in phase with the sea level changes. This scenario is depicted in Figure 29.
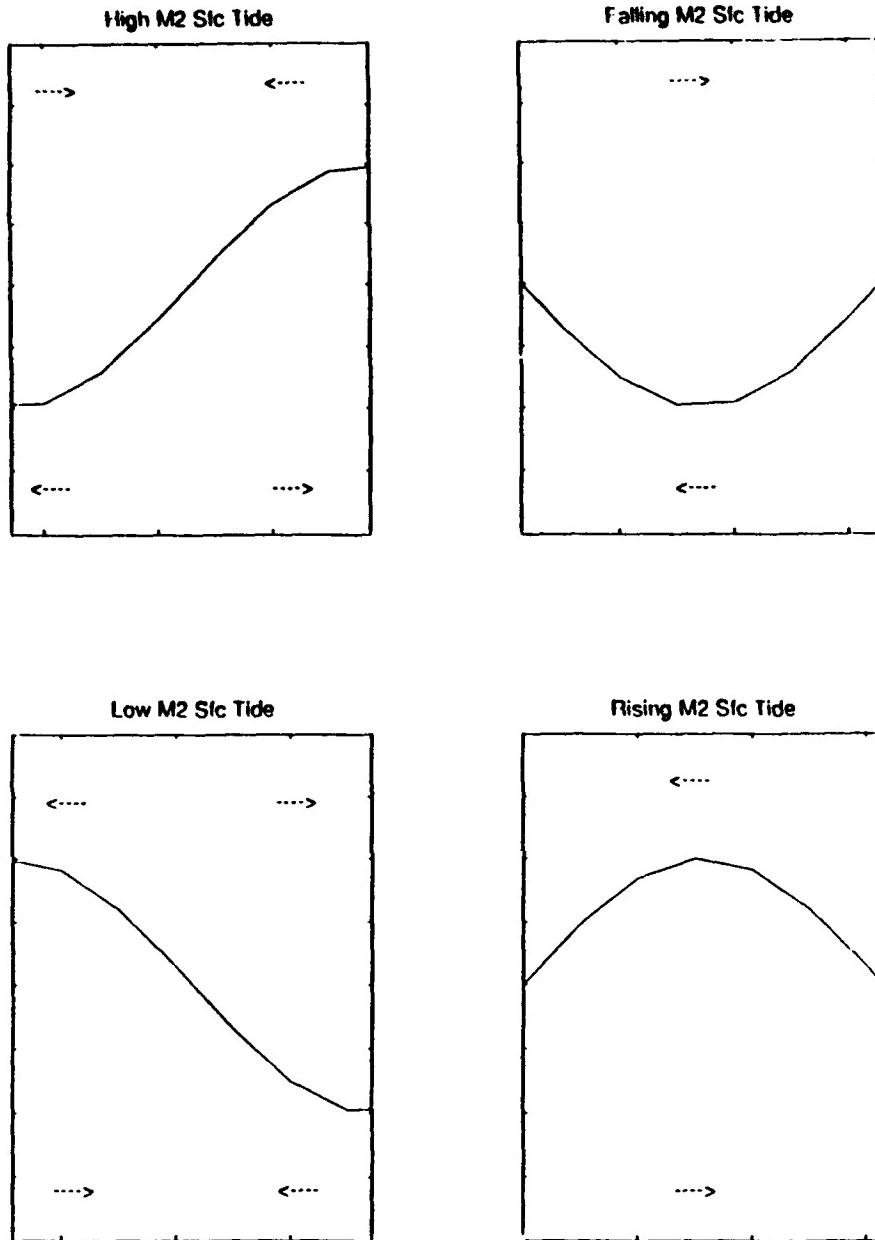
Figure 29. Theoretical Flow Associated With A First Mode Internal Wave of Semidiurnal Period Propagating Up the Monterey Submarine Canyon. The vertical displacement of the isopycnals at the head of the canyon is in phase with the semidiurnal (M2) surface tide. The distance from the mouth of the Bay (the left side of each figure) to the canyon head (on the right side of each figure) is approximately 15 km, and the wavelength of the internal wave is approximately 30 km.

While the internal wave depicted in Figure 29 explains the surface flow over the canyon axis at mid-bay, it is emphasized that the surface flow near the canyon head appears to be dominated by the bathymetric steering of water being pumped in and out of the canyon as these large internal waves shoal at the canyon head.

3. Vertical Structure

The counterclockwise veering of the M2 ellipses with depth appears to be related to stratification. Few discussions of the turning of tidal current ellipses in the upper ocean can be found in the literature, however Harvey and Vincent (1977) state that tidal ellipses in the North Sea rotate counterclockwise through a total angle of 14° as one goes downward through the boundary layer. Prandle (1982a and 1982b) describes the vertical structure of tidal currents as a function of vertical eddy viscosity, quadratic bed stress friction, depth-averaged velocity, frequency, and depth. The dependence on eddy viscosity suggests the possibility of seasonal variations in the vertical structure of tidal currents as stratification conditions change. Figure 14 shows that the upper ocean M2 ellipses veer counterclockwise with depth. In the first record, when the existence of a deep mixed layer is expected, this veering does not become evident until a depth of approximately 100 m. Between 100 and 200 m, the M2 ellipses veer approximately 100°. In the second

record, when the water column appeared to be continuously stratified, the M2 ellipses veered approximately 85° counterclockwise between 17 and 200 m, and the veering was apparent at all depths.

B. DIURNAL TIDES

Although the diurnal sea level response to tidal forcing is relatively strong, the diurnal period currents analyzed during this study appeared to be dominated by periodic wind forcing. The exceptionally strong K1 signal in the CODAR-derived tidal currents is most likely due to sea breeze effects. The northwest-southeast orientation of the K1 ellipses is in agreement with the expected direction of Monterey Bay sea breezes, which flow into the Salinas Valley southeast of the Bay (Round, 1993 and Foster, 1993). The northwest-southeast orientation of the K1 ellipses was also evident in the ADCP-derived tidal currents. The clockwise rotation of the K1 ellipses is in agreement with the clockwise rotation of the sea breezes (Foster, 1993).

Though internal waves of semidiurnal period appear to influence semidiurnal current flow in Monterey Bay, internal waves of diurnal period are not expected at this latitude since only those internal waves with periods less than the inertial period will propagate freely. This may explain why the depth-averaged O1 currents were weaker than the S2 and N2 currents (see Figure 10).

C. LONG PERIOD TIDES

Although the sea level response to long period tidal forcing was minute, the long period signals in the ADCP and CODAR measurements were exceptionally strong. There are three mechanisms to explain the existence of these low frequency currents. These mechanisms are discussed in the following paragraphs.

1. Astronomical Forcing

Although long period tides may be a direct result of astronomical forcing, it is unlikely that the strong fortnightly and monthly currents observed in this study are the direct result of astronomical forcing. If this were the case, a significant sea level response at the same frequency would also be expected, however the low frequency tidal heights were negligible.

2. Meteorological Forcing

Periodic wind forcing may contaminate tidal current analyses, expecially if the analyses are based on short records. This has already been seen to be the likely cause of the relatively strong K1 ellipses. The northwest-southeast orientation of the monthly (MM) and fortnightly (MSf) constituents is suggestive of meteorological forcing, as this is the predominant direction of the local land-sea breeze cycle. In the harmonic analysis of a 33-day record, two

exceptionally strong land-sea breeze events spaced two weeks apart could be resolved as a fortnightly signal.

3. Nonlinear Interaction

Besides gravitational and meteorological forcing, contributions to currents in these frequency bands are also produced through nonlinear interaction among the stronger tidal constituents. These interactions are described by the advection and friction terms in the shallow water wave equations. Godin (1972), Thompson and Wilson (1987), and Parker (1991) discuss long period tidal modulation through nonlinear interaction of the major diurnal and semidiurnal tides. The interaction of the M2 and N2 tides result in a difference frequency harmonic with a frequency equal to that of the MM constituent. Interaction of the S2 and M2 gives rise to a component equal in frequency to MSf, while interaction of the K1 and O1 components generate a longer period fortnightly constituent equal to Mf. Numerous higher frequency "overtides" are also produced through the interaction of these constituents.

The production of a long period (difference frequency) harmonic by the interaction of two constituents with frequencies σ_1 and σ_2 may be examined by letting $u = A_1 \cos(\sigma_1 t - \theta_1) + A_2 \cos(\sigma_2 - \theta_2)$, (where the right side of the equation is the sum of the two interacting tidal constituents), and then expanding the advection term, $u\, \partial u / \partial x$.

Both σ and θ are functions of x, and numerous terms result from the expansion. The terms which describe the difference frequency harmonic are:

$$A_1 A_{2_x} \frac{1}{2} \cos \left[(\sigma_1 - \sigma_2) t + (\theta_1 - \theta_2) \right]$$

and

$$A_{1_x} A_2 \frac{1}{2} \cos \left[(\sigma_1 - \sigma_2) t + (\theta_1 - \theta_2) \right]$$

It is thus seen that the phase of the long period harmonic should be equal to the difference of the phases of the two interacting constituents ($\theta_{\text{HARMONIC}} = \theta_1 - \theta_2$).

Applying this theory to the M2, S2, and MSf currents analyzed during this study, this phase relationship was readily apparent at all depths in the second set of ADCP measurements (9/1-10/4/92), but only at the deepest depths in the first set (1/17-2/19/92). The phase errors of the depth-averaged M2, S2, and MSf currents, which are representative of the phase errors in the bin-by-bin tidal analyses, are approximately 1° for M2, 5° for S2, and 10-15° for MSf (Tables 4A and 4B). Thus, differences between θ_{MSf} and ($\theta_{\text{S2}} - \theta_{\text{M2}}$) which are less than 20° are not significantly different from zero. The phase relationships of the ADCP-derived M2, S2, and MSf ellipses are presented in Table 6.

TABLE 6. OBSERVED M2, S2, AND MSF PHASE RELATIONSHIPS

ADCP BIN	1/17-2/19/92			9/1-10/4/92		
	$G_{S2}-G_{M2}$	G_{MSf}	Δ	$G_{S2}-G_{M2}$	G_{MSf}	Δ
2	54.5	154.5	100.0	23.3	30.3	7.0
3	52.6	154.5	101.9	36.5	28.2	8.3
4	49.6	154.3	104.7	24.1	28.0	3.9
5	43.7	156.0	112.3	25.1	29.2	4.1
6	41.3	156.7	115.4	32.3	32.2	0.1
7	41.8	158.4	116.6	34.4	36.1	1.7
8	49.8	158.1	108.3	33.4	38.7	5.3
9	56.5	156.3	99.8	31.9	43.4	11.5
10	62.3	156.4	94.1	36.9	48.0	11.1
11	62.5	158.6	96.1	36.0	52.7	16.7
12	69.5	161.3	91.8	31.2	52.4	21.2
13	95.9	163.4	67.5	32.5	51.1	18.6
14	112.5	164.8	52.3	40.7	48.2	7.5
15	125.7	172.9	47.2	41.0	42.3	1.3
16	141.0	184.5	43.5	35.2	38.5	3.3
17	146.4	195.4	49.0	26.3	33.0	6.7
18	155.3	219.9	64.6	17.2	27.3	10.1
19	209.4	252.6	43.2	19.1	17.9	1.2
20	230.4	262.0	31.6	21.6	9.8	11.8
21	242.4	263.9	21.5	19.2	4.7	14.5
22	246.1	263.1	17.0	11.2	-3.6	14.8
23	256.4	260.5	4.1	4.3	-9.6	13.9
24	267.8	257.9	9.9	-2.7	-11.5	8.8
25	264.8	256.5	8.3	-5.4	-13.4	8.0

It should be pointed out that the shorter period fortnightly constituent, the Lunar-fortnightly (Mf), could not be resolved in the tidal current analyses conducted in this study due to the short record lengths. Thus any contributions to tidal current flow due to this constituent (or due to a difference frequency harmonic resulting from interaction of K1 and O1) would be lumped together in the analysis with the MSf currents.

Although the expected phase relationship for the M2, S2, and MSf phases was only occasionally evident in the CODAR-derived ellipses, there is other evidence in the CODAR records to suggest nonlinear interaction between M2 and S2. Parker (1991) states that nonlinear interaction between tidal constituents may result in significant momentum transfer from the interacting constituents to the resulting harmonic. The loss of momentum in the interacting constituents may cause the harmonic to be stronger than either main constituent. This may be the case in the generation of the relatively strong fortnightly tidal currents over the deeper end of the canyon. The M2 ellipses are strongest near the canyon head and weakest over the deep end of the canyon (see Figure 18). The S2 ellipses, which are not depicted, are slightly weaker than the M2 currents but follow the same pattern in terms of relative strength. The MSf ellipses (Figure 20) exhibit the opposite pattern; they are strongest over the deep end of the canyon near the mouth of the Bay and weakest near the canyon head.

92

Thus, although it is quite possible that the low frequency currents observed during this study are the result of non-tidal (meteorological) forcing, there is a pattern which suggests that momentum transfer from the M2 and S2 currents to a difference frequency harmonic (equal in frequency to that of the MSf tide) may occur near the mouth of Monterey Bay.

V. SUMMARY AND RECOMMENDATIONS

A. SUMMARY

Analysis of year-long sea level records obtained at Santa Cruz and Monterey (the north and south ends of Monterey Bay) indicates that the mixed, mainly semidiurnal sea level response is generally uniform across the Bay. Slight phase differences between the main semidiurnal constituents (3-6°) at these two locations suggest a possible southward progression of the semidiurnal constituents within Monterey Bay. This is a surprising result, in view of the northward phase progression of the M2 tide along the west coast of North America.

Near the mouth of the Bay, tidal currents account for 50% of the total current variance in the upper 200 m of the ocean. Within the Bay, the Monterey Submarine Canyon clearly influences the direction and strength of semidiurnal tidal currents. Amplification of the semidiurnal tidal currents occurs near the canyon head, apparently in response to large internal waves of semidiurnal period which propagate up the canyon axis. M2 surface currents were approximately 5 cm/s near the mouth of the Bay and 15 cm/s near the canyon head. Analysis of the vertical structure of the M2 currents revealed significant counterclockwise turning of the M2 ellipses in the

upper 200 m of the ocean, as well as a reversal in flow direction over depth. The northwest-southeast orientation and the surprising strength of the K1 surface currents (30 cm/s) suggest that currents at this frequency are dominated by sea breeze effects over month-long periods in the winter and late summer. Strong fortnightly surface currents (15 cm/s) were observed near the mouth of the Bay. There is some evidence to suggest that these fortnightly currents are the result of nonlinear interaction between the M2 and S2 currents. With the exception of the K1 currents, good agreement exists between HF-radar and ADCP-derived tidal currents.

B. RECOMMENDATIONS

Current records of at least six months in length should be analyzed in order to obtain a clearer picture of the behavior of tidal currents in Monterey Bay. Longer time series of current measurements would allow distinctions to be made between the K1 and P1 currents, and might help distinguish between diurnal tidal currents and wind forced (sea breeze) currents. Additionally, comparison of longer current records and concurrent wind records might clear up the cause of the strong low frequency currents. More could be learned about the persistent internal waves in Monterey Bay by comparing the phases of temperature and current oscillations, especially in the vicinity of the canyon.

It is clear that successful modeling of the tidal currents in Monterey Bay will require consideration of baroclinic effects. In view of the strong fortnightly tidal currents observed in this study, it is possible that nonlinear effects will need to be incorporated in future modeling efforts as well.

Although the measurement of surface currents with HF radar has not found widespread use in the U.S., this study demonstrates the capability of this technology to provide reliable, long term current measurements over a large area. The use of HF radar to study tidal and subtidal currents should continue.

Appendix A

ERROR ESTIMATION OF THE TIDAL HEIGHTS HARMONIC ANALYSIS

Residual sea level, i.e. the difference between the observed and calculated sea level changes, represents the expected error of the tidal heights analysis. The residual signal can be attributed to errors in the coefficients of the sine and cosine terms chosen as the best fit in the least squares matrix (Godin, 1972). The errors in the sine and cosine coefficients are propagated in the subsequent calculations of the amplitudes and phases of the various tidal constituents. In order to find the errors associated with each analyzed tidal height constituent then, the variance of the residual energy in each tidal band (low frequency, diurnal, semidiurnal, etc...) must be determined and then related to the standard deviation (or expected error) of the amplitudes and phases of the tidal constituents (Filloux and Snyder, 1979, and Tee, 1982).

The variance of some variable **x** is defined as

$$\sigma_x^2 = \frac{1}{N} \sum_{n=1}^{N} (x_n - \bar{x})^2$$

where σ_x is the standard deviation of x, N is the total number of observations of x, and $x_n - \bar{x}$ is the difference between the

mean and the nth observed signal. Similarly, the variance of the residual tidal heights may be expressed as:

$$\sigma_H{}^2 = \frac{1}{N}\sum_{n=1}^{N} (H_n - \overline{H})^2 .$$

Godin (1972) and Foreman (1978) assume the variance of the residual signal to be constant across the spectrum (i.e., "white noise"). Filloux and Snyder (1979) and Tee (1982) take a more rigorous approach in describing the residual signal by finding the variance of the noise in each of the major tidal bands. This more detailed method was also used in this study. In practice, σ_H was calculated for a given frequency band as follows. The residual sea level signal was determined by subtracting the calculated tidal contribution (the time varying signal resulting from the sum of the analyzed tidal constituents) from the measured sea level. A one-sided power spectrum of this residual signal was then computed, and the average variances in the various tidal bands (low frequency, diurnal, semidiurnal, terdiurnal, etc...) were determined. The average variances were calculated by integrating the spectral density in each band, dividing by the number of spectral estimates in the given band, and multiplying by two to account for the use of a one-sided spectrum. The standard deviation (or expected error) of the amplitude for each major tidal constituent was then defined as the square root of the

98

average variance of the noise in the appropriate frequency band.

1. **Tidal Constituent Amplitude Error**.

The variance can be shown to depend on the errors in the sine and cosine coefficients (A and B) as follows. If x is a function of two variables, r and s, the following approximation can be made:

$$x_n - \overline{x} \approx \frac{\partial f}{\partial r}\bigg|_{\overline{r}} (r_n - \overline{r}) + \frac{\partial f}{\partial s}\bigg|_{\overline{s}} (s_n - \overline{s}).$$

The variance of x can then be expressed as:

$$\sigma_x^2 = (\frac{\partial f}{\partial r})^2 \sigma_r^2 + (\frac{\partial f}{\partial s})^2 \sigma_s^2 + 2\frac{\partial f}{\partial r}\frac{\partial f}{\partial s}\sigma_{rs}^2. \qquad (1)$$

As was stated in Chapter II, the harmonic representation of the sea level response to forcing by the ith constituent can be expressed as $H_i(t) = Z_i \cos(\sigma_i t - \phi_i)$. Expansion of this equation yields (dropping the i subscript):

$$H(t) = Z(\cos\sigma t \cos\phi + \sin\sigma t \sin\phi).$$

Letting $A = Z\cos\phi$ and $B = Z\sin\phi$, we have

$$H(t) = A\cos\sigma t + B\sin\sigma t.$$

and

$$Z = \sqrt{A^2 + B^2}.$$

Since we are looking for the error in the calculated tidal amplitude, we substitute Z for x in Equation 1, obtaining:

$$\sigma_z^2 = \left(\frac{A}{Z}\right)^2 \sigma_A^2 + \left(\frac{B}{Z}\right)^2 \sigma_B^2 + 2\left(\frac{A}{Z}\right)\left(\frac{B}{Z}\right)\sigma_{AB}^2. \qquad (2)$$

For gap-free records of sufficient length to separate the major constituents (29 days, using a Rayleigh Factor equal to 1) the following assumptions can be made (Tee, 1982):

- The covariance of the sine and cosine terms is equal to zero ($\sigma_{AB}^2 = 0$).

- The variances of the sine and cosine terms are equal ($\sigma_A^2 = \sigma_B^2 = \sigma_H^2$).

We can then simplify Equation 2 as follows: $\sigma_z^2 = \sqrt{\dfrac{\sigma_H^2}{Z^2}(A^2 + B^2)}$,

or since $Z = \sqrt{A^2 + B^2}$,

$$\sigma_Z = \sigma_H. \qquad (3)$$

Equation 3 simply states that the expected error of the calculated tidal amplitude is equal to the standard deviation (the square root of the average variance) of the residual sea level amplitude (noise) in the specified frequency band.

2. Tidal Constituent Phase Error.

Using the definition of A and B given above, the phase (ϕ) of the tidal constituent can be expressed as $\phi = \tan^{-1}\frac{B}{A}$.

Substituting ϕ for x in Equation 1, we obtain:

$$\sigma_\phi^2 = \left(-\frac{B}{Z^2}\right)^2\sigma_A^2 + \left(\frac{A}{Z^2}\right)^2\sigma_B^2 + 2\left(-\frac{B}{Z^2}\right)\left(\frac{A}{Z^2}\right)\sigma_{AB}^2$$

which, after applying our two assumptions from above, simplifies to

$$\sigma_\phi = \frac{\sigma_H}{Z^2}\sqrt{(A^2+B^2)} = \frac{\sigma_H}{Z}.$$

Thus the expected error of the calculated phase for a given constituent in the tidal heights record is easily found by dividing the standard deviation of the residual sea level in that band by the calculated amplitude of the constituent.

Appendix B

ERROR ESTIMATION OF THE TIDAL CURRENTS ANALYSIS

The determination of the errors associated with the calculated tidal current ellipse parameters employs the same basic method used to find the errors of the amplitudes and phases of the tidal heights constituents. The residual currents (the "noise" in the signal) contribute to errors in the coefficients of the sine and cosine terms chosen as the best fit in the least squares matrix, and these errors are propagated in the subsequent calculations of the lengths of the semimajor and semiminor axes, the phase, and the inclination of the tidal current ellipse.

In Appendix A the amplitude and phase for a given constituent in the tidal heights were shown to be functions of two variables, the coefficients of the sine and cosine terms. In the case of tidal currents, there are sine and cosine terms for both the east-west and north-south components of flow. Thus, the tidal current ellipse parameters are functions of four variables: two cosine coefficients (A_1 and A_2) and two sine coefficients (B_1 and B_2). The variance of a quantity which is a function of four variables ($x = f(A_1, B_1, A_2, B_2)$) is approximated by:

$$\sigma_x^2 = \left(\frac{\partial f}{\partial A_1}\right)^2 \sigma_{A_1}^2 + \left(\frac{\partial f}{\partial B_1}\right)^2 \sigma_{B_1}^2 + \left(\frac{\partial f}{\partial A_2^2}\right) \sigma_{A_2}^2 + \left(\frac{\partial f}{\partial B_2^2}\right)^2 \sigma_{B_2}^2 + \text{higher order terms.} \qquad (1)$$

The higher order terms are associated with the covariances of A_1, B_1, A_2, and B_2.

As in Chapter II, the magnitude of the semimajor axis can be expressed as

$$U_{maj} = a^+ + a^-$$

$$= \frac{1}{2}\left[(A_1+B_2)^2 + (A_2-B_1)^2\right]^{\frac{1}{2}} + \frac{1}{2}\left[(A_1-B_2)^2 + (A_2+B_1)^2\right]^{\frac{1}{2}}.$$

An expression for the variance of the calculated semimajor axis is obtained by substituting U_{maj} for x in Equation 1. As in the tidal heights error analysis (Appendix A), we can assume that the higher order terms in Equation 1 are negligible, and that $\sigma_{A_1}^2 = \sigma_{B_1}^2 = \sigma_u^2$ and $\sigma_{A_2}^2 = \sigma_{B_2}^2 = \sigma_v^2$. The variance of the calculated semimajor axis then simplifies to:

$$\sigma_{U_{maj}}^2 = \sigma_u^2\left[\left(\frac{\partial U_{maj}}{\partial A_1}\right)^2 + \left(\frac{\partial U_{maj}}{\partial B_1}\right)^2\right] + \sigma_v^2\left[\left(\frac{\partial U_{maj}}{\partial A_2}\right)^2 + \left(\frac{\partial U_{maj}}{\partial B_2}\right)^2\right].$$

The partial derivatives of U_{maj} with respect to A_1, B_1, A_2, and B_2 are then determined, and the calculated values of the sine and cosine coefficients (determined during

103

the least squares analysis) are plugged into these expressions. The standard deviation of the noise in the u and v components of flow (σ_u and σ_v) were determined as follows.

The residual currents were determined by subtracting the time series representing the u and v components of the total tidal current (resulting from the summation of all analyzed tidal constituents) from the time series representing the u and v components of the measured currents. As in the tidal heights error analysis, one-sided power spectra of these residual signals were computed, and the average variances in each tidal band were found by integrating the power spectrum in each band, dividing by the number of spectral estimates in the band, and multiplying by two to account for the use of one-sided spectra. The standard deviation of the residual u and v signals in each tidal band were then obtained by taking the square root of the variance in the appropriate band.

The procedures to determine the errors in the semiminor axis length (U_{min}), the ellipse orientation (INC), and the phase (G) are similar. The expressions for U_{min}, INC, and G were substituted for x in Equation 1, the values of A_1, A_2, B_1, and B_2 and the appropriate σ_u and σ_v were plugged into the resulting expressions, and the variances of these parameters were calculated for each of the major tidal constituents. The standard deviation (expected error) for

each parameter was obtained by taking the square root of the calculated variances.

LIST OF REFERENCES

Baines, P.G., "The Generation of Internal Tides by Flat-Bump Topography", *Deep Sea Research*, 20, pp. 179-205, 1973.

Barrick, D.E., Evans, M.W., and Weber, B.L., "Ocean Surface Currents Mapped by Radar", *Science*, 198, pp. 138-144, 1977.

Barrick, D.E., Lipa, B.J., and Lilleboe, P.M., "HF Radar Surface-Current Mapping: Recent U.S./Canadian Advances", paper sponsored by the Current Measurement Technology Committee of the Ocean Engineering Society Institute of Electrical and Electronic Engineers, 1986.

Battisti, D.S., and Clarke, A.J., "A Simple Method for Estimating Barotropic Tidal Currents on Continental Margins with Specific Application to the M2 Tide off the Atlantic and Pacific Coasts of the United States", *Journal of Physical Oceanography*, 12, pp. 8-16, 1982.

Bolin, R.F. and Abbot, D.P., "Studies on the Marine Climate and Phytoplankton of the Central Coastal Area of California, 1954-1960", *California Cooperative Oceanic Fisheries Investigation Reports*, 9, pp. 23-45, 1963.

Breaker, L.C., and Broenkow, W.W., *The Circulation of an Embayment Bisected by a Major Submarine Canyon: Monterey Bay*, Moss Landing Marine Laboratories, Moss Landing California, Technical Publication 89-1, 1989.

Broenkow, W.W., and McKain, S.J., *Tidal Oscillations at the Head of Monterey Submarine Canyon and Their Relation to Oceanographic Sampling and the Circulation of Water in Monterey Bay*, Moss Landing Marine Laboratories, Moss Landing, California, Technical Publication 72-05, 1972.

Broenkow, W.W., and Smethie, Jr., W.M., "Surface Circulation and Replacement of Water in Monterey Bay", *Estuarine and Coastal Marine Science*, 6, pp. 583-603, 1978.

Caster, W.A., *Near-Bottom Currents in Monterey Submarine Canyon and on the Adjacent Shelf*, Master's Thesis, Naval Postgraduate School, Monterey, California, 1969.

Chelton, D.B., "Seasonal Variability of Alongshore Geostrophic Velocity off Central California", *Journal of Geophysical Review*, 89, pp. 3473-3486, 1984.

Crombie, D.D., "Doppler Spectrum of Sea Echo at 13.56 Mc/s", *Nature*, 175, pp. 681-682, 1955.

Crombie, D.D., "Resonant Backscatter from the Sea and its Application to Physical Oceanography", *Oceans '72 Conference Records*, IEEE Publishing number 72CHO660-1022, pp. 173-179, 1972.

Defant, A., *Physical Oceanography*, vols. I and II, Pergamon Press, Oxford, England, 1961.

Dooley, J.J., *An Investigation of Near-Bottom Currents in the Monterey Submarine Canyon*, Master's Thesis, Naval Postgraduate School, Monterey, California, 1968.

Fernandez, D.M., *High Frequency Radar Measurements of Coastal Ocean Surface Currents*, PhD Dissertation, Stanford University, Stanford, California, 1993.

Filloux, J.H., and Snyder, R.L., "A Study of Tides, Setup and Bottom Friction in a Shallow Semi-Enclosed Basin. Part I: Field Experiment and Harmonic Analysis", *Journal of Physical Oceanography*, 9, pp. 158-169, 1979.

Foreman, M.G.G., *Manual for Tidal Currents Analysis and Prediction*, Institute of Ocean Sciences, Patricia Bay, Sidney, British Columbia, Canada, (1st ed. 1978; reprinted 1979, 1982, 1984.)

Foster, M.D., *Evolution of Diurnal Surface Winds and Surface Currents for Monterey Bay*, Master's Thesis, Naval Postgraduate School, Monterey, California, 1993.

Gatje, P.H., and Pizinger, D.D., *Bottom Current Measurements in the Head of Monterey Submarine Canyon*, Master's Thesis, Naval Postgraduate School, Monterey, California, 1965.

Gill, A.E., *Atmosphere-Ocean Dynamics*, pp. 262-264, Academic Press, Inc., 1982.

Godin, G., *The Analysis of Tides*, University of Toronto Press, 1972.

Godin, G., "The Analysis of Tides and Currents", *Tidal Hydrodynamics*, pp. 675-709, John Wiley and Sons, Inc., 1991.

Harvey, J.W. and Vincent, M.A., "Observations of Shear in Near-Bed Currents in the Southern North Sea", *Estuarine Coastal Marine Science*, 5, pp. 715-731, 1977.

Heard, J.A., *A Kinematic Model of Baroclinic Tidal Currents At the Head of Monterey Submarine Canyon*, Master's Thesis, Moss Landing Marine Laboratories, San Jose State University, Moss Landing, California, 1992.

Hickey, B.M., "The California Current System - Hypothesis and Facts", *Progressive Oceanography*, 8, pp. 191-274, 1979.

Hollister, J.E, *Currents in Monterey Submarine Canyon*, Master's Thesis, Naval Postgraduate School, Monterey, California, 1975.

Hotchkiss, F.S. and Wunsch, C., "Internal Waves in Hudson Canyon with Possible Geological Implications", *Deep-Sea Research*, 29, pp. 415-442, 1982.

Huyer, A., Kosro, P.M., Fleischbein, J., Ramp, S.R., Stanton, T., Washburn, L., Chavez, F., and Cowles, T., "Currents and Water Masses of the Coastal Transition Zone off Northern California, June to August 1988, *Journal of Geophysical Research*, 96, pp. 14,809-14,831, 1991.

Koehler, K.A., *Observations and Modeling of Currents Within the Monterey Bay During May 1988*, Master's Thesis, Naval Postgraduate School, Monterey, California, 1990.

Lazanoff, S.M., *An Evaluation of a Numerical Water Elevation and Tidal Current Prediction Model Applied to Monterey Bay*, Master's Thesis, Naval Postgraduate School, Monterey, California, 1971.

Lentz, S.J., "The Accuracy of Tide-Gauge Measurements at Subtidal Frequencies", *Journal of Atmospheric and Oceanic Technology*, 10, pp. 238-245, 1993.

Lynn, R.J., and Simpson, J.J., "The California Current System: The Seasonal Variability of its Physical Characteristics", *Journal of Geophysical Research*, 92, pp. 12,947-12,966, 1987.

McKay, D.A., *A Determination of Surface Currents in the Vicinity of the Monterey Submarine Canyon by the Electromagnetic Method*, Master's Thesis, Naval Postgraduate School, Monterey, California, 1970.

Munk, W., Snodgrass, F., and Wimbush, M., "Tides Offshore: Transition from California Coastal to Deep-Sea Waters", *Geophysical Fluid Dynamics*, 1, pp. 161-235, 1970.

National Ocean Service, *Tidal Current Tables 1992, Pacific Coast of North America and Asia North*, National Oceanic and Atmospheric Administration, 1991.

National Ocean Service, *Tide Tables 1992, West Coast of North and South America Including the Hawaiian Islands*, National Oceanic and Atmospheric Administration, 1991.

Neal, T.C., *Analysis of Monterey Bay CODAR-Derived Surface Currents, March to May 1992*, Master's Thesis, Naval Postgraduate School, Monterey, California, 1992.

Njus, I.J., *An Investigation of the Environmental factors affecting the near-bottom currents in Monterey Submarine Canyon*, Master's Thesis, Naval Postgraduate School, Monterey, California, 1968.

Noble, M., Beardlsey, R.C., Gardner, J.V., Rosenfeld, L.K., and Smith, R.L., "Tidal Currents Seaward of the Northern California Continental Shelf", *Journal of Geophysical Research*, 92, pp. 1655-1681, 1987.

Parker, B.B., "The Relative Importance of the Various Nonlinear Mechanisms in a Wide Range of Tidal Interactions (Review)", *Tidal Hydrodynamics*, pp. 237-268, John Wiley and Sons, Inc., 1991.

Prandle, D., "The Vertical Structure of Tidal Currents and Other Oscillatory Flows", *Continental Shelf Research*, 1, pp. 191-207, 1982a.

Prandle, D., "The Vertical Structure of Tidal Currents", *Geophysical and Astrophysical Fluid Dynamics*, 22, pp. 29-49, 1982b.

Pugh, D.T., *Tides, Surges and Mean Sea-Level*, John Wiley and Sons, Ltd., 1987.

RD Intruments, *Acoustic Doppler Current Profilers Principles of Operation: A Practical Primer*, 1989.

Rosenfeld, L.K., and Beardsley, R.C., "Barotropic Semidiurnal Tidal Currents off Northern California During the Coastal Ocean Dynamics Experiment (CODE)", *Journal of Geophysical Research*, 92, pp. 1721-1732, 1987.

Rosenfeld, L.K., "Baroclinic Semidiurnal Tidal Currents Over the Continental Shelf off Northern California, *Journal of Geophysical Research*", 95, pp. 22,153-22,172, 1990.

Rosenfeld, L.K., Schwing, F.B., Garfield, N., and Tracy, D.E., "Bifurcated Flow From an Upwelling Center: A Cold Water Source for Monterey Bay", *Continental Shelf Research*, in press, 1993.

Round, R.D., *Climatology and Analysis of the Monterey Bay Sea Breeze*, Master's Thesis, Naval Postgraduate School, Monterey, California, 1993.

Schomaker, C.W., *A Model for Tidal Circulation Adapted to Monterey Bay, California*, Master's Thesis, Naval Postgraduate School, Monterey, California, 1983.

Schureman, P., *Manual of Harmonic Analysis and Prediction of Tides, Government Printing Office*, Washington D.C., (1st ed. 1924; reprinted 1940, 1958, 1988).

Shea, R.E., and Broenkow, W.W., "The Role of Internal Tides in the Nutrient Enrichment of Monterey Bay, California", *Estuarine, Coastal and Shelf Science*, 15, pp. 57-66, 1982.

Shepard, F.P., Marshall, N.F., McLoughlin, P.A., and Sullivan, G.G., *Currents in Submarine Canyons and Other Seavalleys*, AAPG Studies in Geology No. 8, American Association of Petroleum Geologists, 1979.

Shih, H.H., and Baer, L., "Some Errors in Tide Measurement Caused by Dynamic Environment", *Tidal Hydrodynamics*, pp. 641-671, John Wiley and Sons, Inc., 1991.

Simpson, J.J., Koblinsky, C.J., Pelaez, J., Haury, L.R., and Wiesenhahn, D., "Temperature-Plant Pigment-Optical Relations in a Recurrent Offshore Mesoscale Eddy Near Point Conception, California", *Journal of Geophysical Research*, 91, pp. 12,919-12,936, 1986.

Skogsberg, T., "Hydrography of Monterey Bay, California. Thermal Conditions, 1929-1933", *Transactions of the American Philosophical Society*, 29, pp. 1-152, 1936.

Stoddard, H.S., *Feasability Study on the Utilization of Parachute Drogues and Shore-Based Radar to Investigate Surface Circulation in Monterey Bay*, Master's Thesis, Naval Postgraduate School, Monterey, California, 1971.

Strub, P.T., Allen, J.S., Huyer, A., and Smith, R.L., "Seasonal Cycles of Currents, Temperatures, Winds, and Sea Level Over the Northeast Pacific Continental Shelf: 35° N to 48° N", *Journal of Geophysical Research*, 92, pp. 1507-1526, 1987.

Tee, K., "The Structure of Three-dimensional Tide-generating Currents: Experimental Verification of a Theoretical Model", *Estuarine, Coastal and Shelf Science*, 14, pp. 27-48, 1982.

Thompson, R.E., and Wilson, R.E., "Coastal Countercurrent and Mesoscale Eddy Formation by Tidal Rectification Near an Oceanic Cape", *Journal of Physical Oceanography*, 17, pp. 2096-2126, 1987.

Tisch, T.D., Ramp, S.R., and Collins, C.A., "Observations of the Geostrophic Current and Water Mass Characteristics off Point Sur, California, From May 1988 Through November 1989", *Journal of Geophysical Research*, 97, pp. 12,535-12,555, 1992.

Werner, F.E., "Tidal Hydrodynamics, Quantitative Aspects", *Encyclopedia of Earth System Science*, 4, pp. 351-367, Academic Press, Inc., 1992.

Wunsch, C., "Internal Tides in the Ocean", *Review of Geophysics*, 13, pp. 167-182, 1975.

INITIAL DISTRIBUTION LIST

		No. Copies
1.	Defense Technical Information Center Cameron Station Alexandria VA 22304-6145	2
2.	Library, Code 052 Naval Postgraduate School Monterey CA 93943-5002	2
3.	Oceanography Department Code OC/CO Naval Postgraduate School 833 Dyer Rd RM 331 Monterey CA 93943-5122	1
4.	Meteorology Department Code MR/HY Naval Postgraduate School 589 Dyer Rd RM 252 Monterey CA 93943-5114	1
5.	Dr. Jeffrey D. Paduan Code OC/PD Naval Postgraduate School 833 Dyer Rd RM 331 Monterey CA 93942-5122	1
6.	Dr. Leslie K. Rosenfeld Code OC/LR Naval Postgraduate School 833 Dyer Rd RM 331 Monterey CA 93942-5122	1
7.	LT Emil T. Petruncio, USN SMC 2834 Naval Postgraduate School Monterey CA 93943-5122	1
8.	Dr. Melbourne G. Briscoe Director, Office of Ocean and Earth Sciences NOAA, National Ocean Service 1305 East-West Highway SSMC4 Station 6616 Silver Spring, MD 20910	1

9. Dr. Stephen K. Gill   1
    N-OES 22
    SSMC 4 Rm 7109
    1304 East West Highway
    Silver Spring, MD   20910

10. Dr. W.W. Broenkow   1
    Moss Landing Marine Laboratory
    P.O. Box 223
    Moss Landing, CA 95039

11. Library   1
    Moss Landing Marine Lab
    California State Colleges
    Sandholdt Road
    Moss Landing, CA   95039

12. Harold A. Miller Library   1
    Hopkins Marine Station
    Stanford University
    Cabrillo Point
    Pacific Grove, CA 93950

13. Library   1
    Scripps Institute of Oceanography
    Code C-075
    University of California, San Diego
    La Jolla, CA 92093